Real time course of transmitter release of SSVs and LDCVs; SNARE function analysed in synaptobrevin2 and cellubrevin knock out mice

Dissertation
zur Erlangung des Doktorgrades
der Mathematisch-Naturwissenschaftlichen Fakultäten
der Georg-August-Universität zu Göttingen

Vorgelegt von
Ying Zhao
aus Wuhan, China

Göttingen 2003

D 7

Referent: Prof. Dr. F.W.Schümann

Korreferent:Prof. H.D.Söling

Tag der mündlichen Prüfung:

Abbreviations

Acetic acid	Glacial acetic acid
2-ME	ß-mercaptoethanol
APS	ammonium persulphate
ATP	adenosine triphosphate
BoNT	botulinum neurotoxine
BSA	bovine serum albumine
Cy3	indigocarbocyanine
DMEM	Dulbecco's minimal essential medium
DMSO	Dimethyl sulfoxide
Dopmine	2-(3,4-Dihydroxyphenyl)ethylamine hydrochloride
EB	Ethidium Bromide
ECL	super signal west dura extended Durati substrate
EDTA	ethylenediaminetetraacetic acid
EGTA	ehtylene glycol-bis[ß-amino-ethylether]
EtOH	ethanol
FCS	foeral calf serum
HEPES	N-[2-Hydroxyethyl]piperazine-N'-[2-ethanesulfonic acid]
HRP	horse radish peroxidase
Ig	Immunoglobulin
ITSX	Insulin-Transferrin-selenium-X
kb	kilo base pairs
KDa	kilodalton
KO	knock out
LDCVs	large dense core vesicles
NSF	N-ethylmaleimide sensitive factor
PAGE	polyacrylamide gel electrophoresis
Pen-Strep-Sol	Penicillin-streptomycin solution
PBS	phosphate buffered saline
PCR	polymerase chain reaction
PFA	Paraformaldehyde
PK	proteinase-K
PonceauS	3-Hydroxy-4-(2-sulfo-4-[4-sulfophenylazo]phenylazo)-2,7-Naphthalenedisulfonic acid sodium salt
2-propanol	Isopropyl alcohol , Isopropanol
rpm	rotations per minute
Rotiphorese Gel30	Roti-phenol/chloroform
RT	room temperature
SDS	sodium dodecyl sulfate
SNAP	soluble NSF attachment protein
SNAP-25	synaptosomal associated protein of 25 kDa
SNARE	SNAP-receptor

SSVs	small synaptic vesicles
sucrose	ß-D-Fructofuranosyl-α-D-glucopyranoside
syb2	synaptobrevin2
syx	syntaxin
TAE	Tris-Acetic/EDTA
TBS	Tris-buffered saline
TE	Tris-EDTA
TEMED	1,2-Bis-(dimethylamino)-ethane
TeNT	tetanus neurotoxin
Tris	tris-(hydroxymethyl)-aminoethane
Triton 100X	t-Octylphenoxypolyethoxyethanol
Tween-20	polyoxyethylenesorbitan monolaurate
UV	ultra violet
v/v	volume to volume
vol	volume
w/v	weight to volume
w/w	weight to weight
WT	wild type

Contents

1. Synapses and synaptic transmission

The intercellular communication resulting in the relaying of information from one cell of the nervous system to another is the essence of nervous system function. The brain is clearly distinguished from other organs by this information transfer. The task is carried out by a unique and highly specialized structure called synapse. The term synapse, derived from a Greek word meaning "connect", was introduced by the British physiologist Charles Sherrington near the end of the nineteenth century. According to the nature of signal transmission, synapses can be classified as chemical and electrical synapses. Although chemical and electrical synapses exit side by side in most nervous systems and both mediate intercellular information transfer, they do so by different mechanisms. The intercellular signaling at electrical synapses is mediated by the movement of small ions from one cell to another through cell-to-cell gap junction channels. The extent of electrical connectivity in the central nervous system is not clear. In the mammalian system, synaptic transmission is mediated mainly by chemical synapses. Fast chemical synapses are composed of three compartments 1) the presynaptic cell, 2) the synaptic cleft, and 3) the postsynaptic cell. In such synapses, when an action potential generated at the axon hillock of a presynaptic neuron travels down to the presynapses, where it causes opening of voltage-gated Ca^{2+} channels, Ca^{2+} ions enter the cytosol and trigger the fusion of synaptic vesicle with the plasma membrane leading to the release of neurotransmitters contained in the vesicles. These transmitters diffuse through the synaptic cleft and bind to the receptors on the postsynaptic neurons eliciting a specific cellular response, *e.g.*, the opening of ligand-gated ion channels which causes an electrical signal called synaptic potential.

2. Synaptic vesicles, synaptic transmitters and exocytotic pathways

Central synapses reveal morphologically specialized release sites where synaptic vesicles (SVs) are attached to the presynaptic membrane. SVs are small organelles (~50nm, diameter) and contain neurotransmitters. The presynaptic boutons of central nervous system (CNS) contain a large reservoir of SVs that can be functionally

divided into three pools. At about 200nm away from the active zone a resting pool consisting of hundreds of vesicles exists. At the border of the active zone a pool of 5-20 docked SVs bound to the presynaptic plasma membrane is present at any given time, this is called the readily releasable pool (RRP). Situated between the two pools is the reserve pool of ~17-20 SVs that appears to be located near the active zone (Murthy and Stevens, 1999).

Two major classes of synaptic transmitters are identified, low molecular weight transmitters, and peptides. Acetylcholine, dopamine, noradrenaline, octopamine, serotonin, histamine, ATP, gamma-aminobutyric acid (GABA), glutataurine, tyramine, and the diadenosine polyphosphates are the members in the first class. The other class, the peptides, is synthesized under direct genetic control. They enter intracellular membrane compartments from the rough endoplasmic reticulum and are packaged into secretory vesicles via the Golgi apparatus. Afterwards they are transported to the axon terminal.

Nerve cells posses two principle pathways for exocytosis. The constitutive pathway serves constant secretion and the incorporation of membrane constituents into the plasma membrane and it can take place at any point of the neuronal surface. In contrast, regulated exocytosis occurs only when the cell is activated by a specific signal, *e.g.*, the influx of Ca^{2+} ions and it is confined to specific sites of the plasma membrane where the molecular machinery exists to respond to a cellular signal, to dock the vesicles, and to elicit membrane fusion.

3. SNAREs-mediated exocytotic fusion

The fusion of vesicles with target membranes involves the merger of two phospholipid bilayers. The fusion process is controlled by a cascade of protein-protein interactions. In eukaryotic cells several protein families, including SNAREs, Rab proteins, and Sec1/Munc-18 related proteins (SM-proteins) are involved in this process. However, it is generally accepted that the SNARE complex form the core of

the machinery for intracellular membrane fusion and that formation of a SNARE complex is crucially important.

3.1 SNARE proteins

SNAREs (soluble NSF attachment protein receptors) consist of three synaptic membrane proteins, the synaptic vesicle protein synaptobrevin called v-SNARE (also known as vesicle-associated protein, VAMP) and the plasma membrane proteins called t-SNARE, syntaxin1 and SNAP-25 (synaptosome-associated protein of 25kDa). These proteins were originally identified as membrane receptors for an ATPase called NSF (N-etylmaleimide-sensitive factor), and SNAPs (soluble NSF attachment proteins). The neuronal SNAREs, synaptobrevin2, syntaxin, and SNAP-25 assemble into a stable ternary complex with a 1:1:1 stoichiometry, which is disassembled after fusion by NSF, in conjunction with α-SNAPs (Sollner *et al*., 1993; Rothman, 1994). *In vitro*, this very stable complex is resistant to heat, the detergent SDS, protease digestion and clostridial neurotoxin cleavage (Fasshauer *et al*., 1998; Poirier *et al*., 1998). Most SNARE proteins are attached to membranes through their C-terminal membrane anchor, a transmembrane domain. The SNARE superfamily is characterized by the presence of SNARE motif which is about 60 amino acid residues long (Jahn and Südhof, 1999). The SNARE motif is placed close to the membrane anchor and is responsible for SNARE-SNARE interactions and complex formations. SNARE proteins can contain one or two SNARE motifs. Criteria for the division of SNAREs into subfamilies are the sequences of the SNARE motifs.

The structure of the SNARE-complex is well known now (Sutton *et al*., 1998). The crystal structure was obtained from recombinant SNARE motifs without transmembrane domains. The crystal structure shows a parallel bundle of four α-helices formed by one helix of synaptobrevin2, one of syntaxin1 and two of SNAP-25 (*Fig. 1A*). In the SNARE complex 16 layers can be identified, in which amino acid residues from all four helices are oriented into the inside of the bundle and interact with each other (*Fig. 1B*). In the layers most amino acid residues are hydrophobic, but one arginine (R) residue of synaptobrevin interacts with three glutamine (Q) residues

of other helices in the zero layer. Thus the proteins are divided into R-SNAREs and Q-SNAREs on the basis of having an arginine or glutamine residue in the position predicted to form the zero layer of the complex (Fasshauer *et al*., 1998). Amino acid residues intended to form the 16 layers of the bundle are highly conserved in different SNAREs and the highest degree of conservation is found in the zero layer. The surface of the synaptic complex is highly grooved and possesses distinct hydrophilic, hydrophobic and charged regions. These characteristics may be important for membrane fusion and for binding of regulatory factors affecting neurotransmission (Sutton *et al*., 1998).

3.2 Common steps in SNARE-mediated fusion reactions

The secretory process requires many different steps and stages. Vesicles must be formed and transported to the target membrane. They must be tethered or docked at the appropriate sites and must be prepared for fusion (priming). At final step, a fusion pore is formed and the contents are released. Such SNARE mediated fusion reactions can be summarized into 5 different phases, 1) SNARE proteins located on the SNARE core complex are disassembled by NSF; 2) the synaptic vesicles are attached to the plasma membrane; 3) syntaxin, synaptobrevin and SNAP-25 form trans-SNARE complexes and lead to an approximation of the opposing lipid bilayers; 4) the membrane bilayers merge to open the fusion pore; 5) fusion pore expansion leads to completion of the reaction (Jahn and Südhof, 1999).

A

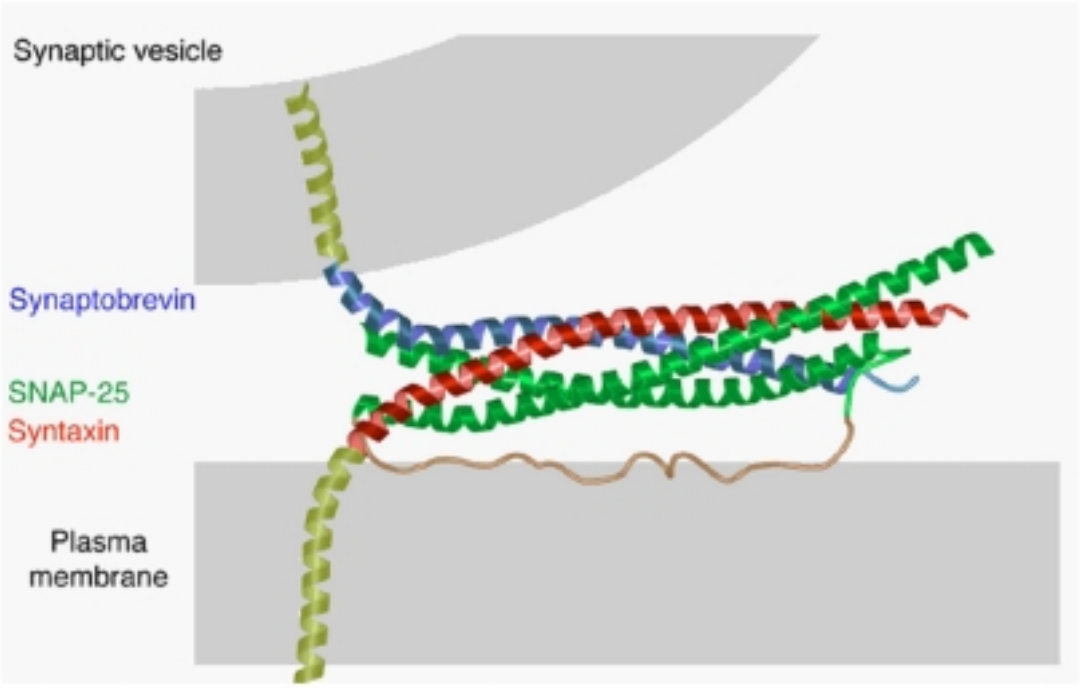

Sutton, Fasshauer, Jahn, Brunger (1998) Nature 395, 347-353

B

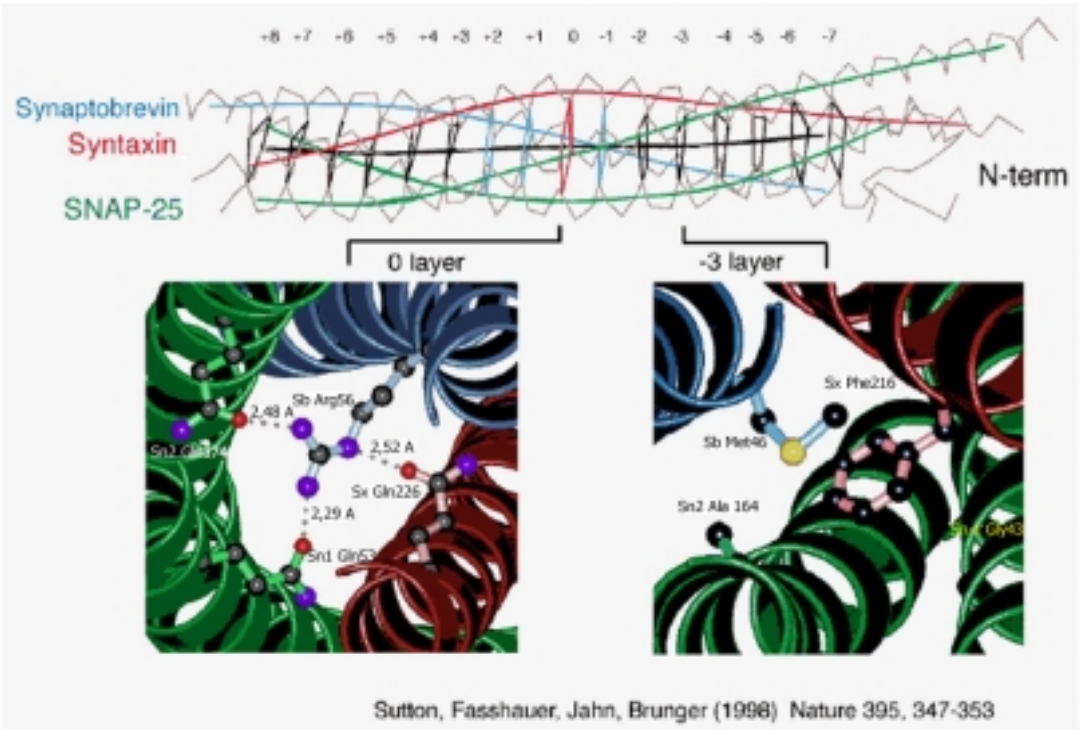

Figure 1. Model of neuronal SNARE complex consisting of synaptobrevin, syntaxin, and SNAP-25 based on the crystal structure.

3.3 The cleavage of SNARE proteins by clostridial neurotoxin blocks neurotransmitter release.

Eight different clostridial neurotoxins have been identified (Schiavo *et al*., 2000): one tetanus toxin (TeNT) and seven botulinal toxins (BoNT/A, B, C1, D, E, F, and G). TeNT and BoNT are bacterial proteins that comprise a light chain (M(r) approximately 50) disulfide linked to a heavy chain (M(r) approximately 100). The heavy chains mediate targeting of the toxin to the presynaptic nerve terminal. After binding to specific membrane acceptors, BoNTs and TeNT are internalized via endocytosis into nerve terminals. Subsequently, their light chains (a zinc-dependent endopeptidase) are translocated into the cytosolic compartment where they cleave one of three essential proteins involved in the exocytotic machinery: syntaxin, SNAP25 and synaptobrevin/VAMP. Tetanus and botulinum B neurotoxin cleave VAMP (Link *et al*., Schiavo *et al*., 1992), the remaining six botulinum neurotoxins cleave either VAMP, syntaxin 1, or SNAP-25. (Bittner *et al*., 1989; Lomneth *et al*., 1991). Cleavage of the neuronal SNARE proteins by these toxins causes a complete block of exocytosis, illustrating the importance of SNARE proteins for membrane fusion.

4. Electrophysiological techniques allow monitoring of single fusion events

The development of the so-called patch clamp technique and the electrochemical technique with a carbon fiber electrode provide a highly spatial and temporal resolution of release process and permit the analysis of transmitter release at the level of single secretory vesicles.

4.1 Cell-membrane capacitance techniques

The patch clamp technique, in whole-cell configuration, allows the detection of single fusion events by measuring changes in cell membrane capacitance (Fleig and Penner, 1995; Hamill *et al*., 1981). Since the exocytotic process involves vesicle-membrane fusion, it is associated with an increase in the plasma membrane area of the cell. Biological membranes have a rather constant specific capacitance of ~1μF/cm^2.

Therefore, the expansion of membrane area due to exocytosis results in a proportional increase in the plasma membrane capacitance. Following exocytosis, subsequent membrane retrieval by endocytosis leading to a decrease of capacitance of cell membrane can also be measured (Fernandez *et al*., 1984; Lindau *et al*., 1994; Neher and Marty, 1982a).

4.2 Amperometry

4.2.1 Amperometry can detect released transmitter molecules.

The amperometric method based on the oxidation or reduction of specific transmitters allows for exquisitely sensitive measurements of secretion at the level of single secretory organelles. Compared to the capacitance method, amperometry has several advantages, *e.g.*, no intervention by overlapping endocytosis, immediate monitoring of transmitter discharge, fewer limitations of cell shape, and it is a "noninvasive" method. Furthermore, in the case of chromaffin cells, the electrochemical approach is more sensitive than capacitance methods for detecting individual secretory quanta (Chow and Rüden, 1995).

In amperometry, molecules are electrochemically reduced or oxidized and the current of the reaction is measured. By utilizing Faraday's law, amperometric measurements can quantitatively reveal the number of molecules (oxidased)

[1] $$Q = \int I dt = zFM / N_A = zeM$$

here, Q represents the total charge involved in the redox reaction, which is obtained by integrating the current (*I*) transient; *M* represents the number of molecules reacted; *Z* is the number of moles of electrons transferred per mole of compound reacted; *F* is Faraday's constants, 96,485 coul/mol; N_A is Avogadro's number, 6.023×10^{23}; and e is the elementary charge, 1.6×10^{-19} coul. Using amperometry, the contents of very small vesicles can be quantified. For example, amperometry was applied to detect release of synaptic vesicles from cultured leech neurons that contain about 4,700 5-HT molecules (Bruns and Jahn, 1995).

Amperometry has an excellent temporal resolution and allows for a detailed real time

analysis of the kinetic processes involved in extrusion of vesicular content into the extracellular space. The time span between 50% and 90% amplitude (rise time) and the duration of the current transient at half height of its peak amplitude (half width) are often used to evaluate the time course of an individual secretion event. With a microelectrode pressed firmly against the individual cell membrane, losses of exocytotic materials due to diffusional mass transport are minimized, and the area of the cell analyzed is mostly determined by the surface of the microelectrode.

4.2.2 Diffusion theory

After opening of fusion pore the released molecules diffuse out of the vesicle to the surface of the detector (applied with ~ 650 mV) to be oxidized. Thus the kinetics of the transient currents recorded by the carbon fiber is determined by the time course of release process and the diffusion over the cell-electrode spacing (Chow and Rüden, 1995). The slowing of amperometric kinetics due to the diffusional broadening is described by *Einstein-Smolochowski* equation (one dimensional diffusion)

[2] $$\chi^2 = 2Dt$$

here, χ^2 is the mean squared displacement, D is the diffusion coefficient, and *t* is time. It indicates that the time for diffusion increases with the square of distance and is inversely proportional to the diffusion coefficient. For non-instantaneous, in order to record amperometric signals with reasonable fidelity of real time course of release process, placing carbon fiber on the cell surface as close as possible helps to minimize the diffusional “smearing”.

Amperometric spikes recorded from embryonic chromaffin cells are often preceded by a slower pedestal, called the foot signal, indicating that a small amount of catecholamine escapes from a nascent fusion pore (the foot) before the pore fully opens to release the remaining contents of the granule (the spike). In some cases, the foot signals are not followed by a spike due to the closure of fusion pore, and they are termed as foot-alone events.

4.3 Patch amperometry

The investigation of the fusion pore formed during Ca^{2+}-triggered exocytosis and its role in transmitter release are restricted, due to the small size of the secretory vesicles containing neurotransmitter. Lindau and his colleagues (Albillos *et al*., 1997) combined cell-attached capacitance measurements with electrochemical detection of catecholamines by inserting a carbon-fiber electrode into the patch pipette, termed as "patch amperometry". The technique allows the simultaneous determination of the opening of individual fusion pores and of the kinetics of catecholamine release from the same vesicle and extends the measurements of the time course of fusion and release from single vesicles to small vesicles with capacitance as small as 0.1fC.

5. Leech neurons and chromaffin cells

Secretory vesicles and their regulated exocytosis have been most extensively studied in a few cell types chosen either as model systems due to certain experimental advantages or due to their crucial physiological or pathophysiological interest. Current spikes have been electrochemically observed from several different cells often used as models for Ca^{2+}-triggered exocytosis, *e.g.*, mast cells, chromaffin cells, PC12 cells, Retzius cells. Since Retzius cells and chromaffin cells will be used as models in my study, they are discussed in detail here.

5.1 Leech neurons

The use of invertebrate preparations has contributed greatly to our understanding of the mechanism of neurotransmitter release. The leech is especially useful for studying exocytosis and its underlying mechanism. A pair of giant Retzius neurons is found in each segmental ganglion of the CNS in the leech (*Hirudo medicinalis*). They can be removed individually and plated in culture, where they retain their characteristic physiological properties, grow neuritis and form specific synapses that are chemical or electrical, depending on the neuronal identities.

The results obtained from the electrophysiological studies (amperometry) of Retzius cells advance our understanding of the kinetics of neurotransmitter release and molecular mechanism of exocytosis. Bruns & Jahn (1995) characterized the release of 5-HT from isolated Retzius cells of the leech. Two types of action potential-evoked spikes were observed and they are believed to correspond to Ca^{2+}-dependent exocytosis of small clear synaptic vesicles (SSV) and large dense core vesicles (LDCV). Electron microscopy confirmed that SSVs are located close to the plasma membrane of the axon stump, in contrast, LDCVs are present in more remote areas of the cytoplasm of the soma and axon in Retzius cells. The amperometric spikes attributed to small vesicles occurred more rapidly and frequently than LDCV spikes following a single action potential stimulus. Furthermore, it is found that the quantal variability for SSVs and LDCVs results from the size difference of the organelles and that transmitter is stored at similar concentration in SSVs and LDCVs (Bruns, 2000).

The formation and physiology of the synapses between the Retzius cell and its partners have been well characterized. Retzius cells form purely chemical, inhibitory synapses with pressure-sensitive (P) cells where 5-HT is the transmitter. Bruns *et al*., (1997) studied the unique properties of Retzius-P cell synapse. Their data demonstrate a direct correlation between the inhibition of transmitter release and the ability of clostridial neurotoxins to cleave their targets and support the view that SNARE ternary complex formation is an important step leading to synaptic vesicle exocytosis.

5.2 Chromaffin cells

The adrenal glands are a pair of endocrine organs that are situated cranially to the kidneys and serve to secret hormones from their cortices and catecholamines from their medulla into the bloodstream. The adrenal medulla is composed mainly of adrenergic and noradrenergic chromaffin cells, which are specialized for the synthesis, storage, and the secretion of catecholamines. Adrenaline and noradrenaline are released from adrenal medulla chromaffin cells by regulated exocytosis of the secretory granules in the cells (Aunis and Langley, 1999; Burgoyne, 1995; Perlman and Chalfie, 1977).

The chromaffin cell system (and its tumor counterpart the PC12 cell line) is well studied and many aspects of the mechanisms by which exocytosis is mediated in chromaffin cells are now well understood in detail providing insights into neuroendocrine secretion in general (Barnard *et al*., 1997; Burgoyne *et al*., 1996; Graham and Burgoyne, 2000). Due to their similarities of exocytotic mechanism to that of neurons, many of the results obtained from chromaffin cells can be applied to neurons as well. This makes chromaffin cells an ideal model system for the study of neuronal exocytosis.

Most of the proteins that mediate the formation, targeting, docking, and fusion of secretory granules have been identified in chromaffin cells (Baltazar *et al*., 2000; Fisher *et al*., 2001; Hohne-Zell and Gratzl, 1996; Roth and Burgoyne, 1994; Sorensen *et al*., 2002; Tagaya *et al*., 1995; Xu *et al*., 1999a; Xu *et al*., 1999b). As a model system, chromaffin cells provide the combination of biophysical techniques, *e.g.*, patch clamp, amperometry, with biochemical assays allowing to study exocytosis on single-vesicle level, and to perform specific biochemical modifications in the protein machinery involved in exocytosis (Baltazar *et al*., 2000; Chow *et al*., 1992; Graham *et al*., 2000; Heinemann *et al*., 1993; Moser and Neher, 1997; Neher and Marty, 1982b). Chromaffin cells remain a powerful model to address new and still open questions in the field of secretion.

6. Over-expression recombinant proteins by using SFV expression system

Recombinant protein expression is today a prerequisite for basic research. Owing to the high transfection efficiencies in mammalian cells, replication-deficient alphavirus vectors, specifically Semliki Forest virus (SFV) have become attractive alternatives for rapid and high-level gene delivery (Liljestrom and Garoff, 1991). The SFV expression system has already been used for overexpression of a single synaptic protein in chromaffin cells allowing for quantitative secretion measurements.

SFV has an enveloped, polydenylated single-stranded RNA genome, which functions as mRNA in infected cells. When the RNA genome of the recombinant SFV is

delivered to the cytosol and it is transcribed, an internal subpromoter leads to the transcription of a subgenomic RNA that encodes for a recombinant protein. SFV vector is engineered to express different proteins in a broad range of mammalian host cells (Lundstrom, 1999). The virus is modified to express a green fluorescence protein, which faithfully reports the infection and expression of the recombinant proteins of interest. Two SFV vectors are generated according to two different approaches for introducing an EGFP reporter into the virus genome, $SFV_1X_{IRES}EGFP$ and $SFV_1EGFP_{sub}X$, here, X is the sequence of interested protein. $SFV_1EGFP_{sub}X$ gives maximal expression of the reporter EGFP and a more limited expression of the recombinant protein. In contrast, $SFV_1X_{IRES}EGFP$ produces a maximal expression of the recombinant protein and a more limited expression of the EGFP reporter.

1 Animals

1.1 Leech

Retzius cells from leech *(Hirudo medicinalis)* were isolated and cultured for the experiments, as described in section 2.3.1.

1.2 Transgenic mice

C57BL/6J synaptobrevin2-deficient ($syb2^{+/-}$) mice (male and female) were obtained from the laboratory of Thomas Südhoff (University of Texas Southwestern Medical Center, Dallas, Texas, USA). $Syb2^{+/-}$ males were paired with $syb2^{+/-}$ females, and embryonic mice at the age of E17.5 ~E18.5 were prepared for the experiments.

C57BL/6J cellubrevin (VAMP3)-deficient ($VAMP3^{+/-}$) mice (male and female) were obtained from the laboratory of Jeffery E. Pessin (University of Iowa, Iowa, USA). $VAMP3^{+/-}$ males were paired with $VAMP3^{+/-}$ females, and embryonic mice at the age of E17.5 ~E18.5 were prepared for the experiments.

2 Genotyping of mice

2.1 Preparation of mice genomic DNA

Proteinase K stock solution

Dissolve Proteinase K (Roche) 10mg in 1ml autoclaved H_2O. Store at -20°C.

Lysis Buffer

Tris-HCl	pH 7.5, 0.01M
EDTA	pH 8.0, 0.01M
NaCl	0.1M
SDS	0.5%

Roti-Phenol / Chloroform (Roth)

A 25: 24:1 mix of TE –equilibrated phenol, chloroform, and isoamyl alcohol. Store at 4 °C to slow down evaporation of chloroform.

2-Propanol (Merck)

Keep 2-Propanol in the dark.

70 % Ethanol (Merck)

TE solution

Tris	pH 7.5, 10mM
EDTA	1mM

Fresh 0.5~1.0 cm pieces of mice tails were put each into a 1.5 ml eppendorf tube. 500µl Lysis buffer containing 25µl Proteinase K stock solution was added to each tube. The mixtures were incubated with gentle shaking at 55°C overnight. An equal volume of phenol / chloroform / isoamylalcohol (25/24/1mixture) was added to DNA solution, mixed by gently inverting the tubes several times till emulsion was formed. Samples were centrifuged in a tabletop centrifuge at full speed (13000 rpm) at room temperature for 15min. A blue pipette tip was cut off and 350µl viscous supernatant was transferred into a new tube. 350µl 2-propanol was added to each tube and DNA was pelleted for 10 minutes at 13000 rpm at room temperature. The supernatant was decanted as much as possible, and the DNA pellet was washed in 400µl 70 % ethanol. After centrifugation at 13000 rpm for 2min, Ethanol was removed, and 200µl TE solution was added to each tube. All the samples were kept at 37°C over night to let the genomic DNA dissolve completely.

2.2 Genotyping of mice embryos

PCR ingredients

10x PCR buffer containing 15mM $MgCl_2$ (Genecraft)

dNTPs (20mM, Genecraft)

BioThermTMDNA Polymerase (Taq, 5units / µl, Genecraft)

DMSO (Sigma)

Autoclaved H_2O

5x Soriano Buffer (SB)

Ammoniumsulphate	83mM
Tris	335mM
$MgCl_2$	33.5mM
2-ME	25mM.

Adjust pH to 8.8.

Primers for wt PCR

wt sense (100pmol /µl , MWG) 5'-GCC CAC GCC GCA GTA CCC GGA TG-3'

wt antisense (100pmol /µl , MWG)5'-GCG AGA AGG CCA CCC GAT GGG AG-3'

Primers for mutant PCR

Mutant sense (100pmol /µl, MWG) 5'-CAG CAG ACC CAG GCC CAG CG-3'

Mutant antisense (100pmol /µl, MWG) 5'-CAC CCT CAT GAT GTC CAC CAC-3'

PCR protocols for wt and mutant reactions

WT	1x reaction
SB buffer	5µl
H_2O	14.475µl
DMSO	2.5µl
dNTPs	0.625µl
wt sense primer	1µl
wt anti sense primer	1µl
Taq	0.4µl

Each reaction volume is 25µl. Add 1µl DNA template to each reaction system.

A cycling program for the genomic DNA with a 500bp amplified region is 93°C, 10min (initial denaturation); followed by 40 cycles of 93°C, 30s; 60°C, 45sec; 65°C, 1.5min; final extension 65°C, 10min; hold 4°C.

Mutant 1x reaction

10xPCR buffer (containing 1.5mM $MgCl_2$)	3µl
H_2O	25.14µl
dNTPs	0.6µl
mutant sense primer	0.48µl
mutant antisense primer	0.48µ
Taq	0.3µl

Each reaction volume is 30µl. Add 1µl DNA template to each reaction system.

A cycling program for the genomic DNA with a 550bp amplified region is 93°C, 5min (initial denaturation); followed by 30 cycles of 93°C, 50s; 55°C, 45s; 72°C, 1.5min; final extension 72°C, 10min, hold 4°C.

2.3 Agarose gel electrophoresis for DNA separation

For separation of DNA fragments of different length agarose gels were used. 1.8% agarose was chosen depending on the size of the DNA fragments. The necessary amount of agarose was boiled in 1× TAE buffer using a microwave oven. Ethidium bromide was added (final concentration 0.5µg/ml) to the boiling agarose solution. The agarose was put into a chamber for electrophoresis directly and chilled at room temperature till the gel was solidified. The chamber was then filled with 1×TAE buffer, DNA probes were mixed with sample buffer (end concentration 1×) and put into gel pockets. The left gel pocket was always filled with 5µl of 100bp DNA-ladder (Gibco) as standard. The electrophoresis was done at a voltage of 5V/cm. Due to intercalation of ethidium bromide, DNA fragments were visible as stripes under UV-light and photo pictures of gels were taken.

3 Cell culture

3.1 Removal and culturing of Leech neurons

Desheathed ganglia from freshly obtained leeches were exposed to a solution of Leibowitz-15 medium (Gibco, Germany) supplemented with gentamycin (0.1mg/ml; Merck, Germany) and glucose (4mg/ml) and containing collagenase-dispase (2mg/ml for 1; Boehringer Mannheim, Germany). After 1~1.5h at room temperature, the ganglia were washed with enzyme-free supplemental medium. Individual neurons were then removed by aspiration into a fire-polished micropipette (Dietzel, 1986). Retzius cells were identified by their positions in the ganglia and by their size (70μm in diameter). The cells were cultured at room temperature (21°C~23°C) on nonadhesive culture dishes (Falcon No.3001). The cells were transferred after 24h into culture dish (Falcon No.1008) and filled with Leibowitz medium. After settling down of the neurons, the medium was supplemented with 6% heat-inactivated fetal calf serum. Retzius cells had an initial axonal process of 100-200μm in length that sometimes bifurcated at its tip. These processes retracted overnight after the cells were plated on dishes, leaving only a stump at the cell body. Under these experimental conditions, the cells did not develop extended neuritis and were used for electrophysiological measurement at room temperature (21°C~23°C) on days 1-2 of cultures.

3.2 Preparation and culturing of chromaffin cells

Locke's solution

NaCl	154mM
KCl	5.6mM
HEPES	5.0mM
$NaHCO_3$	3.6mM
Glucose	5.6mM

Enzyme solution (papin)

DMEM (Gibco, high Glucose, Glutamax I, without Sodium-Pyruvat)	250ml
L-Cysteine (sigma)	50mg
100mM $CaCl_2$	2.5ml
50mM EDTA (Sigma)	2.5ml

Filter the solution, make aliquots into 10ml and freeze them. Before use, add 20-25 units Papin / 1ml Enzyme solution and bubble with carbogen (5% CO_2 in O_2) for 25min.

Inactivating solution

DMEM (Gibco, high Glucose, Glutamax I, without Sodium-Pyruvat)	225ml
FCS (Gibco, heat inactivated for 30min)	25ml
Trypsin Inhibitor (Sigma)	625mg
Albumin (Sigma)	625mg

Filter the solution, make aliquots into 10ml and freeze them.

Culture medium

DMEM (Gibco, high Glucose, Glutamax I, without Sodium-Pyruvat)	100ml
Pen-Strep-sol (Gibco, 10,000units/10mg/ml)	1ml
ITSX (Gibco, 100x, without Sodiumpyruvat)	1ml

Warm up the medium to 37°C before use.

The pregnant mouse was decapitated at the age of E17.5~E18.5. The abdominal cavity was opened and the uterus was taken out. Embryos were released and decapitated rapidly. Both adrenal glands of the embryo were exposed under the microscope and transferred into a drop of Locke's solution in a petri dish (Falcon 1008). Tissues around the gland were removed into Locke's solution and the capsule of the gland was opened by a sharp forceps. Next each pair of glands was transferred into another drop of enzyme solution in the same petri dish. Each pair of glands was incubated in a sterilized 15ml FALCON tube containing 200µl

enzyme solution for 40min at 37°C in the shaking water bath. 150µl inactivating-solution was added to each sample and incubated for another 10min at 37°C in the shaking water bath. The solution was sucked off and replaced with 400µl culture medium leaving the glands at bottom of the tube. The glands were gently triturated (10-30 times) until no pieces of tissues were visible in the medium. The sample solution was plated into sterilized 35mm petri dishes (Falcon 3001, 50µl / dish). The cells settled down for 15min in the incubator (37°C, 8.5%CO_2). In the end, 2ml culture medium was added to each dish and the next day the chromaffin cells were used for experiments.

4 Transfection and determination of overexpressing level of protein

4.1 Transfection of chromaffin cells with Semliki Forest virus constructs

Virus production was performed as described (Ashery *et al*., 1999).

10xPBS solution

NaCl	1.36M
KCl	25mM
KH_2PO_4	15mM
Na_2HPO_4	65mM
$CaCl_2$	5mM
$MgCl_2$	20mM.

Adjust pH to 7.4.

Culture medium

DMEM (Gibco, high Glucose, Glutamax I, without Sodium-Pyruvat)	100ml
Pen-Strep-sol (Gibco, 10,000units/10mg/ml)	1ml
ITSX (Gibco, 100x, without Sodiumpyruvat)	1ml

Warm up the medium to 37°C before use.

Chymotrypsin (Boehringer) 2mg/ml in PBS with Ca^{2+} and Mg^{2+}. Store in aliquots

at -20°C.

Aprotinin (Boehringer) 6mg/ml in PBS with Ca^{2+} and Mg^{2+}. Store in aliquots at -20°C.

An aliquot of frozen virus (450µl) was thawed and 450µl of DMEM medium without ITSX were added. To activate the virus, 100µl of chymotrypsin were added and incubated for 30-50 min at 37°C. Then, 100µl of aprotinin were added to inactivate chymotrypsin and incubated for 3-5 min at room temperature. 1ml medium was sucked out from each 35mm plate and 120-150µl of the activated virus was added. After incubation for 1h at 37°C, the virus-containing medium was replaced with 1ml of conditioned medium. After 6~7h the expression level was optimum for the experiments. Initial GFP detection was performed with an inverted microscope (Zeiss Axiovert 100, Oberkochen, Germany) using a GFP filter set.

Immunofluorescence on chromaffin cells

Freshly prepared transfected $syb2^{-/-}$ and $syb2^{+/+}$ chromaffin cells in 35mm plastic plates were fixed for 20-30 min at room temperature with 4% PFA in PBS, and washed three times in PBS for 10 min each, followed by blocking in PBS containing 6% BSA for 1 h. They were then incubated with primary antibody diluted 1:500 for 1hr (mouse monoclonal antibody against syb2, 69.1, Synaptic System, Göttingen). Samples were washed 5 times in PBS for 10 min each, followed by 1h incubation with the secondary antibody (Cy3-coupled goat-anti-mouse; Dianova, Hamburg, Germany) diluted 1:1000 in PBS. After washing three times in PBS for 10 min each, samples were mounted into a special mounting medium under the coverslips and left at room temperature to solidify the mounting medium. Circumference of the coverslip was sealed by nail polish to prevent drying out. Samples were analyzed under the fluorescence microscope.

Fluorescence microscopy

Samples were analyzed using either a Zeiss Axiophot 2 or a Zeiss Axiovert 100TV fluorescence microscope with a 100X1.4 NA plan achromate objective. For imaging I used either a front-illuminated slow-scan CCD-camera (1317X1035 Kodak chip, 6.8X6.8 μm pixel size; Princeton Instruments Inc.) or a back-illuminated frame transfer CCD-camera (2X512X512-EEV chip, 13X13 μm pixel size; Princeton Instruments Inc.) with a magnifying lens (1.6Xoptovar). EGFP fluorescence was detected using Zeiss filter set 10 (excitation filter BP 450-490, BS 510, emission filter BP 515-565); for Cy3-flurescence Zeiss filter set 15 was used (excitation filter BP 540-552, BS 580, emission LP 590). Images were analyzed with Metamorph (Universal Imaging Corporation, West Chester, PA).

5 Protein biochemistry

10×TBS

Tris-HCl	200mM, pH 7.5
NaCl	1.5M

Blotto

TBS 1 ×

Tween-20	0.1%
fat free milk powder	5%

Stacking buffer

Tris	0.5 M, pH 6.8
SDS	0.4%

Separating buffer

Tris	1.5 M, pH 8.8
SDS	0.4%

Composition of separating gel of 13% polyacrylamide (for two gels)

DH_2O	2.95ml
Separating buffer	2.5ml
30/0.8% polyacrylamid	4.33ml
TEMED	5µl
10% APS	250µl

Composition of stacking gel of 3.75% polyacrylamide (for two gels)

DH_2O	3.07ml
stacking buffer	1.25ml
30/0.8% polyacrylamid	0.625ml
TEMED	5µl
10% APS	50µl

5.1 Preparation of tissue homogenates

The brain samples and adrenal glands of mice were removed from the animal bodies rapidly. Samples were homogenized in the 1× TBS containing 2% Triton (Merck) at 4°C.

5.2 Determination of protein concentration using Bradford reagent

Bradford reagent 4× (BIORAD, München)

The Bradford reagent was diluted 1:4 and stored at 4°C before usage. 2µl tissue homogenate was adjusted to a volume of 200µl. A solution of BSA protein (1mg/ml) was used as standard. 1µl, 2µl, 3µl, 4µl, 5µl of BSA protein solution was pipetted and the volumes were adjusted to 200µl. The reaction was started in the protein standards and in the samples by addition of 800µl BIORAD reagent. The extinction at λ=595nm was measured at room temperature. A curve was plotted from the standard values and the protein concentrations in the samples were calculated from that curve.

5.3 SDS-polyacrylamide-gel electrophoresis (SDS-PAGE) of proteins

Separation of protein mixes was done using discontinuous SDS-polyacrylamide-gel electrophoresis.

Electrophoresis was done always in vertical directed glass plates (the size of glass plates is: 10×7cm, 1mm spacer). Glass plates were put together with spacers between and hermetically sealed by the pad. Freshly mixed separating gel was poured between plates and 1ml H_2O was put on the top. After 45 minutes of polymerization at RT, H_2O was sucked out, stacking gel was poured and a comb was inserted. After 30 minutes of polymerization, the comb was removed and the gel pockets were filled with 1X running buffer for electrophoresis. Protein probes were adjusted to the same protein concentrations and mixed with 5X sample buffer, denatured for 5 minutes at 95°C, centrifuged for 1 minute at 13000 rpm at room temperature. 10~20 μg of protein probe was loaded into each gel lane. Electrophoresis was run at 25mA for 1~1.5 h.

5.4 Semi-dry protein transfer (western-blotting)

4 pieces of GB 005 gel-blotting-paper (Schleicher & Schuell, Germany) and nitrocellulose transfer membrane (Schleicher & Schuell, Germany) were cut out in a size of the gel and soaked in semi-dry buffer just before usage. After SDS-PAGE, the stacking gel was removed and the resolving gel was soaked in the semi-dry buffer shortly, before placing it onto the membrane. Gel-blotting-paper was placed directly onto an electrode surface (2 layers), then the nitrocellulose membrane was placed on the top the paper. The gel surface was covered again with 2 layers of wet gel-blotting-paper and the air bubbles were removed. A second electrode was put onto the top of the unit so the device was fully assembled and then connected to a power supply. The transfer followed from cathode to anode for 45 minutes at 50mA/gel. The efficiency of the transfer was controlled using Ponceau solution that stained the protein bands on membranes. The membrane was soaked in the solution for 5 minutes and rinsed with water till

an excess of Ponceau was removed. The membrane was used for coupling.

5.5 Antibody-staining and enhanced chemiluminiscent (ECL) assay for protein detection

The protein of interest was identified via interaction with a mouse or rabbit antibody specific to that protein (*e.g.* syb2, 1:1000; syntaxin, 1:1000; snap-25, 1:1000), which was detected by goat-HRP conjugated antibody directed against either mouse or rabbit IgG.

A protein-blot was washed in water till the Ponceau disappeared and blocked in blotto for 1h at room temperature. The desired primary antibody was diluted in blotto and the blot was put into this solution. The blot was then incubated overnight at 4°C, followed by washing three times in TBS-Tween for 15 minutes each. The membrane was incubated again for 1h with anti-mouse or anti-rabbit secondary antibody diluted in blotto at room temperature. Finally the membrane was washed with TBS-Tween three times for 15 minutes each at room temperature. The membrane was put into SuperSignal mixture and incubated for 2 minutes with shaking at room temperature. The membrane was then exposed to KODAK film or luminescent image analyzer for different exposure times, depending on signal intensity.

6 Electrophysiology

Commercial carbon fiber electrodes (CFE) were used (ALA Scientific Instruments, Inc. USA). Amperometric currents were recorded with a List EPC-7 amplifier (Heka Electronics, Lambrecht, Germany) with output range of ± 10 V. The reference electrode, which is connected to the ground, is a silver/silver chloride pellet and is placed in the bath. The CFE is connected to input of the amplifier and has a holding potential of +650 mV versus reference electrode. The tip-refreshing of the carbon fiber is done by the technique developed in the lab of Professor Bruns. The tip of the CFE is partially inserted into a glass pipette tip with inner diameter of 8-10μm and broken by the edge of a small piece of

platinum blade (3×5mm) against which the CFE is gently pressed (*Fig 1*). Normally, after such breaking-treatment, the tip of CFE has a very even surface and a good signal to noise ratio during the measurements. Transsected tip is examined for irregularities at 800 × magnification (Olympus ULWD CD Plan 40 × objective) on the stage of a microforge (Narishige, MF-90, Tokyo, Japan) and is re-broken if the exposed CFE surface is visibly uneven.

For the measurements in Retzius cells, the actual membrane potential is recorded with an additional glass microelectrode penetrating the soma of the Retzius cell. The microelectrode (borosilicate glass, GC150F10, Clark Electromedical Instruments) is connected to a conventional bridge amplifier. Microelectrodes are back filled with 3M KCl and have resistances ranging from 30 to 50 MΩ. Experiments are performed on the stage of an inverted microscope (Zeiss Axiovert 100, Oberkochen, Germany), which is mounted on a vibration-isolated table. For the positioning of the CFE and the glass microelectrode, the custom-made micromanipulators are used. Amperometric signals are filtered in two steps with EPC-7 and a pre-amplifier (Retzius cells, 10 kHz plus 10 kHz; chromaffin cell, 10 kHz plus 3 kHz, 8-pole, Bessel) and are acquired by 12 bit ADC, and are stored on a personal computer. Afterwards, signals are again digitally filtered at 3 kHz. The sampling interval is adjusted according to the cell types (Retzius cells, 10~20 μs; chromaffin cell, 40 μs). For data collection and evaluation, the programs pClamp6 (Axon Instruments, Foster City, CA) and Autesw (NPI Electronics, Tamm, Germany) are used. Amperometric signals are analysed with an AutesW-based customized event detection routine (written by Bruns). Current transients that exceed the average baseline noise by 4 standard deviations are selected. External solution is delivered from a multichannel perfusion pipette placed ~340μm from the cell. Change of superfusion solutions is accomplished by triggered electromagnetic valves (The Lee Co., Westbrook, CT). The slow solution exchange (time constant, 600-800 ms; Bruns *et al*., 2000), as determined by tip potential measurements with a microelectrode placed at a distance of 2-10μm from the cell, does not affect the charge integral of the amperometric signal

measured over a time period of 40ms. The external saline contained (in mM): 130 NaCl, 4 KCL, 2 $CaCl_2$, 48 Glucose and 10 HEPES-NaOH (pH 7.3); high potassium saline contained (in mM): 50 NaCl, 84 KCL, 2 $CaCl_2$, 48 Glucose and 10 HEPES-NaOH (pH 7.3)

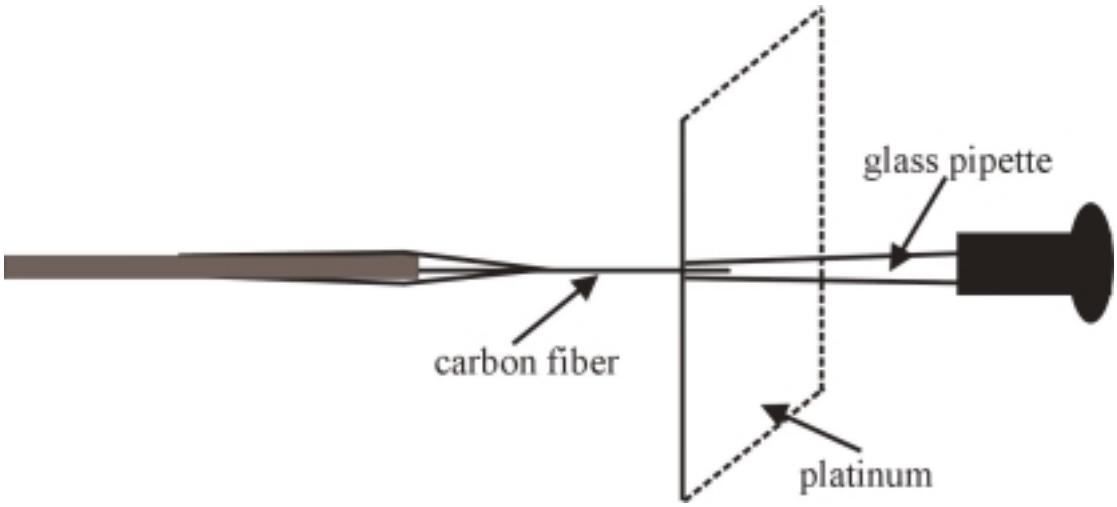

Figure 1. A schematic view of the set up for breaking CFE.

1 The aim of the first project

Synaptic transmission is a highly regulated function of the nervous system. Nerve cells communicate with each other or with muscle cells by regulated exocytosis of neurotransmitter-containing synaptic vesicles. It is generally acknowledged that the kinetics of transmitter release from large dense core vesicles (LDCVs) is slower than that from small synaptic vesicles (SSVs) and it is not instantaneous. Compared to LDCVs, SSVs have very rapid kinetics of release process, which is very important for the signaling between neurons in the brain. Two principal hypotheses concerning the process of neurotransmitter release have been proposed. First, the exocytosis of SSVs is so rapid that the real time course of transmitter release can be negligible therefore the release process can be treated as an instantaneous event. The second hypothesis proposes that the release process is not as fast as expected and needs certain time to proceed which leads to a series of important physiological consequences, *e.g.*, the discharging time of neurotransmitter can modify the concentration profile of the transmitter molecules in the synaptic cleft which probably prevent the saturation of postsynaptic receptors binding neurotransmitters.

The controversy still remains about whether the release process of SSVs is instantaneous or non-instantaneous. Due to the small size and fast release process of SSVs, the study of the real time course of transmitter release is technically difficult. So far the real time course of transmitter discharge of SSVs has not been exactly measured.

In this thesis, one of my aims is to study the real time course of neurotransmitter release from SSVs. I also investigate the temperature effect on the release kinetics of SSVs. Furthermore, a model for the mechanism underlying the release dynamics is developed.

2. Real Time Course of Transmitter Release From Small Synaptic Vesicles (SSVs) and Large Dense Core Vesicles (LDCVs)

2.1. "Classical" amperometric recordings of SSV release events: real or artificial?

Small synaptic vesicles show very rapid transmitter discharge after the opening of fusion pore, making the analysis of the real time course of transmitter release technically difficult. "Classical" individual amperometric recordings of SSVs (*Fig. 1*) show very fast kinetics with half-width (the duration of current transient at half- height of its peak amplitude) and 50-90% rise time (the time span between 50% and 90% amplitude) about 250μs and 45μs, respectively. When measuring biophysical events of such fast kinetics, the questions that arise are: Is the release of the entire contents of the vesicle instantaneous and the kinetics of amperometric events simply governed by diffusion? If the release is non-instantaneous, how fast does it occur and what is the mechanism responsible for such rapid process?

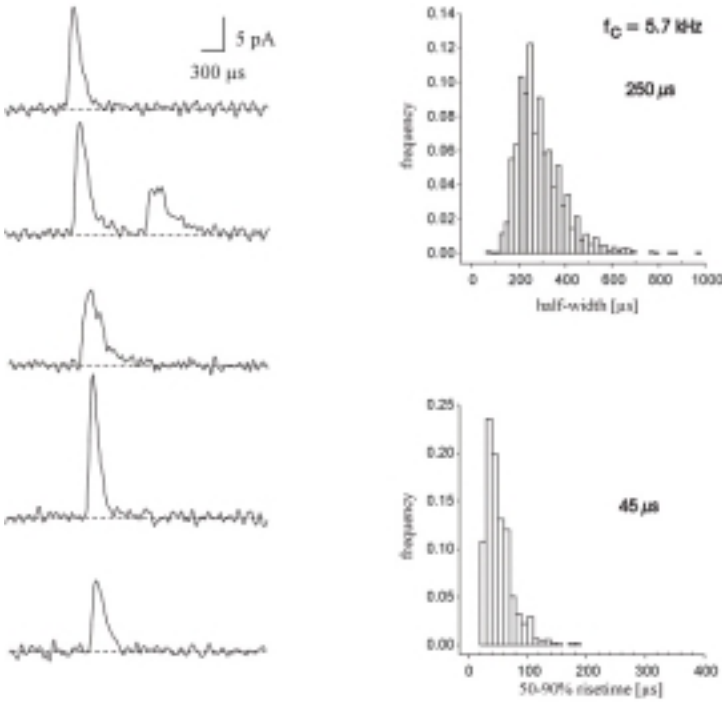

Figure 1. Kinetics of transmitter discharge from SSVs in Retzius cells of the leech Hirudo medicinalis (reproduced from Prof. Bruns)

Left side, example recordings of amperometric measurements of SSVs, transient currents were filtered with 5.7 kHz. Right side, frequency distributions of half-width and of 50-90% rise time for SSV events. Number indicates the median values of 250µs and 45µs of half-width and 50-90% rise time, respectively.

2.2 An experimental approach to the real time course of SSV and LDCV events

I decided to approach these questions on the basis of current knowledge of the variables affecting current signals. I know that amperometric current signals for single vesicles reflect the time courses of transmitter release and the diffusion from the transmitter release site to the detector (Chow and von Rüden, 1995).

[1] signal (measured) = diffusional broadening + real time course

For the half-width, it follows

[2] $HW_{signal} = HW_{diffusion} + HW_{real}$

The problem is that, while I can experimentally measure the first term of the equation (signal), I cannot distinguish between the contributions of the two components of diffusion and real time course. I reasoned that, by obtaining amperometric recordings in two experimental situations with different diffusion coefficients, I would be able to reformulate in these terms

[3] $HW_A = (HW_B - HW_{real}) \times K + HW_{real}$

where HW_A is the HW determined in the experiment with diffusion coefficient A, HW_B is the HW determined in another experiment with diffusion coefficient B, HW_{real} is the HW of the real time course, and K is the ratio of diffusion coefficient B versus A. Equation *[3]* has over equation *[1]* the advantage that only one of the variables cannot be measured experimentally, namely HW_{real}. In this way, the problem would be reduced to setting up recordings in two different diffusion conditions, and then applying the experimental data so obtained to solve equation *[3]* for HW_{real}.

Of course the standard experimental conditions using Ringer's solution can be used to obtain HW_B. To determine HW_A, I have to find different, non-standard experimental conditions with different diffusion coefficient.

2.3 The diffusion coefficient of transmitter molecules decreases by a factor of 1.5 in the presence of Dextran molecules

It is well known that the addition of Dextran molecules is suitable to slow down the diffusion of transmitter molecules. I decided to set up amperometric recordings in which the carbon fiber electrode was bathed with a Ringer-Dextran solution and the diffusion coefficient of transmitter molecules can be measured in the presence of Dextran (MW 40,000).

Dopamine is one intensively studied neurotransmitter and is readily oxidizable. Controlled release of dopamine with a concentration of 500mM from an iontophoretic pipette with a high resistance of 100 MΩ was obtained by positive current-pulses (pulse duration was 10 ms and pulse amplitude was 99 nA), which ejected the positively charged dopamine molecules out of the tip of the pipette. In the interval between the pulses, the leakage of dopamine from the pipette was stopped by a negative holding current. The iontophoretic pipette tip was kept always in the same position, and the distance between the pipette tip and detector was adjusted by moving the tip of carbon fiber. A constant overpotential of 650 mV was applied to the carbon fiber. The oxidation currents were recorded at different distances between the source (discharging place) of dopamine molecules and the detecting surface of the carbon fiber (*Fig. 2B*). The relationship between diffusion-based signals and the path over which the molecules must diffuse is given by the Einstein-Smolochowski equation for three-dimensional diffusion

[4] $$r^2 = 6 \times D \times t$$

where r^2 is the squared distance between the tip of the dopamine-releasing pipette and the tip of the detecting carbon fiber; D is the diffusion coefficient, and t is the

time to peak (the duration from onset to peak of the amperometric signal), showing that the time (t) for a diffusing particle to travel some distance (r) is proportional to the square of the distance.

As shown in *Fig. 2C*, the signal (green) recorded in Ringer-Dextran solution showed a longer time to peak and lower peak amplitude than that (red) recorded in Ringer's solution, indicating that the signal kinetics was slowed down by the introduction of Dextran molecules. The values of square of distance (r^2) were plotted against the corresponding values of time to peak, and the combined sets of data were fitted with a linear regression that had slopes of 3.8 and 2.5, with respect to Ringer and Ringer-Dextran conditions, thus the ratio of $slope_{Ringer}$ / $slope_{Dextran}$ is 1.5 (*Fig. 2A*). Since the slope is equal to 6 × D, the ratio of D_{Ringer} / D_{Dex} should also be 1.5. After the calculation, the diffusion coefficient (D_{Ringer}) of dopamine in the Ringer's solution was $6.4\times10^{6}cm^{2}sec^{-1}$and the diffusion coefficient ($D_{Dextran}$) of dopamine in the 9.2% Dextran solution was $4.3x10^{-6}$ cm^{2} sec^{-1}. So the diffusion coefficient of transmitter molecules was slowed down by a factor of 1.5 in the presence of Dextran molecules.

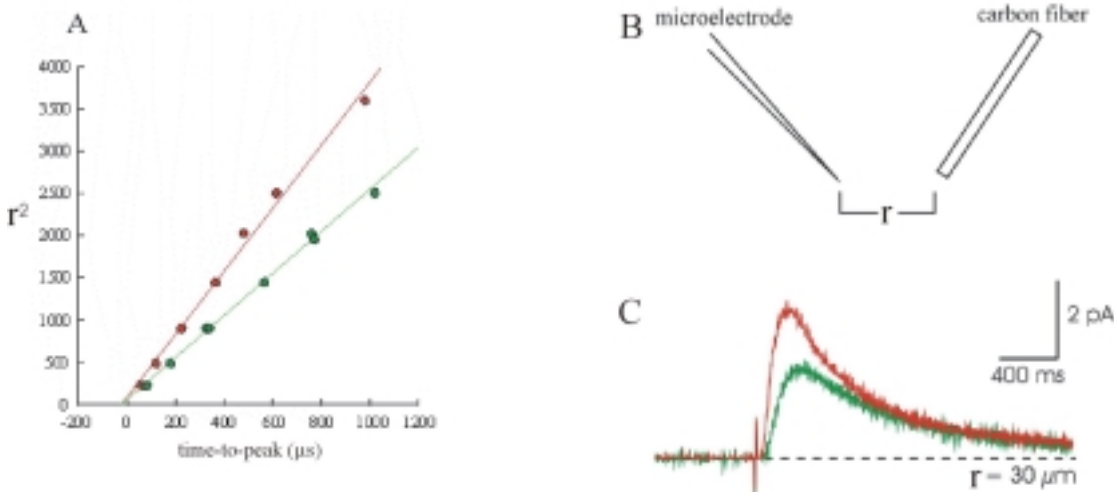

Figure 2. Dextran: a tool to slow down diffusivity of neurotransmitter molecules.

(A) The time-to-peak (µs) determined from individual dopamine spikes recorded under Ringer (red) and Ringer-Dextran (green) conditions were plotted against the square of

corresponding distance (r^2) between the source of dopamine molecules and the detecting surface of the carbon fiber.

(B) Illustration of the orientations of microelectrode and carbon fiber. Dopamine molecules are discharged from the tip of the microelectrode with controlled current-pulses. After discharging the dopamine molecules diffuse to the surface of the carbon fiber over certain distance (r) and become oxidized.

(C) Examples of oxidation currents of dopamine recorded in Ringer (red) and Ringer-Dextran (green) solutions, respectively. Note that both spikes were recorded over the same distances (30 μm), the green one showed lower amplitude and slower kinetics due to the decreased mobility of dopamine molecules in the Ringer-Dextran solution.

2.4 Monte-Carlo simulations

To test whether the approach is suitable to unmask the diffusional broadening of SSVs signals, I did Monte-Carlo simulations mimicking the conditions of real amperometric experiments. In my study, template-driven releases (SSVs and LDCVs) or the model of instantaneous release are introduced. Therefore I can easily adjudge the validity of my approach (formula *[3]*) by directly comparing the simulation results with template which is already known in advance.

2.4.1 General assumptions for Monte-Carlo simulations

I assume that vesicles underneath the cell membrane are located at the central axis of the carbon fiber where they will discharge the contents (*Fig. 3*). At the release sites, 400,000 oxidizable particles were assumed to be released instantaneously or with a time course determined by a template to mimic properties of noninstantaneous transmitter discharge from SSVs and LDCVs. Afterwards, these particles diffuse in the surrounding medium with a diffusion coefficient of 5.4×10^{-6} cm^2 / s or 3.6×10^{-6} cm^2 / s, corresponding to Ringer and Ringer-Dextran conditions, and are reflected at the cell surface and the cylindrical surface of the fiber, and are absorbed at the disc-like tip of the fiber. The amperometric signals were calculated after particles traveling various distances, ranging from 50 nm to

400 nm or to 1000 nm (increment 50 nm). The minimum step size is determined by

[4] $r^2 = 6 \times D \times t$

here r is the step size, t is the interation time. In order to keep the same step size for each calculation under Ringer and Ringer-Dextran conditions, the ratio of $t_{Dextran}$ versus t_{Ringer} was adjusted to 1.5, and in our study, the t_{Ringer} and $t_{Dextran}$ are 0.6μs and 0.9μs, respectively.

To simulate release from differentially sized SSVs and LDCVs, amplitude, charge of template were scaled proportionally to the volume of the organelle, and the frequency of such signals was adjusted to the frequency distribution of SSV and LDCV diameters at axonal sites (Bruns *et al.*, 2000).

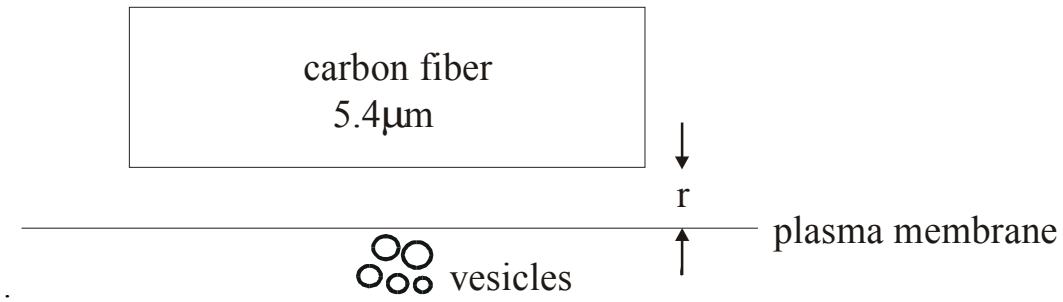

.

Figure 3. Illustration for random walk simulations.

A carbon fiber with diameter of 5.4μm is placed at varying axial distances from the cell membrane. The various cell-electrode spacing (r) increases from minimal axial distance of 50 nm to maximal value of 400 nm or 1000 nm with an increment of 50 nm. Release sites underneath the cell membrane are located at the central axis of the carbon fiber. At the release sites, 400,000 oxidizable particles were assumed to be released instantaneously or with a time course determined by a template (SSVs or LDCVs). After release, molecules diffuse to the carbon fiber in the surrounding medium with diffusion coefficients of $5.4 \times 10^{-6} cm^2/s$ and $3.6 \times 10^{-6} cm^2/s$, corresponding to Ringer and Ringer-Dextran conditions. On the surface of carbon fiber, particles are assumed to be oxidized and calculated as an amperometric spike.

2.4.2 Simulation of SSV template driven release

I performed Monte-Carlo simulations of SSV template driven release over various axial cell-electrode distances ranging from 50-400nm, based on the following "template" with the set of variables: charge integral (2.51fC), peak amplitude (10.08pA), rise time (35µs) and half-width (185µs). Events with amplitudes >3.5pA and charge integrals ranging from 0.5 to 8.0 fC, and recorded under both Ringer and Ringer-Dextran conditions, were analyzed with respect to charge, amplitude, 50-90% rise-time and half-width. I compared the parameters of HW_{Ringer} and $HW_{Dextran}$ and plotted the cumulative frequency distributions of them in *Fig. 4A*. The dashed line represented the real time course of HW from the template. The green curve indicates the calculated real time course of HW_{real} by using the formula (rewritten from *[3]*):

[5] $$HW_{Dex} = (HW_{Ringer} - HW_{real}) \times (D_{Ringer} / D_{Dex}) + HW_{real}$$

As shown in *Fig. 4A*, the calculated real time course almost exactly matched the template value, showing that if I consider axial distance with maximal value of 400nm, the calculated HW_{real} agrees well with the template. The template-driven SSV signals simulated under Ringer and Dextran conditions and the template were plotted in *Fig. 4C*.

Next I want to test whether my formula *[5]* is universally valid within all ranges of separating distances considered. I increased the maximal axial distance up to 1000 nm and executed the simulations. The events were selected with the same criteria (used for simulations with maximal axial distance of 400nm) and analyzed. The curve of cumulative frequency distribution of calculated HW_{real} didn't match the template curve but bent strongly to the right side (*Fig. 4B*).

Why did different maximal axial distances generate completely different simulation results, although I used the same formula? Is the formula *[5]* only valid within a short axial distance? Actually, the prerequisite of utilizing this formula to accurately calculate the real time course (HW_{real}) is that, the detectabilities of events simulated under both conditions must be the same, and based on this, the

formula always holds for any separating cell-electrode distances. So it is clear that the different simulation results were caused by different detectabilities of events, not by the formula itself. What's the factor that can affect the detectability of events? It is the amplitude threshold, which is introduced for selecting events beyond noise level. If events are selected with same amplitude threshold, two types of events recorded under Ringer condition will have more chances to be detected by carbon fiber than that recorded under Ringer-Dextran condition. One type of events are small but recorded over very short distances, the other type of events are big but recorded over long distances. Both types of events have small amplitudes which are on the boundary line of amplitude threshold and the number of the second type of events (big but recorded distantly) goes up with the increase of axial cell-electrode spacing. Theoretically, the different detectabilities of events (recorded under Ringer and Ringer-Dextran conditions) selected by the same amplitude threshold are all the time existing, but to different extents, depending on the separating distance considered. The shorter the distance, the smaller the differences of detectabilities, *vice versa*.

At maximal axial distance of 400 nm, the chance of events (selected by the same amplitude threshold under both Ringer and Ringer-Dextran conditions) to be detected by the carbon fiber are approximately the same, therefore the calculated curve of HW_{real} almost overlapped the curve of template. However, if the axial distance was increased up to 1000 nm, the differences of detectabilities consequently got bigger thus the formula didn't work anymore in this case.

2.4.3 Simulation of SSV instantaneous release

I also made Monte-Carlo simulations of SSV instantaneously driven release. Events with amplitudes > 3.5 pA were selected. I compared the calculated HW_{real} of events recorded over maximal distances of 400 nm and 1000 nm with the assumed real time course of '*zero*' (***Fig. 4D and 4E***). The results showed the similarity to that obtained from simulations of SSV template driven release. The

calculated HW_{real} curve of events recorded within 50-400 nm almost matched the curve of assumed real time course, '*zero*', in contrast, the curve strongly bent to the right side if the events were simulated over axial distance of 50-1000 nm.

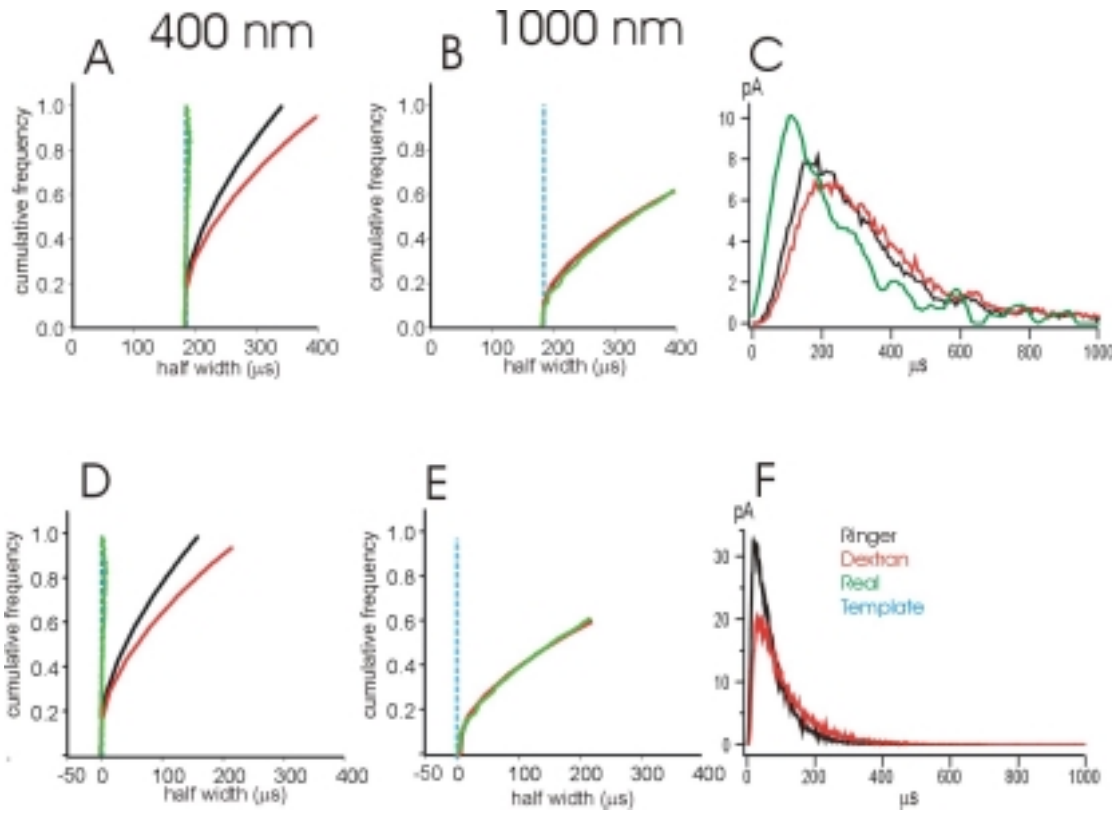

Figure 4. Kinetics of SSV signals as inferred by Monte-Carlo simulation

(A), (B) and (C) The simulations of SSV template driven release.

(A), (B) The comparisons of cumulative frequency distributions of HW_{Ringer} (black), $HW_{Dextran}$ (red), and the calculated real time course of HW_{real} (green) with the HW of template (blue, dashed line). The simulations were performed over varying axial distances and the maximal value of the distance is 400 nm (A) and 1000 nm (B). The calculated HW_{real} curve (400 nm) almost matched the template curve, but the calculated HW_{real} curve (1000 nm) strongly bent to the right side.

(C) Examples of spikes simulated under Ringer (black) and Ringer-Dextran conditions and the SSV template used in the study. Both spikes (black and red) suffered from the diffusional smearing to different extents. The diffusion had even stronger effect on the amperometric kinetics of the spike (red).

(D), (E) and (F) The simulations of SSV instantaneous release.

(D) and (E) The comparisons of cumulative frequency distributions of HW_{Ringer} (black), $HW_{Dextran}$ (red), and the calculated real time course of HW_{real} (green) with the assumed real time course of '*zero*' (blue, dashed line). The simulations were performed with the same procedures as applied to the simulations of SSV template driven release.

(F) The displaying of two spikes originating from an instantaneous release of SSV. The black and red spikes were simulated under Ringer and Ringer-Dextran conditions, respectively.

2.4.4 Simulation of LDCV template driven release

The LDCV events were also simulated on the basis of LDCV template driven release with the properties of charge integral (26.4fC), peak amplitude (16.3pA), rise time (180μs) and half width (1170μs). In the first place, the same amplitude criterion applied to SSV events and the maximal separating distance of 400 nm were introduced. The real time course was calculated by using the formula *[5]*. As shown in *Figure 5A*, the calculated curves of real time courses was very close to the template, showing that the formula can also be used for the calculation of real time course of release process of LDCVs. It could be interesting to test the validity of the formula *[5]* when the same amplitude thresholds are applied in the case of longer separating distance.

The same procedures were applied again to the LDCV simulations, except that the maximal axial distance was extent up to 1000 nm(*Fig. 5B*). The calculated HW_{real} also matched the template value, which was showing that the formula *[5]* can be valid for the calculation of LDCV HW_{real} within a broader range of cell-electrode spacings. The underlying mechanism for such enhanced tolerance to the increase of axial distance is that, the difference of detectabilities of LDCV events simulated under Ringer and Ringer-Dextran conditions dose not change significantly with the increase of separating distance due to their slower release process and larger vesicle sizes compared to the SSVs.

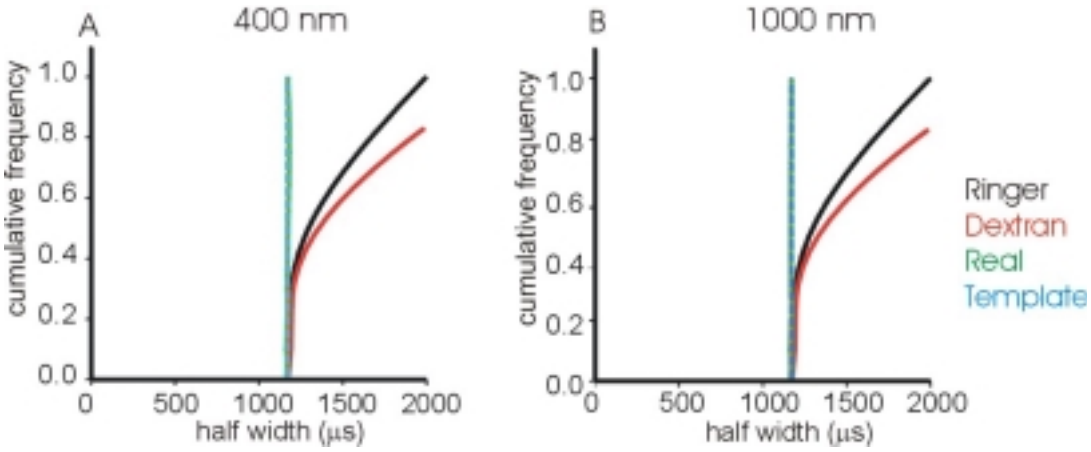

Figure 5. The comparisons of cumulative frequency distributions of HW_{Ringer} (black), $HW_{Dextran}$ (red) and calculated HW_{real} (green) with template HW. The HW_{real} curves fitted well with the template. Events were simulated over various cell-electrode distances ranging from 50-400 nm (A) and 50-1000 nm (B), respectively.

2.5 The real time course of SSVs events

Isolated Retzius cells of the leech *Hirudo medicinalis* were used to study transmitter release under amperometric recording conditions. Single Retzius cells synthesize, store and release serotonin as their only classical transmitter. To facilitate the stimulation of SSV and LDCV exocytosis, I applied the Ca^{2+} ionophore ionomycin (2μM), which should cause a long lasting and spatially uniform intracellular Ca^{2+} rise. Viability of the neurons, as judged from a normal resting potential (-50 ~ - 60 mV) and action potential wave forms, was verified in all experiments by recording the actual membrane potential with an additional microelectrode penetrating the soma of individual Retzius cells. The tip of a carbon fiber (the recording electrode) was pressed gently against the distal end of the axon stump of a single Retzius cell until a visible deformation of the cell membrane was caused. In this way, I minimized diffusional loss of released transmitter and temporal distortion of the amperometric signals.

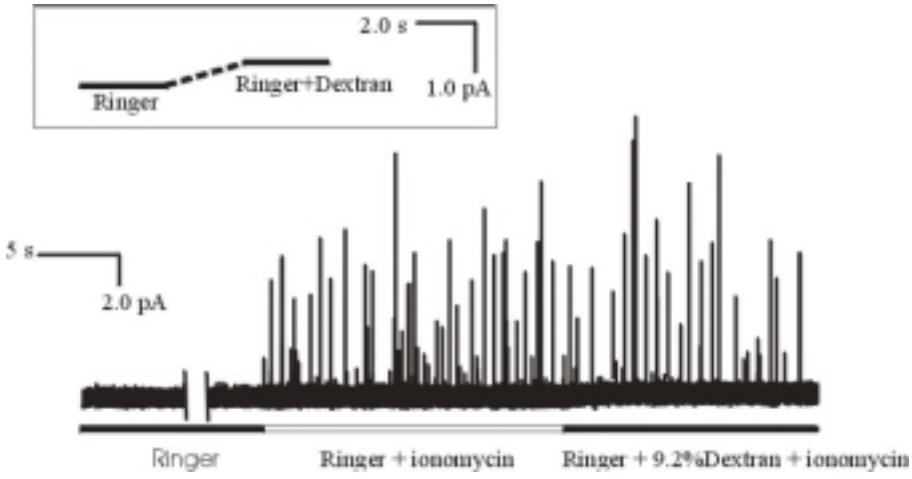

Figure 6. Amperometric events evoked by ionomycin from the vesicles at the axon stump of a Retzius cell. The amperometric spikes were evoked by ionomycin (2 μM) in Ringer (empty bar) and Ringer plus 9.2% dextran solutions (solid bar), sequentially; inset: illustration of the shift of recording baseline resulting from the continuous oxidization of Dextran molecules during the superfusion of Ringer-Dextran solution.

In order to guarantee that events are recorded over the same cell-electrode distance under Ringer and Ringer-Dextran conditions, the Ringer and Ringer-Dextran solutions, each containing 2 μM ionomycin, were superfused on the same cell alternatively. A strong increase in the frequency of amperometric spikes was induced by ionomycin (*Fig. 6)*. All the events were recorded at room temperature. As shown in *Fig. 6,* when the cells were superfused with Ringer-Dextran solution, the baseline slightly drifted up. After 2~3 s the baseline reached up to 0.5pA, then remained constant during the entire superfusion of Ringer-Dextran. When the superfusion was switched back to Ringer solution, the elevated baseline slowly came down to the normal level during 2~3 s. I assume that the shift of baseline is caused by the Dextran molecules, which are continuously oxidized on the surface of carbon fiber. In the future experiments, in order to select the events recorded in the homogenous solutions, I start counting the events 3 seconds after the change of perfusion solutions.

2.5.1 Selection of SSV recordings exhibiting short cell-electrode spacing

The results of Monte-Carlo simulations (*chapter 2.4*) show that the formula *[5]* is valid for the calculation of real time course (HW_{real}) of transmitter release provided the detectabilities of events recorded under Ringer and Ringer-Dextran are the same. This prerequisite for utilizing the formula can be achieved if cell-electrode spacing is short enough.

In order to calculate the real time course (HW_{real}) of transmitter discharge from SSVs in real experiments by using formula *[5]*, it is necessary to select recordings, which exhibits short cell-electrode spacings. The peak amplitudes of signals are strongly influenced by diffusional broadening, the higher the amplitudes, the less the diffusional broadening. The diffusional effects on the signals are dominated by the diffusion distances and therefore event amplitudes can be taken as an indicator to adjudge the cell-electrode spacings.

In the first place, I analyzed the amplitude distributions of all recordings. The data from all cells measured (n=31) showed an amplitude distribution with double peaks (*Fig. 7A*). It was clear that the first peak resulted from the setting of amplitude threshold of 3.5pA, and the second peak was around 10pA. Normally the frequency distribution of amplitudes from amperometric events decreases exponentially due to the various recording distances. Why didn't the data show a normal exponential distribution? And what was the origin of the second peak? The explanation is based on the tightly clustered distribution of SSVs in the axon stump of Retzius cells (*Fig. 8*) (Bruns *et al.*, 2000). If by chance the carbon fiber was placed on the cell membrane exactly underneath which some SSV clusters were located, the events from such clusters would be recorded over a short distance equal for all. These closely recorded events would suffer less from diffusional distortion, compared to others from distant clusters, thus they had higher amplitudes and created the second peak in the frequency distribution of amplitude. Going through individual measurements, I found that only 10 cells showed Gaussian distribution of amplitudes with a peak around 10pA and had median values of amplitudes above 7.0 pA, indicating that, in these 10 cells, the

locations of SSVs clusters were underneath the carbon fiber and for each recording the events were recorded over a short and equal distance. However, the other 21 cells exhibited exponential distribution of amplitudes as normally expected (*Fig. 7C*) and they all had median values of amplitudes below 7.0 pA, showing that most of the events were recorded from the clusters which were located distantly from the carbon fiber. The combination of all the events from the 31 cells was the cause of the double-peak distribution of amplitudes that I observed (*Fig. 7A)*.

Making clear the underlying mechanism of the Gaussian distribution of event amplitudes, I inferred that the 10 cells showing such symmetric distribution of amplitudes with the peaks around 10 pA had very short cell-electrode spacings. Therefore, I decided to select the 10 cells for the calculation of HW_{real} by using the formula *[5]*.

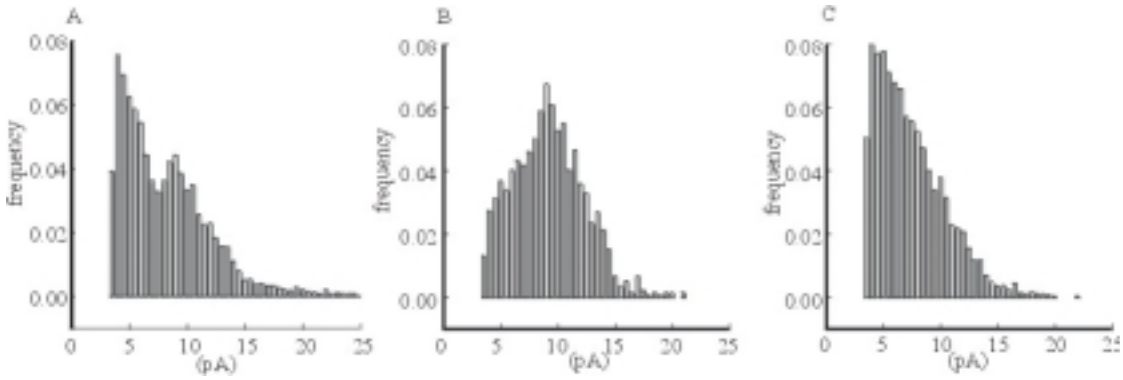

Figure 7. Frequency distributions of amplitudes of SSVs (A, B, C)

(A) Frequency distribution of events pooled from all cells (n=31) exhibited double peaks, around 3.5 and 10 pA separately. The double-peak distribution of event amplitudes implied that some events recorded from the SSV clusters located underneath the carbon fiber generated the second peak of 10 pA.

(B) Frequency distribution of amplitudes of all events pooled from 10 cells each showing nearly symmetric distribution of amplitudes with peak around 10 pA.

(C) Frequency distribution of amplitudes of all events pooled from 21 cells each showing

exponential distribution of amplitudes.

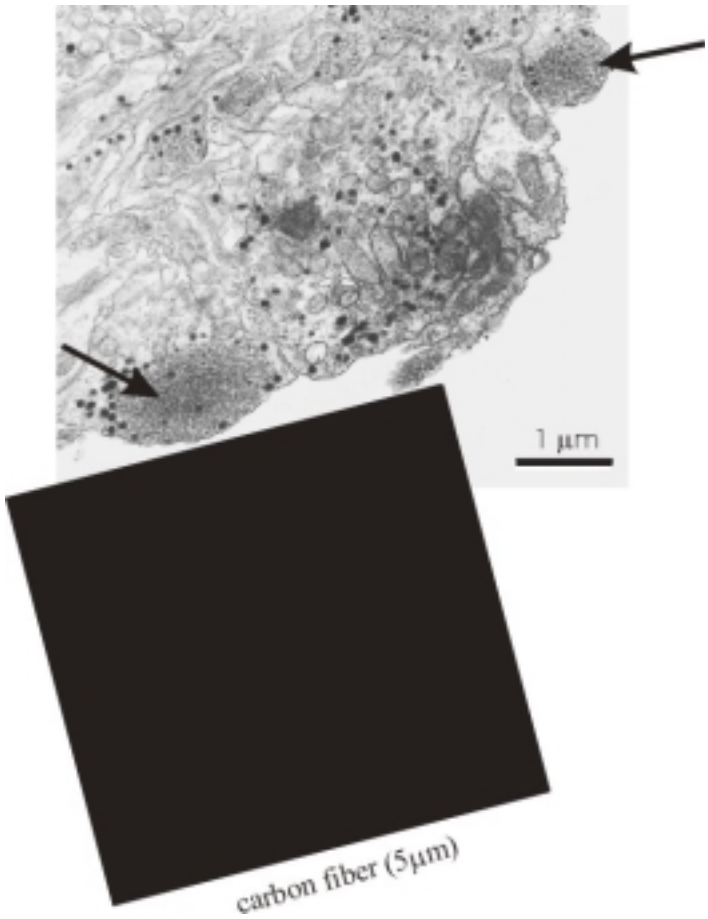

Figure 8. The positioning of carbon fiber on the plasma membrane of Retzius and the characteristics of SSVs distribution in the axon stump of Retzius cell (EM picture reproduced from Bruns, 2000). Clusters of SSVs (arrows) are found underneath the cell membrane of the axon stump. The location of clusters of SSVs very close to the plasma membrane makes the SSVs directly accessible to the carbon fiber.

2.5.2 The "fine" analysis of transmitter release of SSVs.

SSV events with amplitudes > 3.5 pA from the 10 cells (mentioned above) were selected. For each spike, I determined the charge integral, the peak amplitude and the kinetic parameters, with respect to, 50-90% rise time and half width, and plotted the cumulative frequency distributions of these parameters by pooling all the data (*Fig. 9*). The distributions of charge integral, peak amplitude determined under Ringer and Ringer-Dextran conditions were correspondingly similar. The curves of $RT_{Dextran}$ (RT, 50-90% rise time) and $HW_{Dextran}$ shifted to the right side of the curves of RT_{Ringer} and HW_{Ringer}, correspondingly, indicating that the kinetics

of events was slowed down in the presence of Dextran molecules. The curve of HW_{real} calculated by using the formula *[5]*

[5] $$HW_{Dex} = (HW_{Ringer} - HW_{real}) \times (D_{Ringer} / D_{Dex}) + HW_{real}$$

shifted to the left side of HW_{Ringer} curve but didn't go to zero, demonstrating that the process of transmitter discharge from SSVs is not instantaneous.

Surprisingly, the calculated frequency distribution of HW_{real} exhibits a significant scatter showing that release from SSVs occurs with a variable time course, which does not show in the simulation. The scatter can be attributed to the variation in the dimension of fusion pore.

Interestingly, HW distribution of fast events with rise time < 33 μs matches the calculated curve of HW_{real} (dashed curve). This is the expected consequence when under our experimental condition some events are recorded directly at the release sites. The observation also supports the accuracy of the calculation and the validity of this approach.

In order to include each cell with the same weight regardless of the number of spikes recorded, I averaged the median value of each spike parameter in each cell (*Table 1*). No noticeable difference was observed between parameters of events recorded under Ringer's and Ringer-Dextran conditions, with respect to charge and amplitude, which was consistent with the finding in the cumulative frequency distributions of these parameters. The differences between the averaged median values of HW_{Ringer} and $HW_{Dextran}$, as well as of RT_{Ringer} and $RT_{Dextran}$ were small but significant (HW_{Ringer}: 240 ± 10μs; $HW_{Dextran}$: 260 ± 15μs, $p < 0.01$ and RT_{Ringer}: 44 ± 1.7 μs; $RT_{Dextran}$: 49 ± 3.0 μs, $p < 0.05$, paired t-test). The mean value of calculated HW_{real} was 198 ± 17 μs, which was faster by 20% than HW_{Ringer}, indicating that the majority of kinetics of amperometric signals was determined by the release process.

Since in dimensionless term, given by Chow and Rueden (1995), the time to peak relates to the HW by a factor of 0.3882, the equation *[4]* can be rewritten to

[6] $r^2 = 6 \times D \times 0.3882 \times (HW_{Ringer} - HW_{Real})$.

I calculated median values of cell-electrode spacing in individual cell and averaged them; the mean value was about 194 ± 37 nm.

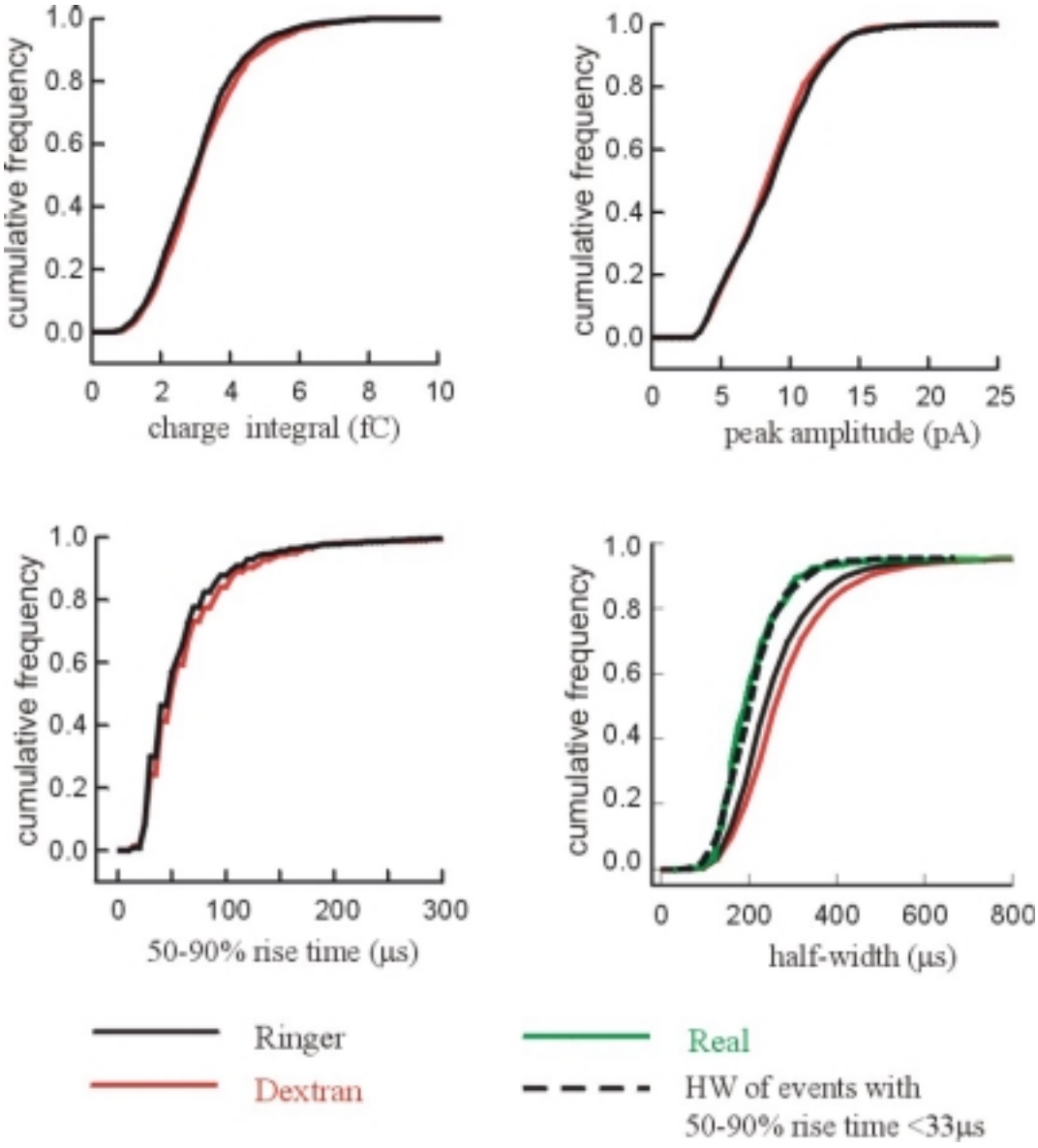

Figure 9. Comparison of cumulative frequency distributions for the charge integral, peak amplitude, 50-90% rise time and half-width of SSV events recorded under Ringer (black) and Ringer-Dextran (red) conditions. The distributions of calculated real time course of half-width (green) and half-width of fast events with rise time <33µs, recorded in Ringer solution (dashed line) are also shown. No differences between parameters of events recorded under Ringer and Ringer-Dextran conditions were observed, with respect to charge integral, peak amplitude were observed. The curves of

$RT_{Dextran}$ and $HW_{Dextran}$ shifted to the right side of the curves of RT_{Ringer} and HW_{Ringer}, showing that the kinetics of events recorded in Ringer-Dextran solution suffered more from the diffusional broadening due to the lower mobility of transmitter molecules. The curves of calculated HW_{real} and fast events (rise time < 33 μs) moved to the left side of the curves of HW_{Ringer} and $HW_{Dextran}$, and both curves almost overlapped, indicating that there were some fast events recorded almost without diffusional slowing and their time courses measured in reality already reflected the real time course of release process.

Table1 Properties of SSV events recorded under Ringer and Ringer-Dextran conditions

	events/cell	charge (fC)	amplitude (pA)	rise time (μsec)	halfwidth (μsec)
Ringer (10 cells)	136 ± 29	2.8 ± 0.13	8.6 ± 0.39	44 ± 1.7	240 ± 10
Dextran (10 cells)	115 ± 34	2.9 ± 0.18	8.5 ± 0.53	49 ± 3.0	260 ± 15

Measurements are given as mean ± SEM of median values determined for the individual cells.

2.5.3 Dextran molecules unmask variable cell-electrode spacings

It is conceivable that SSVs exocytosis occurs locally. Based on this, we would expect that SSVs exocytosis is restricted to certain release site and that the cell-electrode distance is not constant. Application of Dextran should be suitable to uncover the various spacings between the electrode surface and the release site when individual recordings are compared.

I plotted the median values of HW_{Ringer} against the diffusional broadening ($HW_{Ringer} - HW_{real}$) on the left ordinate from corresponding cells (*Fig. 10A*). The data set was reasonably well approximated by a linear regression with a correlation factor of 0.8. Furthermore, the cell-electrode distances corresponding

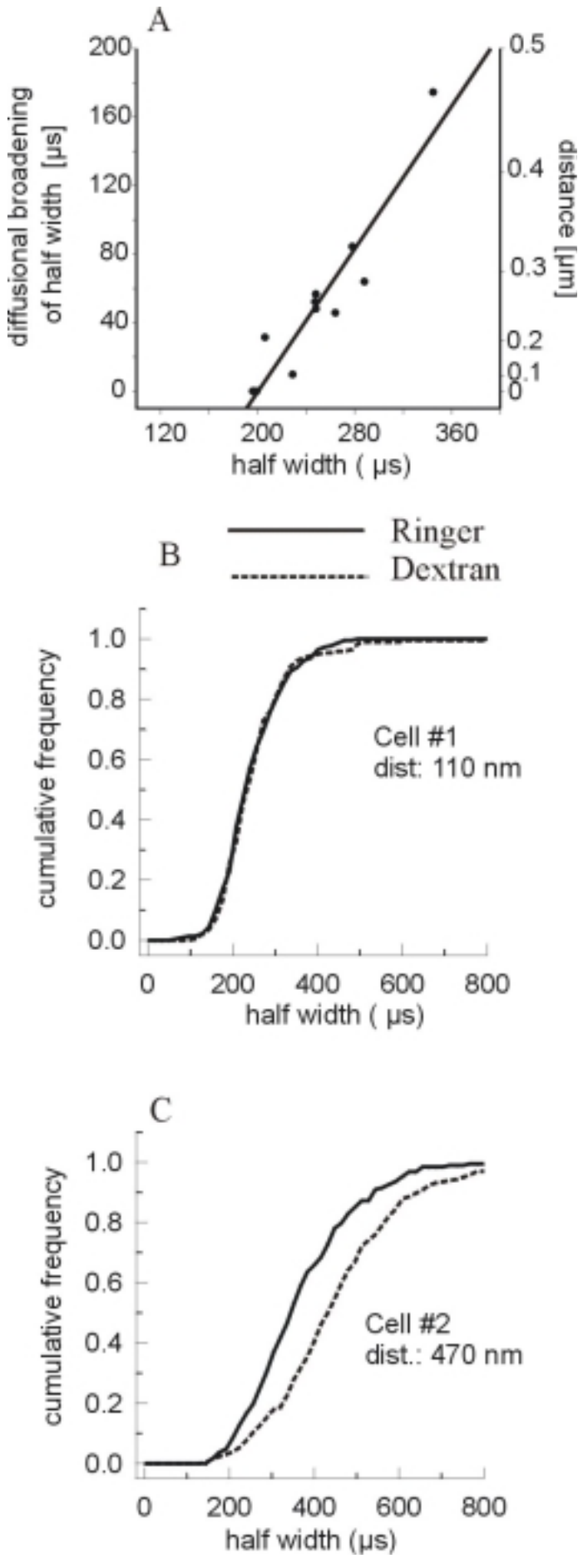
A
diffusional broadening of half width [µs]
distance [µm]
half width (µs)
B
Ringer
Dextran
cumulative frequency
Cell #1
dist: 110 nm
half width (µs)
C
cumulative frequency
Cell #2
dist.: 470 nm
half width (µs)

Figure 10. Dextran molecules reveal the various cell-electrode spacings.

(A) The half-width of events (from the 10 cells mentioned above) recorded in Ringer solution were plotted against the diffusional broadening of half-width (left ordinate, HW_{Ringer}-HW_{Real}) and the cell-electrode distances calculated from corresponding cells. The data in the plot were fitted with a linear regression (red and straight line) with a correlation coefficient of 0.8, strongly indicating that the diffusional effects on the kinetics of amperometric events increases with the widening of the gap between cell and electrode.

(B) and (C) Two example cells (from the 10 cells) were selected with the shortest cell-electrode distance of 110 nm, (C) cell#1, and with the longest cell-electrode distance of 470 nm, (D) cell#2. The cumulative frequency distributions of HW_{Ringer} and $HW_{Dextran}$ from both cells were plotted. Almost no difference was observed between the two curves of HW_{Ringer} and $HW_{Dextran}$ in cell#1 due to the short separating distance, however, a big gap existed between the two curves in cell#2 resulting from the long separating distance.

to values ($HW_{Ringer} - HW_{real}$) on the left ordinate were calculated by formula *[6]* and were shown on the right ordinate. *Fig. 10A* reveals the relationship between diffusional broadening of amperometric events kinetics and the distances, the longer the path which the particles have to travel, the stronger the diffusion effect.

Two extreme cases are presented in *Fig. 10B and 10C*. For cell#1, most of the events were recorded over only 110nm and there was no noticeable difference observed between two cumulative frequency curves of HW_{Ringer} and $HW_{Dextran}$ (*Fig. 10B*). When the distance was up to 470nm, as shown in cell#2 (*Fig. 10C*) , both curves shifted to the right side compared to cell#1, and the difference of median values between two curves was about 30μs, indicating that the effect of the Ringer-Dextran on the diffusion of molecules was aggravated over distance.

2.5.4 The Real time course of transmitter release of LDCV events

LDCVs are loosely and randomly located within the entire cell without exhibiting LDCV clusters underneath the cell membrane (*Fig. 11B*, Bruns, *et al.*, 2000). Due

to the different spatial organizations of SSVs and LDCVs, no subpopulation of LDCV events can be expected to be recorded very close to the release sites. This expectation was confirmed by the frequency distribution of peak amplitude of LDCVs events from all cells measured (n = 31). The amplitude distribution of LDCVs decreased exponentially (*Fig. 11A*), showing that all the events were recorded over long and various cell-electrode spacings. Under such LDCV situations, is it possible to calculate the real time course of HW_{real} by using formula *[5]*, if I applied the same amplitude threshold to select events as I did for SSV events?

There are three reasons which support me to calculate the HW_{real} of LDCVs by utilizing the formula *[5]*. Firstly, the simulation results of LDCVs (*paragraph 2.4.4*) shows that the formula *[5]* remains valid within a broader range of axial distance (~1000 nm) and over such long distance, the calculated HW_{real} matches well the template; secondly, in the real experimental situations, such wide gap of 1000 nm between cell and electrode surface can be visualized under the microscope and is definitely prevented by positioning the carbon fiber on the cell surface with slight deformation of the membrane; thirdly, over various radial distances, the diffusional broadening of the kinetics of LDCV events is less than 8.6% (Bruns, *et al.*, 2000). Based on these three reasons, LDCV events were selected with amplitudes > 3.5 pA and charge > 8.0 fC (Bruns, *et al.*, 2000). I determined the median values of each parameters of events recorded under Ringer and Ringer-Dextran conditions, with respect to charge, peak amplitude, 50-90% rise time and half width (Ringer: n = 1038, charge 27.9 fC, peak amplitude 12.5 pA, 50~90% rise time 203 µs, half-width 1198 µs; Dextran: n = 828, charge 28.9 fC, peak amplitude 11.8 pA, 50~90% rise time 249 µs, half-width 1235 µs). The calculated real time course of HW_{real} was 1133µs. The separating distance calculated was about 240nm, which was reasonably longer than the value of 194 nm determined from the 10 cells exhibiting short cell-electrode spacings (*paragraph 2.5.2*). The frequency and the cumulative frequency distributions of

HW_{Ringer} (black), $HW_{Dextran}$ (red) and HW_{Real} (green) were plotted in *Fig. 11C* and *Fig.11D*, respectively.

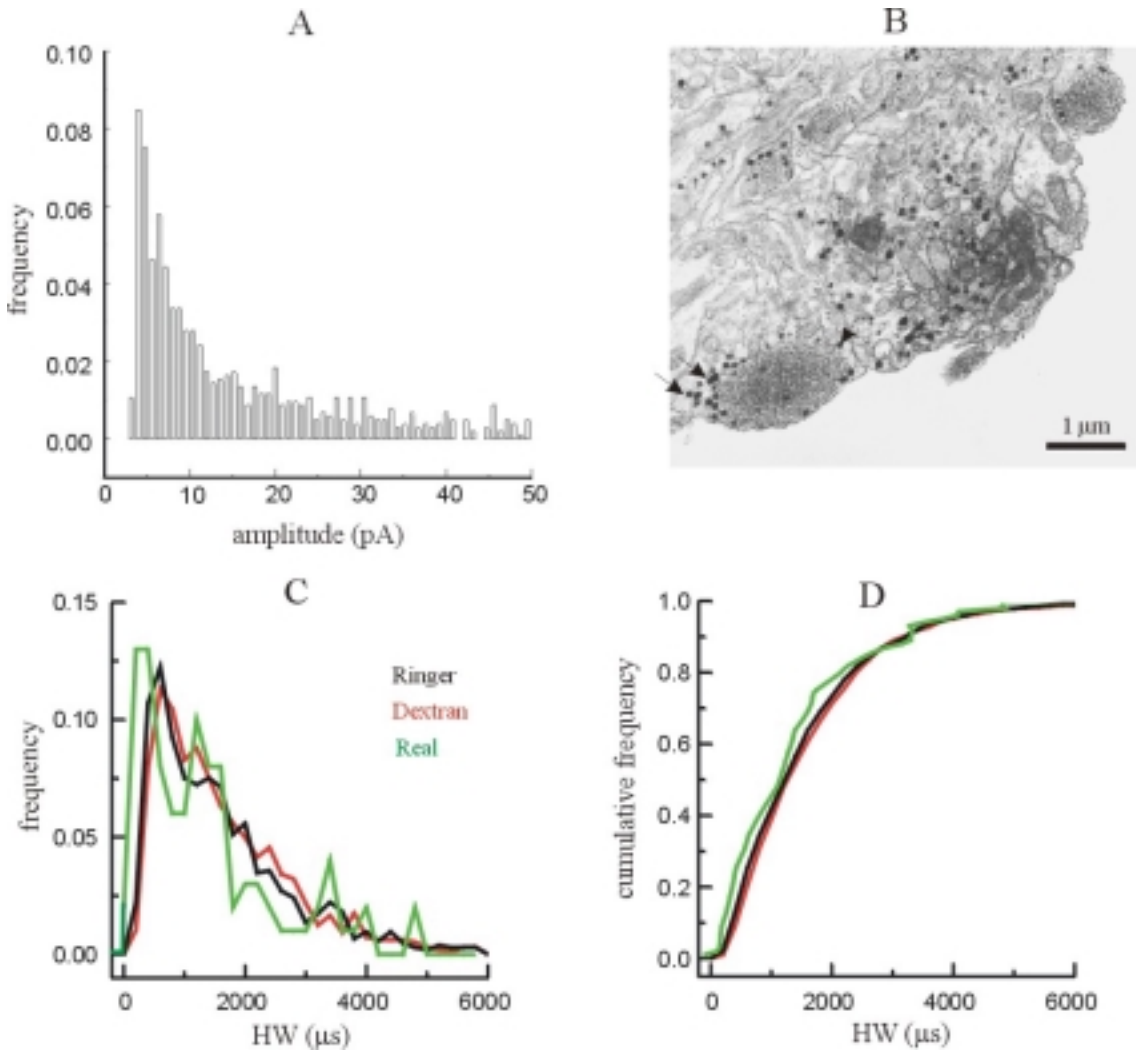

Figure11. Dextran molecules reveal the real time course of transmitter release of LDCVs.

(A) The frequency distribution of amplitudes of LDCV events (pooled from all cells, n = 31) decreases exponentially, indicating that all events were recorded over varying distances from the carbon fiber.

(B) LDCVs (arrows) are located around SSV clusters (EM picture reproduced from Bruns, 2000).

(C) , (D) Frequency and cumulative frequency distributions of HW_{Ringer} (black) and $HW_{Dextran}$ (red) of LDCV events (pooled from all cells, n = 31) and calculated HW_{real} (green).

3. Effects of the Temperature on the SSV Release Process

The previous data demonstrate that the release of SSVs is not instantaneous and it lasts about 198 μs. To illustrate the underlying mechanism for the release process, I next study the effects of temperature on the real time course of SSVs transmitter release?

3.1 Temperature effects on the transmitter release

3.1.1 The setup to perform the rapid temperature jump during the recording on the same cell

In order to change the temperature on the same cell, a customized set up was used for rapid temperature change. A schematic view of this equipment is shown in *Figure 12*.

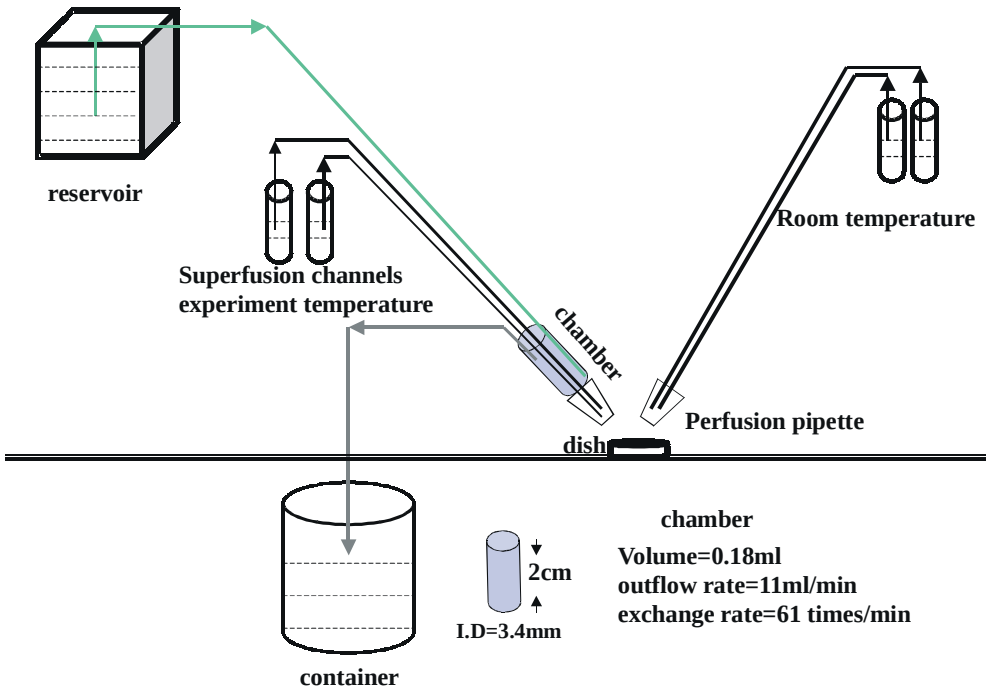

Figure12. Diagram of customized setup for temperature changing.

A small cylinder was used as a heat exchange chamber. The inner diameter, the length, and the volume of the chamber are 3.4 mm, 2 cm and 1.8 ml, respectively.

The chamber was filled with water as medium of heat exchange. The source of this water was a heat-insulated reservoir placed above the chamber. The water temperature inside the chamber was adjusted to the experimental temperature by setting the water temperature in the reservoir. The experimental temperature of water inside the chamber remained constant by continuous inflow and outflow of the water through the chamber, and the water inside the chamber was renewed at the rate of 61 times per minute. Therefore, the experimental temperature of the stimulation solution in the superfusion channel was achieved inside the chamber.

The local temperature-changing rate was determined. A temperature sensor with a diameter of 33μm was positioned at the bottom of a 35mm Petri dish to measure the local temperature. Two perfusion pipettes with diameter of 375μm were placed from both side of the sensor at the height of ~490μm from the bottom of dish. Perfusion solutions at test and room temperature flowed out from the two pipettes separately, and temperature changes were measured by the sensor. It took ~2.4 seconds for a complete temperature change (*Fig. 13*).

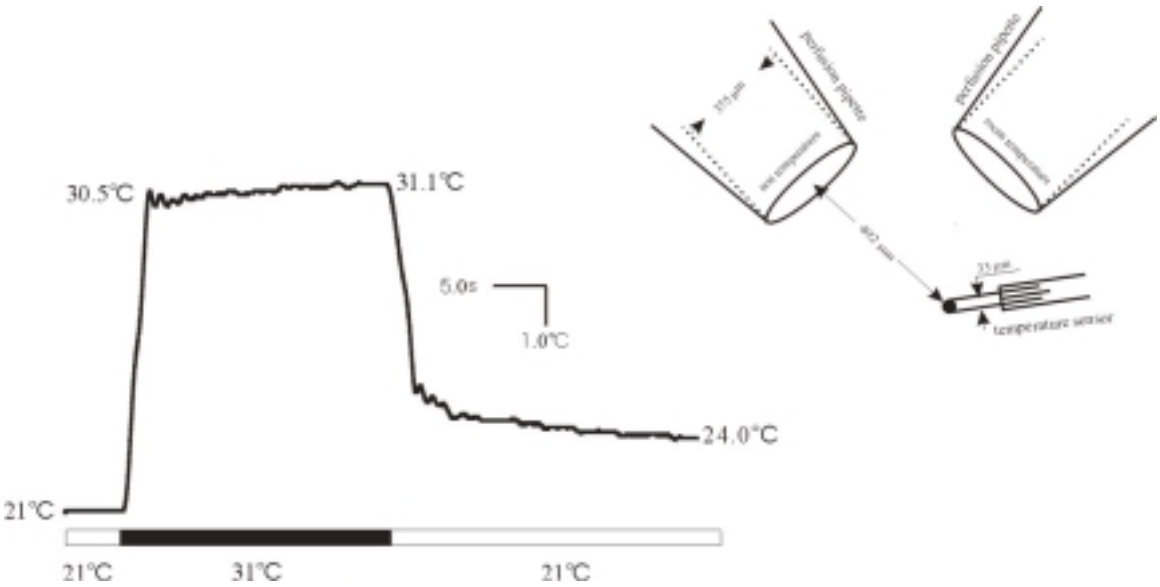

Figure 13. Local temperature at the center of 35mm petri dish can be changed rapidly by using the customized setup. Right-up corner, the spatial positioning of perfusion pipettes and temperature sensor; Left side, the trace of temperature change over the time, as shown, more than 95% of the temperature change was achieved within 2.4s.

3.1.2 Temperature effects on the transmitter diffusion

Equipped with this set up for rapid temperature change, I studied the temperature dependence of transmitter diffusion. A carbon fiber was superfused with 20 μM Dopamine at different test temperatures. The amplitudes of oxidation currents recorded at each test temperature were determined and averaged *(Fig. 14*)

for 21°C an amplitude of 61 ± 2.5 pA

for 13°C an amplitude of 53 ± 2.2 pA

for 31°C an amplitude of 66 ± 3.1 pA

I calculated the Q_{10} according to

$$A_{(13℃)} = A_{(21℃)} \times Q_{10}^{(13℃-21℃)/10}$$

or

$$A_{(31℃)} = A_{(21℃)} \times Q_{10}^{(31℃-21℃)/10}$$

where *A* was the amplitude of oxidation current.

This calculation gave a Q_{10} value of 1.2, which is attributed to a physical process, as opposed to a significant biological process (Precht, 2000).

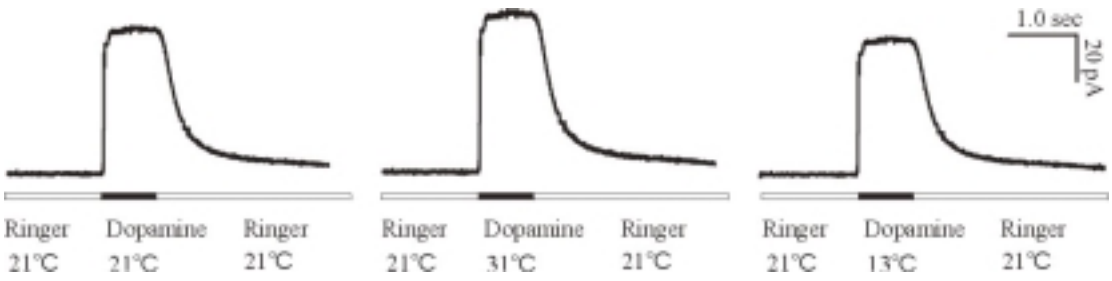

Figure14. The amplitudes of oxidation currents of dopamine recorded at 21ºC , 31ºC and 13ºC were determined. Taking 21ºC (room temperature) as reference point of temperature, physical effect of temperature on the kinetics of amperometric signal was calculated with a $Q_{10\,diff}$ value of 1.2.

3.1.3 Temperature effects on the kinetics of amperometric signals

Single cultured Retzius cells of the leech *Hirudo medicinalis* were superfused

with Ringer's solution containing 2μM ionomycin at 21°C and test temperature, sequentially. The evoked release was recorded by carbon fiber in a cell-attached configuration. It was obvious that release frequency and events amplitudes increased dramatically, when the temperature was changed from 21°C to higher temperature (21°C~26°C and 21°C~31°C) and the opposite change was observed when the temperature was decreased from 21°C to lower temperature (21°C~16°C) (*Fig. 15)*.

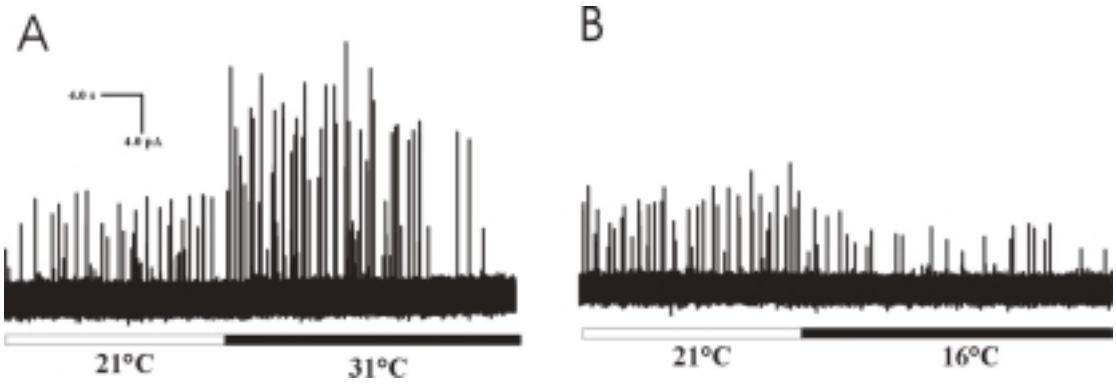

Figure15. Exocytosis from the axon stumps of Retzius cells at different temperature.

(A) Amperometric currents from an example cell stimulated by 2μM ionomycin at 21°C (empty bar) and 31°C (solid bar). Obviously, the amplitude and release frequency of the events measured at 31ºC were increased significantly.

(B) Amperometric currents from an example cell stimulated by 2μM ionomycin at 21°C (green bar) and 16°C (blue bar). Opposite changes of event amplitudes and release frequency were observed at lower temperature of 16°C in comparison with *Fig. 15A.*

The cumulative frequency distributions of spike parameters were plotted (*Fig. 16*). The distributions of cubic roots of charge integral recorded at 21°C, 16°C and 31°C were similar, showing that temperature didn't influence the quantal size of vesicles. The major alterations of signal properties, due to the temperature change, were observed from kinetic parameters. Taking the curves of 50-90% rise time and HW at 21°C as control, I found that the curve at 16°C shifted to the right side and that at 31°C shifted to the left side, showing that signals recorded at high temperature had fast kinetics compared to that recorded at low temperature. Compared to the control values at 21°C, amplitudes of events increased or

decreased dramatically corresponding to 31°C and 16°C, which was consistent with the changes of rise time and half width in our study.

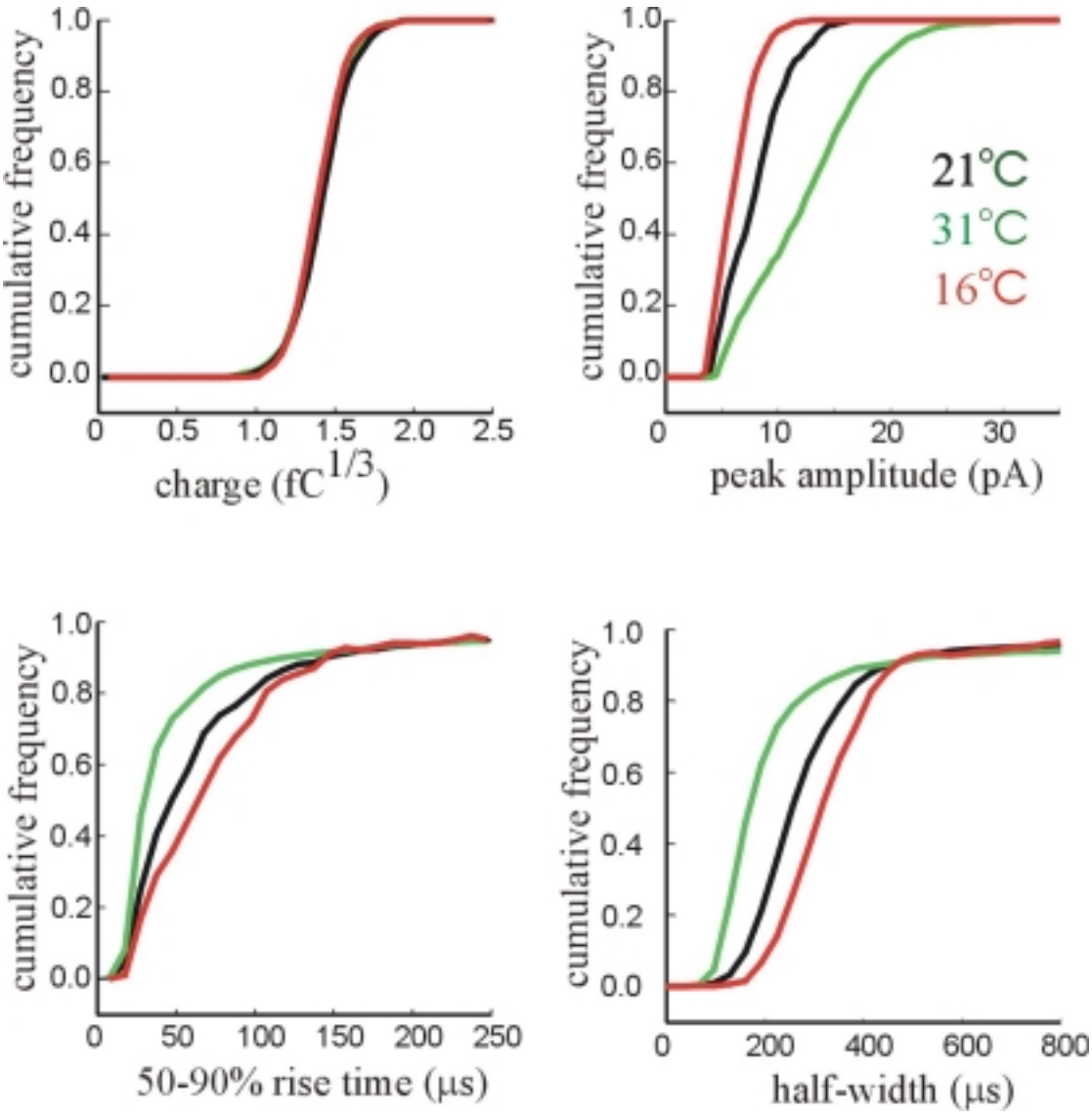

Figure16. Temperature changes the kinetics of amperometric events without altering the vesicle sizes.

Cumulative frequency distributions of all the parameters of events measured at 21°C (black), 31°C (green) and 16°C (red), with respect to cubic root of charge integral, peak amplitude, 50-90% rise time and half-width, were plotted. The test temperatures in this study had no effects on the vesicle size, but strongly influenced the kinetics and amplitudes of events recorded, the higher the temperature, the faster the rise time and half-width and the higher the amplitude, *vice versa*.

I determined the median values of these parameters for each cell, and averaged them within each experiment. The mean values as well as release frequency of the SSV events at each test temperature are given in *Table 2*. For each experiment, I determined the ratio of parameters at test temperature versus that at 21°C, with respect to release frequency, peak amplitude, half width and Q_{10} value for each parameters (*Table 3*). I found that the halfwidth of the amperometric signal was affected by temperature with a $Q_{10\ signal}$ value of 1.6.

Table2. Properties of SSV events recorded at different temperatures

	release frequency (events/sec)	charge (fC)	amplitude (pA)	rise time (μsec)	halfwidth (μsec)
21°C	1.8 ± 0.4	2.7 ± 0.16	7.6 ± 0.39	46 ± 2.6	258 ± 10.0
31°C	10.2 ± 3.0	2.8 ± 0.12	10.8 ± 0.89	34 ± 1.5	162 ± 8.0
21°C	1.5 ± 0.2	3.0 ± 0.07	5.9 ± 0.23	87 ± 8.1	380 ± 16.3
26°C	3.9 ± 0.9	2.9 ± 0.13	7.6 ± 0.68	53 ± 7.1	272 ± 23.0
21°C	2.7 ± 0.4	2.5 ± 0.12	7.6 ± 0.76	49 ± 4.0	257 ± 15.0
16°C	1.4 ± 0.4	2.6 ± 0.12	6.0 ± 0.33	61 ± 3.9	328 ± 10.3

Measurements are given as mean ± SEM of median values determined for the individual cells.

Table3. Ratios of parameter measured at test temperature versus parameters measured at room temperature and the Q_{10} values of each parameters

	31°C / 21°C	26°C / 21°C	16°C /21°C	Q_{10}
release frequency	6.09	2.43	0.51	6.0
amplitude	1.42	1.28	0.79	1.55
halfwidth	0.63	0.72	1.23	1.6

Since the $Q_{10\ diff}$ value is 1.2 and the HW_{signal} is the sum of the contributions of release process (HW_{real}) and transmitter diffusion (HW_{diff}), the net effect of temperature on the release process ($Q_{10\ real}$) can be derived by formula *[7]*,

$$HW_{signal21°C} \times Q_{10signal}^{(21-t)/10} = HW_{real21°C} \times Q_{10real}^{(21-t)/10} + HW_{diff\ 21°C} \times Q_{10\ diff}^{(21-t)/10}$$

here, $HW_{signal21°C}$ is 258 µs, $HW_{real21°C}$ is 198 µs, and $HW_{diff\ 21°C}$ is 60 µs ($HW_{signal21°C}$ - $HW_{real21°C}$). At 21°C $Q_{10signal}$ and $Q_{10\ diff}$ are 1.6, 1.2 respectively. The calculated Q_{10real} is about 1.77, indicating an effect of temperature on the SSV release process. Further I calculated the real time course of HW_{real} at each test temperatures, $HW_{real\ 16°C,}$ $HW_{real\ 26°C}$ and $HW_{real\ 31°C}$, and they are 266,150 and 113µs respectively.

The ratios of each parameters (test°C / 21°C) were plotted against the corresponding temperatures (*Fig. 17*).

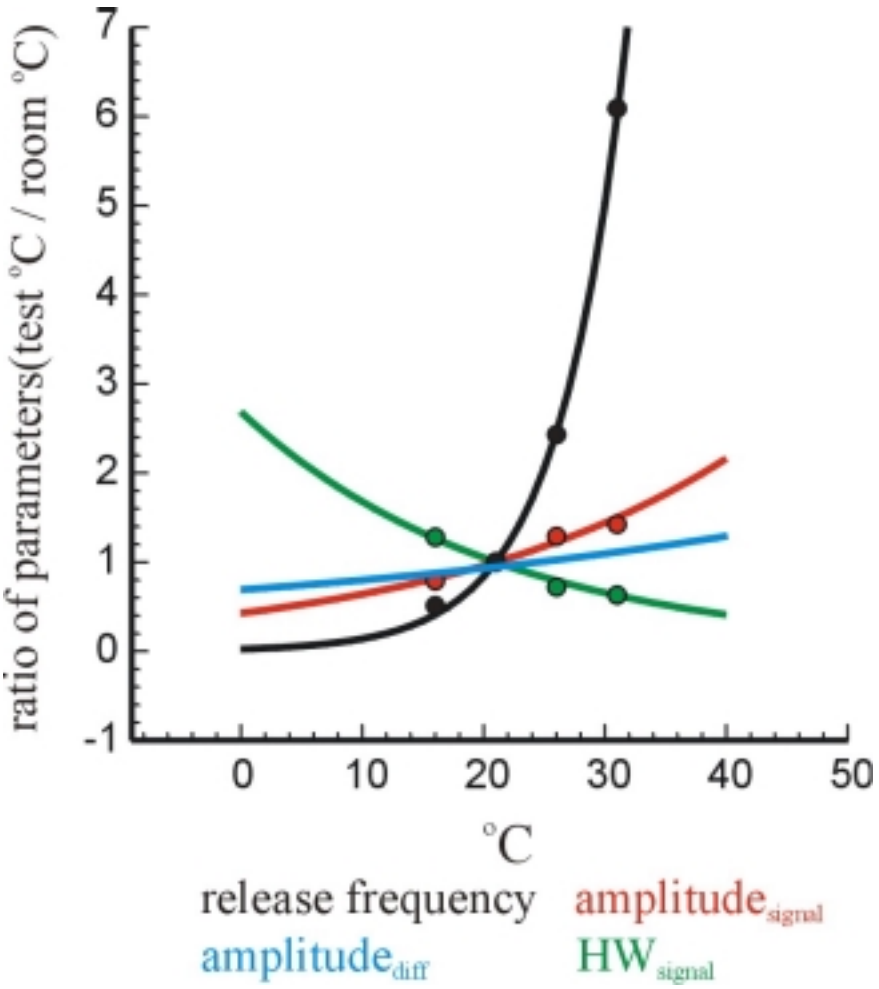

Figure 17. Temperature effects on release frequency and release process of SSVs events.

Different test temperatures were plotted against the ratios of parameters (test°C / 21°C) determined at corresponding temperatures, release frequency of SSVs (black), signal amplitude (red), signal half-width (green) and diffusional effect on signal amplitude . Fitting the data in the plots by using the function, $A_{(test℃)} = A_{(21℃)} \times Q_{10}^{(test℃-21℃)/10}$, generated the Q_{10} values of 1.2, 6.0, 1.55 and 1.6, with respect to pure diffusional effect on signal amplitudes, release frequency, signal amplitude and signal half-width. Here, *A* is the value of the parameter of interest and it is determined at different temperatures indicated by the footnotes.

3.2 The temperature effect on the real time course of SSVs events can be explained by a temperature effect on the speed of fusion pore dilation

I have just described a temperature effect on the release kinetics of SSVs with Q_{10} of 1.77. My question now was: What is the mechanism underlying this effect? The elementary properties of such a fusion pore are similar to an ionic pore. Previous observation in mast cells and chromaffin cells have shown that exocytosis is initiated by opening of a small-sized fusion pore, that allows for high release rate of transmitter molecules, in the range of 10000 mol / ms. According to Hille (1994), the efflux through such a pore is given by the following equation:

[8]

$$efflux = \frac{\pi r^2 Dc}{l + \frac{\pi r}{2}}$$

For an exocytosis vesicle, r is the radius of a fusion pore; C is the concentration of transmitter inside the vesicle; D is the diffusion coefficient of transmitter molecules, and l is the length of the fusion pore. The intravesicular concentration of serotonin of SSVs is 270 mM (Bruns and Jahn, 1995). The dimension of fusion pore is 10-15 nm long and 2 nm (diameter) wide found in mast cells by Spruce *et al.*, (1990).

I assume that, after the initial opening of the fusion pore with radius of 1nm, the pore starts to dilate with a constant rate. Under the assumption that the expansion rate grows with temperature, I accelerated the rate in order to achieve the kinetic properties of simulated signals, which are similar to reality. Two calculated signals were generated at the rates of 2nm/ms and 8nm/ms and they were very similar to the signals recorded at 21°C and 31°C, with respect to charge integral, peak amplitude and kinetic parameters of 50-90% risetime and HW, especially for the ratio of $HW_{2nm/ms}$ / $HW_{8nm/ms}$ of ~1.7, which was very similar to $Q_{10\ real}$ (*Fig. 18*). As shown in the figure, although the dilation rate of the fusion pore was accelerated 4 fold, the kinetics of the signal was only accelerated by ~ 1.7 fold, indicating that the kinetics of signals were strongly influenced by initial pore opening, therefore, the effect of pore dilation on the kinetics was not so dramatic as expected. The simulation provides a simple explanation for the observed temperature effects on the kinetics of SSVs events. The change of fusion pore diameter can be distinguished into two phases, the fast phase representing the initial pore opening and the slow phase representing the pore dilation. The kinetics can be influenced by both phases, but is mostly dominated by the fast one, and the slow phase is probably temperature-sensitive. This interpretation correlates well with my results, that there is only a 1.77 fold change of kinetics of SSVs events for 10°C increments.

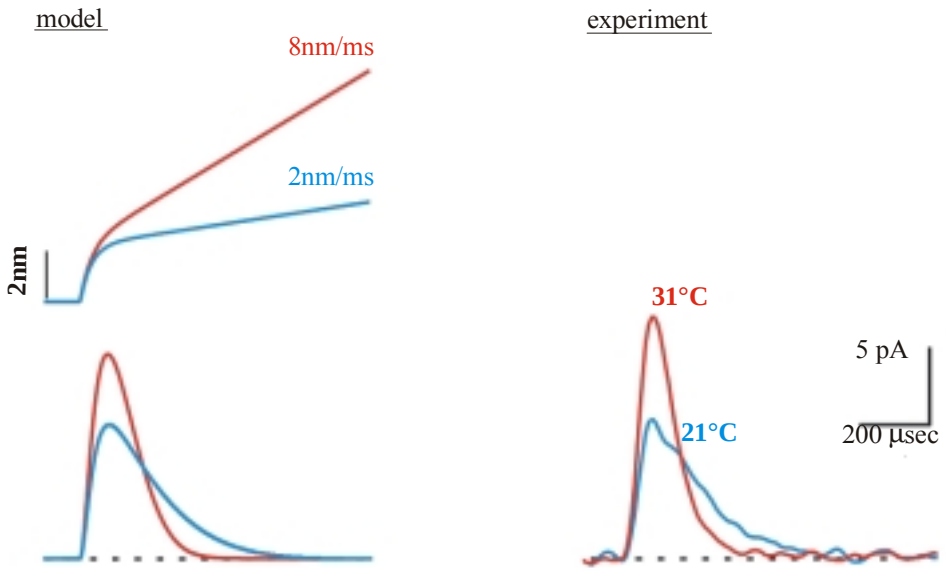

Figure 18. Comparison of simulation results from model of fusion fore expansion of SSVs with experimental data. The upper part on the left side is the model of fusion pore expansion. It is assume that after the opening of fusion pore, the initial pore size is 2nm, afterwards the fusion pore dilates at the speeds of 2nm/ms (blue curve) and 8nm/ms (red curve).

The lower part on the left side is the calculated amperometric signals from the model, corresponding to different expansion rate of fusion pore.

The figure on the right side displays the amperometric signals recorded 21°C (blue curve) and 31°C (red curve). The simulation result fits well with experimental data, with respect to signal charge and kinetic parameters.

4 Discussion

Synaptic transmission is a highly regulated function of the nervous system. Nerve cells communicate with each or with muscle cells by regulated exocytosis of neurotransmitter-containing synaptic vesicles. Synaptic transmission consists of three sets of processes, serially following each other: 1) presynaptic processes, that start with the invasion of the presynaptic terminal by the action potential and end with the release of transmitter from the synaptic vesicles; 2) synaptic gap processes; and 3) postsynaptic processes. These processes form a cascade of events each of which is influenced by the previous and in turn influences the next. The rate of transmitter release from the fusion pore into the synaptic cleft determines the time course of transmitter concentration in an individual synaptic cleft. The profile of transmitter concentration in the synaptic cleft determines the percentage of postsynaptic receptors that bind neurotransmitters, and their degree of desensitization following synaptic activation. Receptor occupancy and desensitization influence the amplitude of the postsynaptic response following release of a single vesicle, the time course of the response, paired-pulse depression, and other important details of synaptic transmission.

Due to their small size and fragility, synapses remain inaccessible to some of the most powerful techniques for examining the kinetics of release. Despite these limitations, still a very detailed picture of the synaptic events has been obtained using a variety of biochemical and electrophysiological techniques and observations.

Khanin *et al.* (1994) provided considerable theoretical evidence that, to generate a sufficiently high (mM range) concentration of transmitter in the vicinity of the postsynaptic receptors (Land *et al.*, 1980; Matthews-Bellinger and Salpeter, 1978), the duration of discharge must be about 100 microseconds in fast synapses. Further, Wathey *et al.* (Wathey *et al.*, 1979), and Clements *et al.* (Clements *et al.*, 1992) combined their biochemical and electrophysiological observations into quantitative models, that predict the time course and size of a synaptic response.

All of the models have assumed that release of the entire contents of the vesicle is instantaneous. However, Van der Kloot (Van der, 1995) noted that the rise times of miniature endplate currents in the frog neuromuscular junction are considerably longer than those predicted by the models. Van der Kloot proposed that the assumption of instantaneous release is probably incorrect and that acetylcholine is released over a period, after vesicle fusion.

Electrochemical measurements with amperometric microelectrodes at isolated adrenal medullary cells provided direct chemical evidence for the quantal nature of exocytosis in real time (Leszczyszyn *et al.*, 1990; Wightman *et al.*, 1991). Amperometric spikes measured with carbon fiber electrodes have been shown to be the result of the oxidation of the catecholamines contained within a single vesicle (Wightman *et al.*, 1991). These measurements have excellent temporal resolution and provide a means to probe the kinetic processes associated with the discharge of amines into the extracellular space (Alvarez *et al.*, 1993; Chow *et al.*, 1992; Jankowski *et al.*, 1993) and its diffusion away from the cell (Kawagoe *et al.*, 1991; Schroeder *et al.*, 1992). The results obtained in this way suggest that the simplest view of exocytosis, instantaneous release from the cell surface followed by diffusion of the catecholamines away from the cell, is incorrect at adrenal medullary cells. Rather, there is a rate-determining step in the secretion process, which is slower than the diffusional rate of mass transport of catecholamines. Evidently, the kinetics of transmitter release from large dense core vesicles (LDCVs) are mainly governed by the release process. Compared to the LDCVs, SSVs have very fast kinetics of exocytosis, which is very important for the signaling between neurons in the brain. Is the kinetics of secretion process of SSVs so rapid that the real time course can be negligible thus can be treated as instantaneous release, or the release process is not as fast as expected and affects the kinetics of amperometric spikes. In the present work, I address these questions by examining exocytosis of SSVs of Retzius cells from leech (*Hirudo medicinalis*) with carbon fiber microelectrodes. The data demonstrated that the process of exocytosis from SSVs is rate limited by the release of serotonin from the vesicle.

It is established that there is a rate-determining step in the secretion that occurs after formation of the fusion pore between the vesicle interior and the plasma membrane.

4.1 Dextran molecules slow down the diffusion of transmitters in the extracellular medium.

The classic Einstein-Smolochowski equation for one-dimensional diffusion: $x^2 = 2Dt$, describes that the time for a diffusing particle to travel some distance, x, goes with the square of x. Following the equation, the diffusion coefficient of serotonin molecules in the extracellular medium was decreased by a factor of 1.5 compared to the normal Ringer's solution, by introducing macromolecules of Dextran (40,000) into the extracellular solution. In the cell-attached configuration, a constant oxidation current of 0.2~0.5 pA recorded by the carbon fiber was observed during the superfusion of 9.2% dextran solution and the minor currents were identified as dextran oxidation currents as it disappeared when superfusion solution was switched back to the Ringer's solution. Thus the slight shifting of the base line of the recording trace due to the oxidation of dextran molecules was taken as an indicator that the macromolecules entered into the cleft of release site and detecting surface. For diffusing molecules, extracellular macromolecules can be considered as obstacles, which impose an additional increase in path length.

4.2 The frequency distributions of amplitudes of SSV amperometric signals correlate to the positioning of carbon fiber microelectrode on the cell membrane.

The typical ultrastructural features of a cultured Retzius cell are studied in detail by Bruns *et al.* (2000). The axon stump of Retzius cell consists of a central cylinder that sends out lateral arborizations forming a condensed network of axonal endings. Many axonal extensions that contain clusters of SSVs are found on the surface of the axon stump, making them directly accessible to carbon fiber amperometry. Within such terminal regions, SSVs are clustered directly opposing

the plasma membrane. Occasionally, axon terminals exhibit active zone-like thickenings (electron-dense bars) to which rows of SSVs are in direct contact with the plasma membrane. The morphological properties of the location of SSVs at the axon stump can explain the different distributions of amperometric signals of SSVs in our study. I recorded the exocytosis from more than 30 cells in the cell-attach configuration. Ten cells with median value of event amplitudes larger than 7.0pA, have nearly symmetric distributions of events amplitudes, peaking around 10pA. In contrast, other cells with a median value smaller than 7.0pA have exponentially decreasing distributions of amplitudes without any peaks. The phenomenon is due to the uneven distribution of SSVs at the axon stump. When the clusters of SSVs are underneath the tip of carbon fiber, the cell-electrode spacing can be extremely short, thus the distortion of signal kinetics due to the diffusional broadening is also small. Under this situation, all the events from these vesicles are measured over equal-distance and the amplitude distributions are more relevant to the vesicle size and secretion process and correlate well with the distribution of charge integral. On the other hand, if the locations of SSVs clusters are further away from the carbon fiber, the transmitter molecules have to travel long distances to reach the recording site, thus all the signals recorded under this condition have kinetics which are mostly dominated by diffusion and there is no correlation between the frequency distributions of amplitudes and charge integrals. As the diffusional smearing has a steep dependence on distance and can influence the event amplitudes (chow and von Rüden, 1995), the longer the distance, the lower the signal amplitudes, increasing the amplitude threshold can restrict the events to be measured underneath the carbon fiber. Based on this assumption, amplitude threshold of median value larger than 7.0pA was applied to select cells, which had very short separating distance between detecting surface and release site. From the data, a weak but obvious tendency was observed, that dextran molecules slightly slowed down the event kinetics, as the risetime and HW of events recorded under dextran condition were longer that those of the events recorded under Ringer condition. It must be noted that the dextran effect is much

less than 1.5 fold, the ratio of D_{Ringer} / $D_{Dextran}$, showing that the release process of SSVs is not instantaneous, otherwise the entire kinetics of the signals are determined by diffusion and $HW_{Dextran}$ should be prolonged by 1.5 fold.

4.3 Determination of real time course of secretion process of SSVs.

The amperometric current signals for single vesicles reflect the time course of transmitter release and diffusion from the release site to the detector, thus, the kinetics of amperometric signals are contributed by both release process and diffusion provided that the release is not instantaneous. I assume that the transmitter release is not instantaneous, although the process can be very rapid. Under this assumption, I built an explicit formula, $HW_{Dextran} = (HW_{Ringer} - HW_{real})\times(D_{Ringer} / D_{Dextran}) + HW_{real}$, showing that, at certain cell-electrode spacing, the pure diffusional effects of different extracellular media on the signal kinetics are only inversely proportional to the ratio of diffusion coefficients of transmitters in these media. Taking the dextran molecules as a tool to change the diffusion coefficient, the real time course of HW_{Real} was calculated from HW_{Ringer} and $HW_{Dextran}$, which were determined from individual events recorded in Ringer's and 9.2% dextran solutions separately. The average of median values of HW_{real} calculated from 10 cells is about 200μs and the diffusional effects on the shape of amperometric signals are ~20%. So like LDCVs, the kinetics of SSVs amperometric signals are also dominated by the real time course of release process, rather than the diffusional rate of mass transport of transmitters.

Furthermore, events with 50-90% rise time faster than 33μs from these 10 cells were selected and analyzed, assuming that these fast events were recorded over very short distance and suffered less from diffusional "smearing", compared with other events having risetime longer than 33μs. As shown in *Fig. 8*, the frequency distribution of HW from these fast events almost overlapped to the curve of HW_{real}, showing that in our recording system, some events, which had very rapid kinetics, were nearly recorded without diffusional distortion.

4.4 Temperature effects on the secretion process of SSVs

What are the determinants of the real time course of transmitter release of SSVs? To probe the mechanism underlying the release process, I studied the temperature effects on it. Firstly, I determined the physical effects of temperature on the diffusion of Dopamine molecules, generating a Q_{10} value of 1.2, which is in very good agreement with Greg Gerhardt and Raiph N. Adams's results (1982), that all the values measured at room temperature can be corrected to test temperatures by applying the standard correction of +2%/°C. I analyzed the kinetic parameters of individual spikes recorded at different temperatures, with respect to peak amplitude, rise-time and half width. After the correction of the physically pure influence of temperature, the kinetic parameter of HW was changed by temperature with Q_{10} value of 1.77, which was the final effect of temperature presented in single spikes. Compared with A. Spruse *et al.* (1990) finding from mast cells, that the mean values for the rate of conductance of fusion pore indicate 3- to 4-fold change for 10°C, our Q_{10} is not as big as I expected.

How to explain this result? One possible hypothesis is that the size and/or the rate of opening of the vesicular fusion pore restricts the rate at which material exits the vesicle (Almers *et al.*, 1989; Alvarez *et al.*, 1993). According to this model the restricted dimension of the fusion pore limits the rate of the serotonin efflux from the vesicle. The fusion pore hypothesis predicts that the time course of secretion will be proportional to the volume of the vesicle. However, the low correlation between HW and total charge of each spike (data not shown) doesn't completely support this hypothesis, at least not completely. Another interpretation, although also based on the opening of the fusion pore or/and the expansion rate of fusion pore, is from Spruse and his colleagues, that the first opening of the fusion pore occurs rapidly, afterwards dilation of the pore is relatively slow, and after the initial pore opening the pore is 2-3nm wide. Thus the change of pore size develops in bi-phases, with rapid opening and slow dilation. Under this assumption, simulations were made by keeping the pore diameter as 2nm after the

first opening and simply increasing the dilation rate from 2nm/ms to 8nm/ms. The shapes of signals, calculated from rates of 2nm/ms and 8nm/ms, fit well with those from real signals recorded at 21°C, 31°C correspondingly. Based on these simulation results, I propose that the diameter of fusion pore changes in two steps, after the first step of dramatically rapid opening, the pore continues dilating with certain speed, and compared to the first step the second step is much slower. From the simulation results, the signal kinetics was only speeded up by 1.6~1.7 fold, although the expansion rate was increased by 4 fold, showing that the release kinetics is mostly determined by the initial opening of fusion pore. From this, I can address that the first opening of fusion pore is the dominant factor for the signal kinetics, the second slow phase of pore dilation also contributes the entire secretion process, but not as much as the fast phase does and the slow phase can be more sensitive to temperature changes.

What's the molecular mechanism of pore expansion? Is the fusion pore predominantly lipidic and is the pore expansion due to lipid-lipid interactions? Our model for fusion pore kinetics, which can explain experimental data well, argues against the idea that the initial rate of pore dilation is determined solely by interactions between lipids: the rate increases much more steeply with temperature (4 fold over 10°C) than the diffusion coefficient of lipid (no measurable change over 10°C when there is no phase transition; Fahey and Webb, 1978). Here, I assume that the pore dilation can be influenced by both lipids and proteins. The lipids within the fusion pore are in contact with proteins and dilation would require the movement of lipid along the protein interfaces, and proteins are more sensitive to temperature changes than lipids.

5 Summary

Neurotransmitter release is mediated by Ca^{2+} dependent exocytosis of synaptic vesicles (SSVs) which have very rapid kinetics of transmitter release. So far, the real time course of transmitter discharge of SSVs has not been directly determined. Using carbon fibers as electrochemical detectors, I measured the release of the neurotransmitter serotonin from cultured Retzius cells of the leech (*Hirudo medicinalis*). The kinetics of amperometric signals reflects the time course of transmitter release and the diffusion of molecules from the release site to the detector. Based on this, I built an explicit formula, $HW_{Dextran} = (HW_{Ringer}-HW_{real}) \times D_{Ringer}/D_{Dextrant} + HW_{real}$ (here, HW is the half-width of individual amperometric spike, and D is the diffusion coefficient of transmitter molecules) to calculate the real time course (HW) of transmitter release of SSVs and LDCVs, by introducing Dextran molecules (40,000 Da) to change the diffusion coefficient. The real time course (HW_{real}) of transmitter release of SSVs is about 198 μs and the contribution of diffusional broadening on the kinetics of individual amperometric signals of SSVs is about 20 %. These results indicate that exocytotic release of SSVs is non-instantaneous and the majority of the kinetics of individual amperometric signals of SSVs is dominated by real time course of transmitter release. The real time course (HW_{real}) of the release process of LDCVs was also determined (about 1133 μs). Furthermore, I investigated the temperature effects on the release process of SSVs. The results show that increasing temperature can accelerate the release kinetics by a Q_{10} value of 1.77 and leads to a dramatic increase of release frequency by a Q_{10} value of 6.0. In the end, the underlying mechanism responsible for the temperature effects on the kinetics of amperometric events can be well interpreted by a model (paragraph *3.2*) developed in this study. It is proposed that, the fusion pore size changes in two steps, the initial opening of the fusion pore which is very rapid, and afterwards the expansion of the pore which is relatively slow. The first step dominates the kinetics of release process, in contrast, the second step of fusion pore dilation contributes less to the kinetics. Compared the first step, the dilation phase is more sensitive to temperature changes, which can

explain that the final change of kinetics is only 1.77 fold for temperature change of 10 ^{o}C.

1 The aim of the work

Neurons and neuro-endocrine cells release neurotransmitters and hormones by regulated exocytosis of small synaptic vesicles (SSVs) or large dense core vesicles (LDCVs). Such intracellular fusion reactions are generally thought to be mediated by SNAREs, a large family of membrane proteins characterized by a common sequence called the SNARE motif. The SNARE proteins consist of syntaxin, synaptobrevin2 (syb2) and SNAP-25. The functional analysis of these proteins has been done in different model systems, *i.e.*, neurons of the hippocampus and neuro-endocrine cells of the adrenal medulla (chromaffin cells) (Schoch *et al.*, 2001; Sorensen *et al.*, 2003). In mice hippocampal neurons deficient in synaptobrevin2 (Schoch *et al.*, 2001), Ca^{2+}-triggered release of neurotransmitter was decreased about 100-fold in comparison with wild type. Although the molecular machinery participating in the release of the two classes of vesicles shows great similarities, functional differences exist between brain synaptic processes and neuro-endocrine exocytotic processes.

In my study, I use synaptobrevin2 (syb2) and cellubrevin (VAMP3) null chromaffin cells of mice adrenal glands as my model systems to investigate the roles of syb2 and VAMP3 in the exocytosis of large dense core vesicles (LDCVs) using electrophysiological technique amperometry as key methodological tool.

2 Result: SNARE Function Analyzed in the Synaptobrevin II Mutant Mouse

2.1 General appearance of the synaptobrevin2 mutant mice

A mouse mutant line carrying a null mutation in the synaptobrevin2 gene and fully backcrossed into C57/B6 background was received from the laboratory of Thomas Südhof (University of Texas Southwestern Medical Center, Dallas, Texas, USA).

Mice heterozygous for the synaptobrevin2 (syb2) mutation were robust, fertile and phenotypically indistinguishable from wild-type littermates. In contrast, homozygous mutants obtained from heterozygous crosses died immediately after birth. At embryonic date (E17.5-18.5), homozygous mutant fetuses were distinguished by their characteristic tucked position, smaller size, and external blotchy appearance, and failed to exhibit either spontaneous movement or sensorimotor reflexes in response to mechanical stimuli.

Genotyping results and protein biochemistry (western blot) were consistent with morphological appearance of embryos (data not shown).

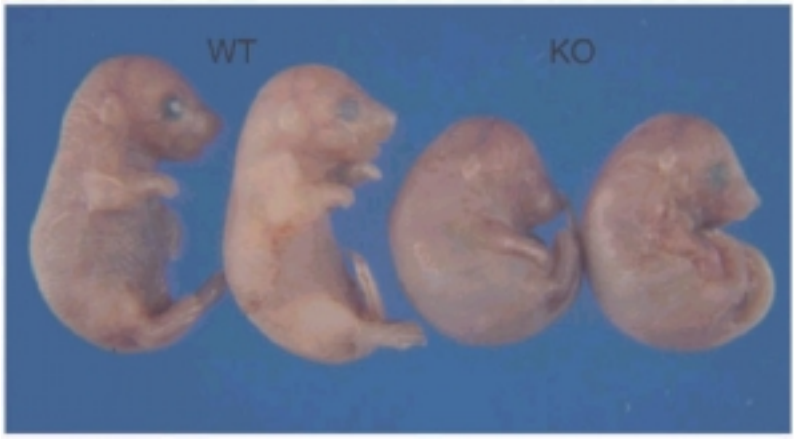

Figure1. Appearance of newborn wild type and mutant mice. Mice from a single litter were photographed immediately after birth (reproduced from Schoch *et al.*, 2001).

2.1.1 Deficiency in synaptobrevin2 does not abolish secretion in mouse chromaffin cells

It has been reported that at least 90% of the calcium-triggered release of small synaptic vesicles is abolished in the hippocampus of mice deficient in synaptobrevin II, showing that synaptobrevin II is essential for the exocytosis of synaptic vesicles. I wanted to know if synaptobrevin II is also essential for the exocytosis of large dense core vesicles (LDCVs), like the ones found in the chromaffin cells of the adrenal gland. These cells represent a well-researched model for calcium-triggered exocytosis (Amatore *et al.*, 2003; Apland *et al.*, 2003; Camacho *et al.*, 2003; Ryan, 2003).

I gently removed the adrenal glands from E17.5-18.5 embryonic mice, then digested the tissue, isolated the chromaffin cells and cultivated them *in vitro* for the experiments.

Upon applying an amperometric electrode to the surface of a chromaffin cell in the cell-contact configuration, exocytosis of a single vesicle registered as a spike of current, caused by the oxidization of catecholamines at the surface of the carbon fiber electrode. These spikes were elicited by depolarization, in this case induced by rapid local application of high K^+ in the presence of 2mM Ca^{2+}. I used a local perfusion system to achieve rapid solution exchange. More than 2 stimuli were applied in the same cell. Considering that a depletion of readily releasable vesicles can occur, a recovery period of 1min between successive stimuli was necessary. The high K^+-evoked exocytosis of LDCVs presented robustly in $syb2^{+/+}$, $syb2^{+/-}$ and $syb2^{-/-}$ cells, showing that the deficiency of syb2 protein doesn't abolish the transmitter release of chromaffin cell (***Fig. 2***). Interestingly, the amplitude of burst often increased at the second application of high K^+ in all the different genotypic cells, implying that the concentration of Ca^{2+} preceding the second stimulation was elevated. Probably after the first application, the Ca^{2+} concentration didn't fall down to the original level but at a higher concentration level, accelerating the "Ca^{2+}-dependent priming" of chromaffin granules.

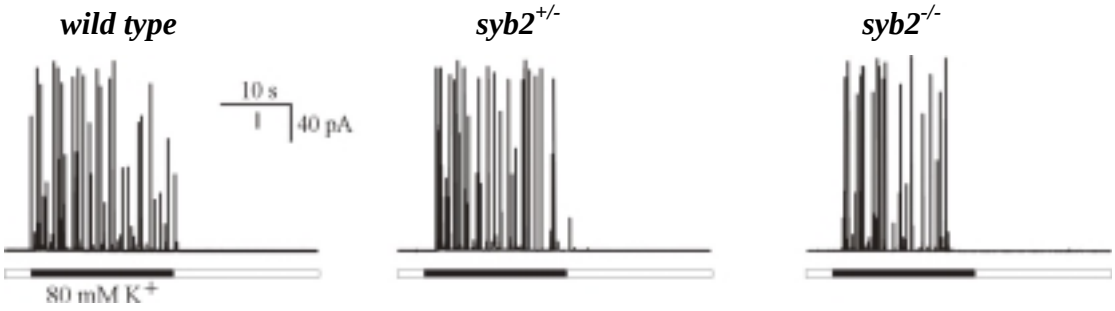

Figure 2. Amperometric currents from example wild-type, syb2$^{+/-}$ and syb2$^{-/-}$ chromaffin cells elicited with 2mM Ca^{2+}, 80mM K^{+} Ringer solution (indicated by solid bar). Each spike represents the fusion of one vesicle. The deficiency of syb2 didn't block the exocytosis in syb2$^{-/-}$ chromaffin cells.

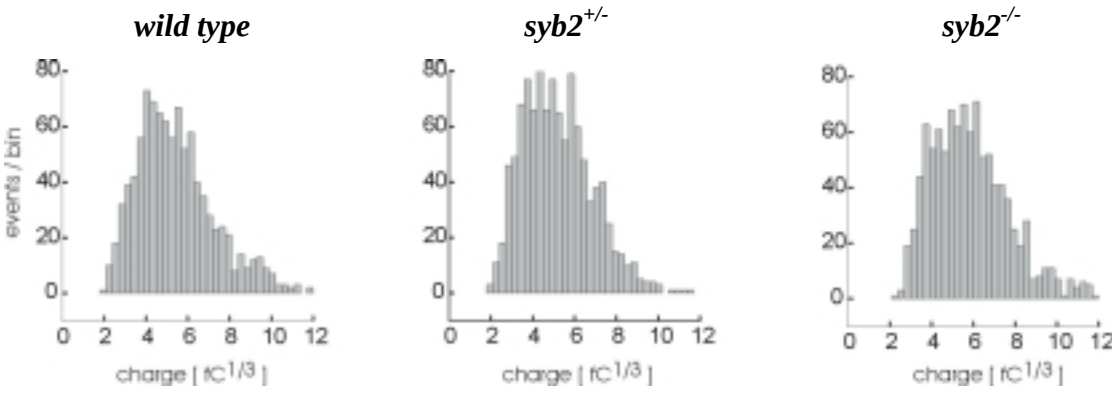

Figure 3. The cube-rooted charge integral of amperometric event is assumed to be proportional to the vesicle inner diameter. Histograms of the cube-rooted charge integral of amperometric spikes measured from wild-type, syb2$^{+/-}$ and syb2$^{-/-}$ chromaffin cells were very similar, showing that the genetic depletion of syb2 does not influence the vesicle sizes.

The vesicles size distribution was examined, as this should reflect dense-core vesicle size (provided that vesicular catecholamine concentration remains the same). The cubic-root of charge integral (cube root transformed to be proportional to vesicle diameter) appeared to be normally distributed and was indistinguishable

between wild type and heterozygous or homozygous, indicating that genetic deletion of synaptobrevin2 didn't change the vesicle size, *Fig. 3***.**

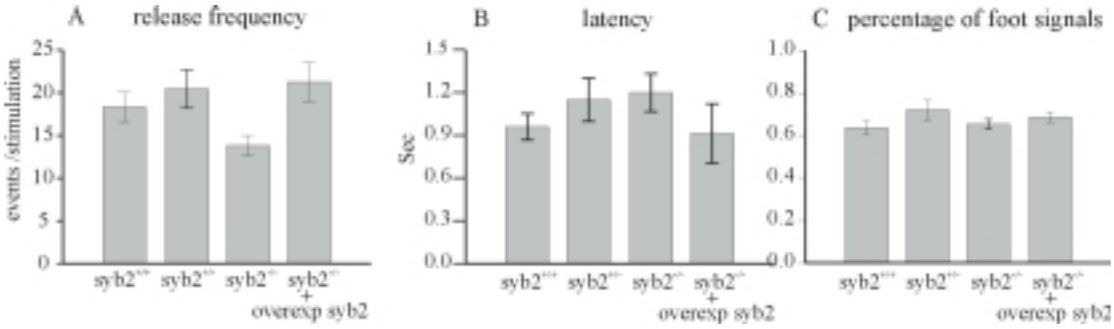

Figure 4. General properties of Ca^{2+}-trigered exocytosis in cultured wild-type, $syb2^{+/-}$, $syb2^{-/-}$ and $syb2^{-/-}$ with overexpression of $syb2^{+/+}$ embryonic chromaffin cells.

The frequency of exocytosis was also analyzed. Because of the irregular nature of the release in a single trial, I counted spikes after the onset of stimulation (*Fig. 4A*). The release frequency of homozygous cells decreased by 23% (wt: 59 ± 4.4 events/cell, n = 44; $syb2^{-/-}$: 46 ± 3.4 events/cell, n = 35, $P < 0.05$, unpaired t-test) compared to the release frequency of wild type cells. No significant difference of release frequency was found between wild type and heterozygous cells

Response to high K^+ was characterized by a latent period with no events, followed by a period of events at irregular intervals. The latency was measured off line as the time between the start of the stimulus and the time at which the amperometric current signal first exceeded the baseline noise by 4 standard deviations (*Fig. 4B*)**.** No significant difference of latency was observed among wild type, heterozygous and homozygous cells, showing that the deficiency of syb2 protein doesn't affect the Ca^{2+} influx due to hyperpolarization and rapid Ca^{2+}-stimulated binding to the SNARE complex.

2.2. Properties of amperometric signals of $syb2^{-/-}$ cells

Amperometric signals recorded by depolarization with high K^+ show a large variability, probably reflecting different kinetics of transmitter discharging. I focused on the spikes preceded by a slower pedestal, called the 'foot' signal (Alvarez *et al.*, 1993; Chow *et al.*, 1992; Neher and Zucker, 1993) to investigate

Table 1. Properties of release and amperometric events (spike phase and foot signal) of LDCVs in syb2$^{+/+}$, syb2$^{+/-}$, syb2$^{-/-}$ chromaffin cells and syb2$^{-/-}$ chromaffin cells with syb2, TeNT overexpression

				spike phase				foot signal				
	number of cells	release frequency	% of foot event	charge (fC)	amplitude (pA)	risetime (ms)	halfwidth (ms)	duration (ms)	charge (fC)	mean amplitude (pA)	amplitude (pA)	% of plateau event
syb2$^{+/+}$	44	59.6±4.4	66±2	178±4.6	82±3.7	0.35±0.02	1.88±0.09	4.8±0.30	21±1.2	4.4±0.2	10±0.37	8±1
syb2$^{+/-}$	32	57.0±6.4	72±2	191±6.6	94±5.4	0.36±0.02	1.78±0.12	5.3±0.34	24±1.9	4.7±0.2	12±0.63	
syb2$^{-/-}$	46	46.0±3.4	64±2	192±5.4	78±5.0	0.46±0.03	2.40±0.17	9.1±0.60	28±1.8	3.4±0.2	10±0.53	15±1.6
syb2 $^{-/-}$ +syb2	18	61.0±7.2	68±3	186±7.1	85±5.5	0.38±0.03	2.00±0.17	4.9±0.44	24±1.9	5.3±0.3	11±0.57	
Syb2 $^{-/-}$ +TeNT	10	0	-	-	-	-	-	-	-	-	-	-

Measurements are given as mean ± SEM of mean values determined for individual cells.

the effects of syb2 on the fusion pore expansion and the transmitter discharging after complete fusion pore dilation.

2.2.1 Deficiency of syb2 prolongs the foot durations of amperometric signals.

Foot signals are most confidently identified in amperometric events that occur when the probability of overlapping individual events is very low. To evaluate the features of the single secretory events consisting of spike phase and foot signal, Ca^{2+} concentration in the stimulating solution was adjusted to 2mM to evoke release at sufficiently low density without significant superposition of independent events.

Spikes preceded by foot signals were selected, with a criterion of amplitude > 4.0pA, charge integral > 50fC and < 500fC. First of all, parameters about foot signals, with respect to foot duration, foot charge and average current (foot integral divided by foot duration) were analyzed. The foot duration was about twofold longer in $syb2^{-/-}$ chromaffin cells than that in $syb2^{+/+}$ chromaffin cells (wt: 4.8 ± 0.25ms; $syb2^{-/-}$: 8.8 ± 0.53ms, $P < 0.001$, unpaired t-test), and there was no distinguishable difference observed between $syb2^{+/+}$ and $syb2^{+/-}$ chromaffin cells (wt: 4.8 ± 0.25ms; $syb2^{+/-}$: 5.3 ± 0.34ms), indicating that syb2 protein functions in the step of fusion pore expansion. An alternative interpretation of the phenomenon, although unlikely, could be that a small event locates just in front of a large one with a partial overlapping. To examine this possibility, I calculated the probability of observing overlapping fusion events from our recordings. For this, the latency times between consecutive fusion events during the constant phase of exocytotic activity was analyzed, and the mean rate of release was 1.63events/sec. The probability of finding two events within a single measurement period (Colquhoun and Sigworth, 1995) is given by:

[1] $$P(\text{time interval} \leq t) = 1 - e^{-t/\tau}.$$

Using the time constant (the inversion of release rate, $\tau = 0.613$s) I calculated the probability of observing two events within a time period that equals the two fold

of the mean half width (t = 3239μs) as 0.02. This will not change the major characteristics of the frequency distribution and agrees with our visual inspection of the current trace, suggesting that the great majority of the exocytotic events were recorded as discrete signals.

Based on this observation, if I propose that the lacking of syb2 protein can interrupt the fusion pore dilation, one might expect that more vesicles under $syb2^{-/-}$ condition could fuse reversibly, with flickering, and that the fusion pore could close again, leading to a 'stand-alone' foot signal without a spike phase, so called "plateau event". The ratios of plateau events to the total events under both $syb2^{+/+}$ and $syb2^{-/-}$ conditions were determined. The ratio from $syb2^{-/-}$ cells was almost 2 fold higher than that from wt cells ($syb2^{+/+}$: 0.08 ± 0.01, $syb2^{-/-}$: 0.15 ± 0.016, $p < 0.01$, unpaired t-test), confirming that syb2 did affect the fusion pore dilation.

Under each genotypic condition, the percentage of events having foot signals was also determined. The ratios were very similar between $syb2^{+/+}$, and $syb2^{+/-}$ or $syb2^{-/-}$ (*Fig. 4C*, wt: 0.66±0.02; $syb2^{+/-}$: 0.72±0.02; $syb2^{-/-}$: 0.65±0.02).

The mean amplitude of foot signals from $syb2^{-/-}$ chromaffin cells was reduced by 20% ($p<0.01$, unpaired t-test) in comparison with amplitudes from $syb2^{+/+}$ and $syb2^{+/-}$ chromaffin cells. The amplitude of foot signal can be influenced by the shape of the fusion pore. The $syb2^{-/-}$ events have lowered foot current amplitudes, suggesting that the protein can alter the structure of the fusion pore, possibly by narrowing or lengthening it. This result, together with the finding that $syb2^{-/-}$ events had prolonged foot durations, strongly indicated that syb2 protein plays a role in the fusion pore expansion.

2.2.2 Depletion of syb2 does not change the spike phase of amperometric signals.

For each individual event headed by foot signals, the characteristics of spike phase, with respect to the charge integral, the 50%-90% rise time, the half width, and the peak amplitude were determined and were given in *table 1*. No significant difference was found between $syb2^{+/+}$, and $syb2^{+/-}$ or $syb2^{-/-}$ chromaffin cells. Our

data doesn't support an effect of syb2 protein on transmitter efflux after the full expansion of fusion pore, the factors controlling this process require further study.

2.3. Rescue of the prolonged foot duration and the decreased release frequency

I examined whether the phenotype of longer duration of foot signal can be rescued by expression of syb2 in syb2$^{-/-}$ chromaffin cells using a Semliki Forest virus (SFV) vector construct. Acutely over-expressing syb2$^{-/-}$ chromaffin cells (6-7 hr after transfection) were studied in parallel with cells from control littermates. As shown in *Fig. 5*, transfection with syb2 virus fully rescued the foot duration to wildtype level. Furthermore, over-expression of synaptobrevin2 protein also increased both the release frequency and mean currents of foot signals of homozygous to wildtype level. I next tested whether overexpression of syb2 in syb2$^{-/-}$ cells changed the parameters of spike phase of amperometric signals, with respect to charge integral, peak amplitude, risetime and halfwidth and I again found no significant differences upon overexpression, table1.

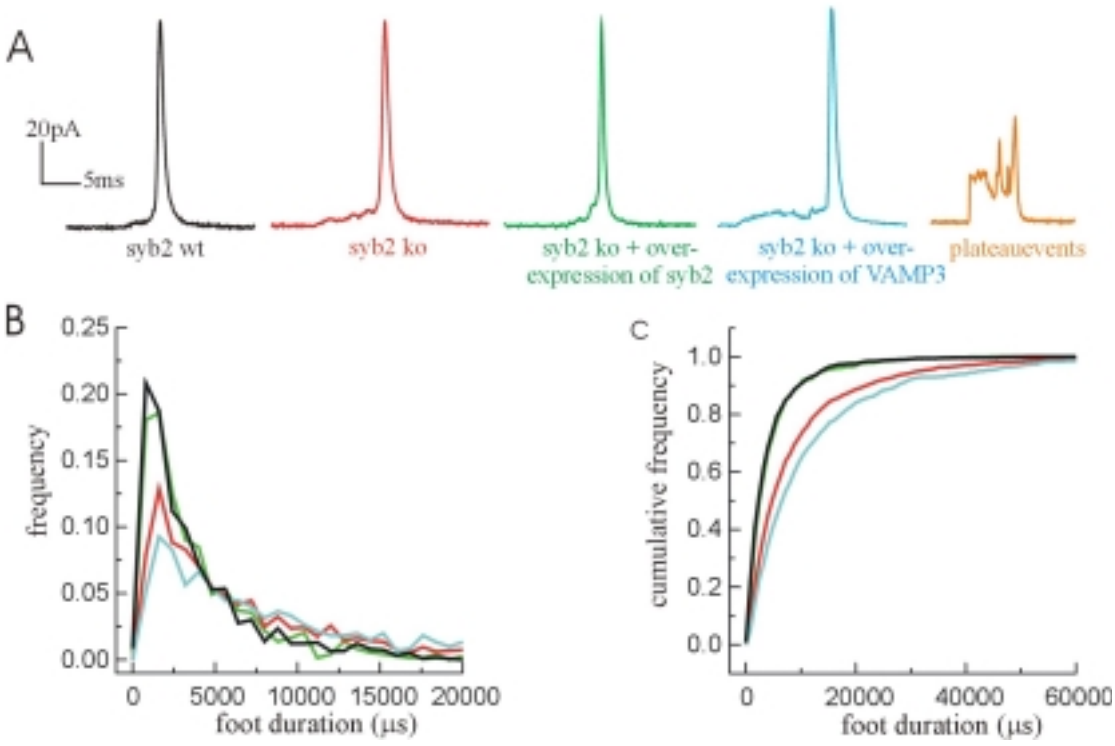

Figure 5. Syb2 and VAMP3 have opposite effects on the speeds of fusion pore expansion.

(A) Examples of amperometric signals having foot signals with different foot durations in wild type (black), syb2$^{-/-}$ (red), syb2$^{-/-}$ with overexpression of syb2 (green) and syb2$^{-/-}$ with overexpression of VAMP3 (light blue) chromaffin cells. The foot signal without following spike phase, so called "plateau event" is also present (orange). The events were chosen in order to illustrate the different life time of fusion pore in all cell types.
(B) and (C) The distributions of frequency cumulative frequency of foot durations from corresponding genetic types of cells. As shown, syb2$^{-/-}$ events had significantly longer foot durations, compared to the wild type events. Overexpression of syb2 fully rescued the foot duration of syb2$^{-/-}$ events to the wild type level. However, overexpression of VAMP3 in the syb2$^{-/-}$ cells made the foot duration even longer, showing opposite effects of syb2 and VAMP3 on the phase of fusion pore dilation.

The level of expression of syb2 protein provided by SFV transduction was investigated using immunocytochemistry. Using an antibody that specifically recognizes syb2 protein, I demonstrated that the viral constructs induced expression of syb2 approximately 17-fold over endogenous levels (*Fig. 6*). *Fig. 6B* is an example fluorescence image of chromaffin cell, which was expressing exogeneous syb2, as indicated by the green fluorescent protein (GFP) fluorescence (green channel). Under the fluorescence microscope, the immunosignals from both transfected and control cells revealed similar dot-staining patterns. The images were collected at different exposure times (wt cells: 5sec; transfected cells: 0.3sec) to prevent the saturation of CCD-camera due to the much stronger intensity of immunofluorescence from transfected cells compared with that from wt cells.

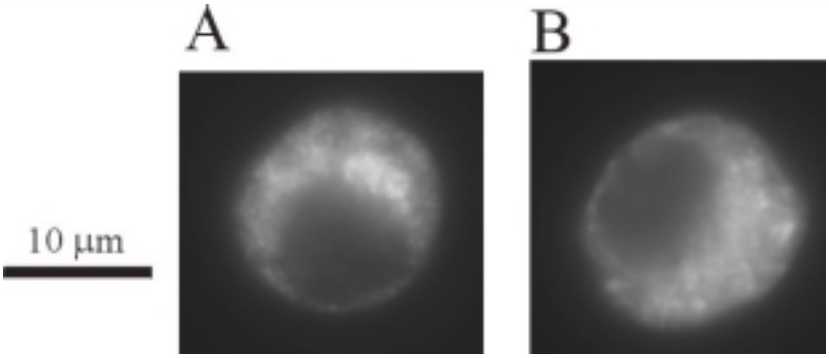

Figure 6. Immunocytochemistry of one wild type embryonic chromaffin cell (A) and one syb2 ko cell with overexpression of syb2 (B). The exposure time was 5sec for the wild type cell, 0.3sec for the transfected cell. The mean fluorescence intensities of the

wild type cell and the transfected cell were 600 ± 157 and 639 ± 180 arbitrary units, respectively. As shown in the figure, the immunosignals from both transfected and control cells revealed similar dot-staining patterns.

2.4 The remaining exocytosis in syb2$^{-/-}$ cells was abolished by overexpression of TeNT.

To examine whether the remaining functionality of fusion in the syb2$^{-/-}$ chromaffin cells was contributed by other members of the synaptobrevin/VAMP family of SNAREs, I overexpressed tetanus toxin light chain (TeNT-LC) in the syb2$^{-/-}$ cells using a Semliki Forest virus (SFV) vector construct, as TeNT-LC can cleave synaptobrevins at the peptide bond between Gln76 and Phe77 (Schiavo *et al.*, 1992a), and therefore blocks the release. After stimulation by high K^+ (80mM), transfected cells displayed a complete absence of exocytosis (*Fig. 7, table 1*), indicating that syb2 was substituted by other proteins, which belong to the synaptobrevin/VAMP family.

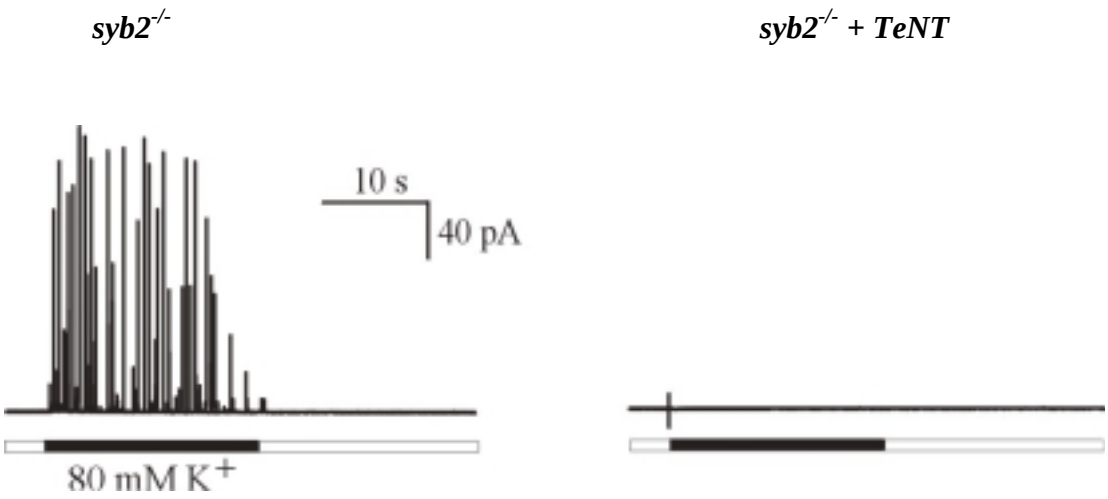

Figure 7. Example of Ca^{2+}-trigerred release in one syb2$^{-/-}$ chromaffin cell (A) and the abolishment of exocytosis in the syb2$^{-/-}$ cell with overexpression of TeNT-LC (B). The cells were stimulated with 80 mM K^+ (indicated by solid bar).

2.5 Properties of secretion and amperometric kinetics of VAMP3$^{-/-}$ chromaffin cells

Cellubrevin (VAMP3) is a member of the synaptobrevin/VAMP family of SNAREs, which has a broad tissue distribution. Furthermore, this protein is abundant in adrenal glands. Cellubrevin and syb2 have a very similar amino sequence in SNARE motif, and they also have the same cleavage site of TeNT (*Fig. 8)*. So cellubrevin is a good candidate to substitute syb2 in the syb2 deficient chromaffin cells. To test this idea, I performed electrophysiological experiments in embryonic mouse chromaffin cells with genetic depletion of cellubrevin.

Embryos deficient in VAMP3 were generated by crossing heterozygous parent animals and prepared at the age of E17.5-18.5. Using the same enzymatic method as used for syb2 ko animals, I prepared isolated embryonic chromaffin cells in parallel from VAMP3$^{+/+}$, VAMP3$^{+/-}$ and VAMP3$^{-/-}$ littermates. The cells were treated with the same stimulation procedure as applied above. No significant differences were observed of secretion and amperometric kinetics, with respect to spike phase and foot signal, between VAMP3$^{+/+}$, VAMP3$^{+/-}$ and VAMP3$^{-/-}$ cells (*Fig. 9, table2)*.

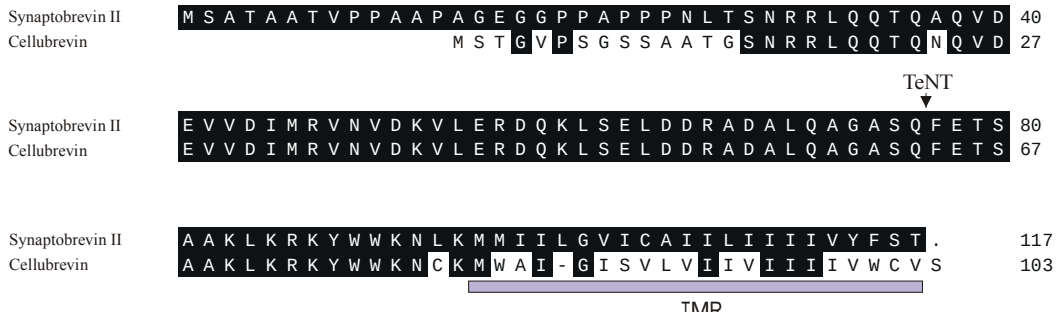

Figure 8. Sequence comparison of synaptobrevin2 and cellubrevin. The TeNT cleavage sites of both proteins are the same and marked with arrow. The putative transmembrane domains are marked by the bar. The sequence of synaptobrevin2 and the amino acids of cellubrevin that are identical to synaptobrevin2 are in dark shadow. Note that the SNARE motifs of both proteins have strong similarity.

Table 2. Properties of release and amperometric events (spike phase and foot signal) of LDCVs in syb2$^{+/+}$, syb2$^{-/-}$ chromaffin cells and syb2$^{-/-}$ chromaffin cells with Vamp3 overexpression

				spike phase				foot signal				
	number of cells	release frequency	% of foot event	charge (fC)	amplitude (pA)	risetime (ms)	halfwidth (ms)	duration (ms)	charge (fC)	mean amplitude (pA)	amplitude (pA)	% of plateau event
Syb2$^{+/+}$	11	93±11	67±3	200±8.2	93±5.9	0.36±0.03	1.8±0.12	4.9±0.46	21±2.7	4.2±0.2	11±0.75	
syb2$^{-/-}$	9	62±12	72±2	193±10	89±7.8	0.42±0.03	2.1±0.22	7.4±1.1	22±3.1	3.2±0.3	12±1.10	
syb2$^{-/-}$ +Vamp3	14	74±11	56±4	205±11	79±7.8	0.52±0.01	2.4±0.40	12.5±1.3	48±4.3	4.2±0.4	11±1.07	27±4

Measurements are given as mean ± SEM of mean values determined for individual cells.

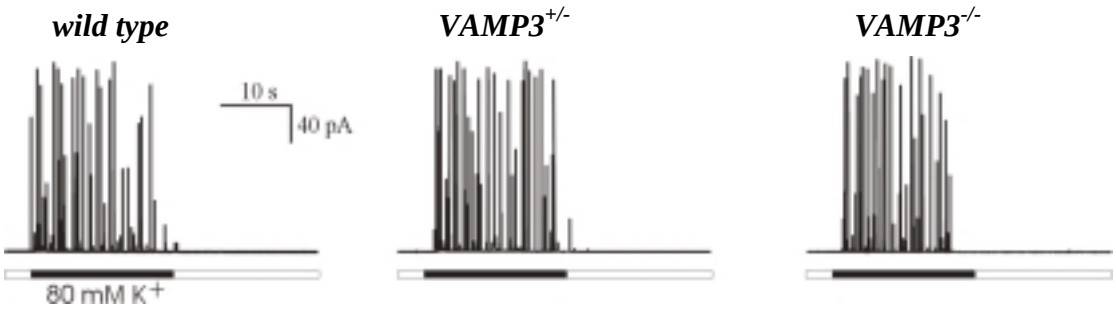

Figure 9. Amperometric recordings from wild type, VAMP3$^{+/-}$ and VAMP3$^{-/-}$ chromaffin cells. The cells were stimulated with 80 mM K^+ (indicated by solid bar). No noticeable differences were found between wild type, VAMP3$^{+/-}$ and VAMP3$^{-/-}$ cells.

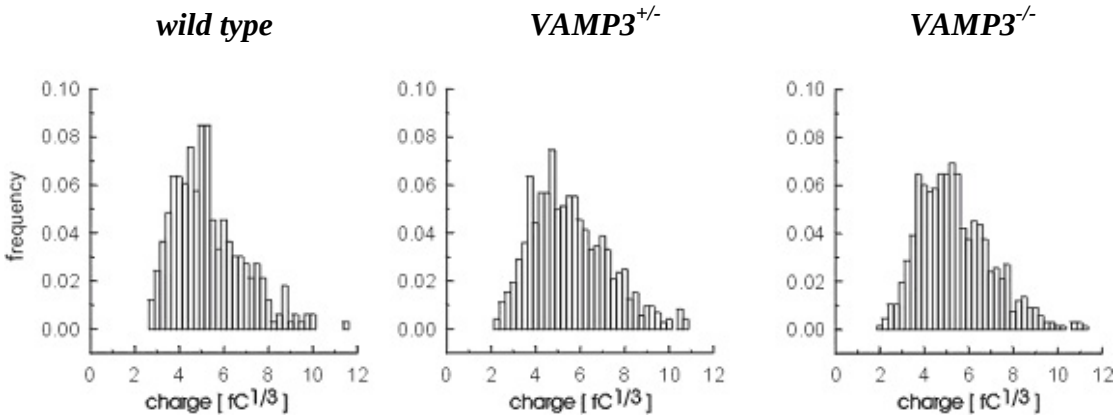

Figure 10. The similar frequency distributions of the cube-rooted amperometric spike charge of the events recorded from wild-type, VAMP3$^{+/-}$ and VAMP3$^{-/-}$ cells show that the deficiency of VAMP3 does not change the vesicle size.

I also compared the frequency distributions of cube-rooted charge integral of amperometric signals from different genotypic cells (*Fig. 10*), results showing that the deficiency of VAMP3 doesn't change the composition of subpopulation of vesicles.

2.6 Overexpressing VAMP3 in syb2$^{-/-}$ cells further prolongs the foot duration.

I next examined whether the prolongation of foot duration of Ca^{2+}-triggered amperometric signals from syb2$^{-/-}$ chromaffin cells can be rescued by expression of VAMP3 using a SFV vector construct. Syb2$^{-/-}$ cells acutely overexpressed

VAMP3 were studied in parallel with untransfected syb2$^{-/-}$ cells and syb2$^{+/+}$ cells from control littermates. Unexpectedly, in transfected syb2$^{-/-}$ cells the events had 3-fold longer foot durations than that in syb2$^{+/+}$ cells, and in untransfected syb2$^{-/-}$ cells the foot durations were still about 2-fold longer compared to that in wild type cells (*Fig. 5, table 3*). Consequently, the foot charges in transfected cells increased by 2-fold in comparison with wild type and untransfected syb2$^{-/-}$ cells. I further determined the percentage of 'plateau events' in transfected cells and compared it with those in wild type and untransfected syb2$^{-/-}$ cells. The transfected cells had a percentage of 'plateau events' up to 27%, which was significantly higher than those in other two types of cells (untransfected syb2$^{-/-}$: 15%, wild type: 5%). The percentage of foot signals in transfected cells was also less than wild type and untransfected syb2$^{-/-}$ cells by ~20%. The release frequency in untransfected syb2$^{-/-}$ cells decreased by 23% compared to that in wild type cells, which was consistent with our early results, and the decrease was only partially rescued by overexpression of VAMP3 (*Fig. 11*). No noticeable differences of amperometric spike phase were found in these three types of cells.

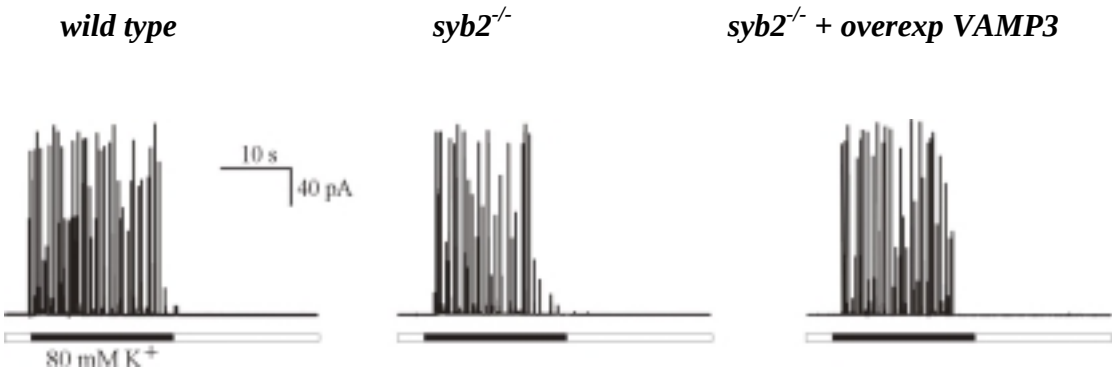

Figure 11. Amperometric recordings from wild type, syb2$^{-/-}$ and syb2$^{-/-}$ with overexpression of VAMP3. The cells were stimulated with 80 mM K^+ (indicated by solid bar). No dramatic changes were observed, with repect to release frequency and event amplitudes between the three types of cells.

Table 3. Properties of release and amperometric events (spike phase and foot signal) of LDCVs in Vamp3$^{+/+}$, Vamp3$^{+/-}$ and Vamp3$^{-/-}$ chromaffin cells

				spike phase				foot signal			
	number of cells	release frequency	% of foot event	charge (fC)	amplitude (pA)	risetime (ms)	halfwidth (ms)	duration (ms)	charge (fC)	mean amplitude (pA)	amplitude (pA)
Vamp3 $^{+/+}$	18	59±8.3	70±3	182±7.1	82±7.1	0.34±0.03	1.84±0.16	5.4±0.27	23±1.8	4.3±0.3	10±0.64
Vamp3 $^{+/-}$	16	53±6.1	67±3	184±8.4	90±8.6	0.32±0.03	1.71±0.17	5.3±0.37	24±1.8	4.6±0.3	11±0.82
Vamp3 $^{-/-}$	13	62±7.2	70±3	181±7.2	84±6.2	0.31±0.02	1.78±0.16	4.7±0.52	22±2.8	4.7±0.4	10±0.82

Measurements are given as mean ± SEM of mean values determined for individual cells.

3. Discussion

Neurons and neuro-endocrine cells release neurotransmitters and hormones by regulated exocytosis of small synaptic vesicles (SSVs) or large dense core vesicles (LDCVs). A vast body of molecular and physiological data has led to a unifying model for this process (Calakos and Scheller, 1996). This model applies to both neuro-transmission and hormone release from a variety of neuroendocrine cells and outlines a molecular mechanism for membrane fusion involving a large number of proteins, including those forming the SNARE complex. This protein complex, consisting of syntaxin, SNAP25 and synaptobrevin2 (syb2), is essential for calcium-triggered exocytosis in neurosecretory cells. The functional analysis of these proteins has been done in different model systems, *i. e.*, neurons of the hippocampus and neuro- endocrine cells of the adrenal medulla (chromaffin cells) (Schoch *et al.*, 2001; Sorensen *et al.*, 2003). The molecular machinery participating in the release of the two classes of vesicles shows great similarities, and data derived from neurons can often be extrapolated to neuroendocrine cells and *vice versa* (Neher, 1998). However, an important difference exists in regard to transmission speed. Whereas classical neurotransmitters (in neurons) are released and give rise to postsynaptic currents within milliseconds, this process is almost 100-fold slower for neuropeptides (Ohnuma *et al.*, 2001) and usually requires more intense stimulation. This fact indicates that, although both neurons and neuro-endocrine cells share a large part of the exocytosis machinery, and in both cases exocytosis is the consequence of a similar chain of events, functional differences exist between brain synaptic processes and neuroendocrine exocytotic processes. This could at least partially be caused by cell-specific gene expression differences, which would be translated into a cell-specific complement of synaptic proteins. Subtle differences in SNARE complex composition, in particular, could account for important changes in the exocytotic process. By systematically investigating the functions of each of the SNARE proteins in synaptic exocytosis of the central nervous system (*e. g.* the hippocampus) and in the exocytotic

processes of cells like the chromaffin cell (adrenal medulla), light is currently being shed on the ultimate functional details of this intricate molecular machinery. This analysis has been considerably facilitated by the use of transgenic mouse lines carrying targeted mutations of a gene of interest (Thomas and Capecchi, 1987).

Synaptobrevin2 (syb2) is one of the components of the SNARE complex (Elferink *et al.*, 1989). Recently, the effect of synaptobrevin2 on the Ca^{2+}-triggered exocytosis of hippocampal neurons has been studied by Schoch and coworkers (2001). They found that in the absence of syb2 the Ca^{2+}-triggered neurotransmitter release was decreased about 100-fold in comparison with wild type. Here I take $syb2^{-/-}$ chromaffin cells of mice adrenal glands as a model system to investigate the role of synaptobrevin2 in the exocytosis of large dense core vesicles (LDCVs).

3.1 The deficiency of syb2 does not abolish exocytosis.

In our study, the Ca^{2+} -triggered release (evoked by local application of potassium) was not completely blocked in syb2 mutant chromaffin cells, and 80% of the release remained. This result contrasts clearly with that previously obtained in hippocampal neurons (Schoch *et al.*, 2001). In addition, in chromaffin cells of mice deficient in SNAP25 (another SNARE protein), exocytosis is completely abolished (Sorensen *et al.*, 2003). One possible explanation for the relatively subtle phenotype of $syb2^{-/-}$ chromaffin cells can be found in the fact that some close structural relatives of syb2 are expressed in these cells, *i. e.,* synaptobrevin1 (syb1), cellubrevin / VAMP3, (Chilcote *et al.*, 1995). At least partially, the function of syb2 could be redundant with that of these isoforms, and so in the absence of syb2, one or some of the synaptobrevin / VAMP isoforms would fill its role and decrease the functional impact of the mutation. I will come back to this hypothesis later (see below), when I discuss the analysis of the VAMP3 mutant line.

3.2 Amperometric techniques cannot resolve the step of exocytosis which is

altered in the syb2 mutants

As I know, vesicles have to follow a number of steps (translocation, docking and priming) before they are ready to fuse to the cell membrane. Due to technical limitations inherent to the amperometric technique, it is not possible from our data to learn which of these steps is altered in the syb2 mutant cells. I foresee to carry out capacitance measurements on these cells in order to clarify this question.

3.3 Pore expansion short and long: contribution of different synaptic proteins

That 80% of the release remained in the mutant does not mean that exocytotic release is entirely normal in the absence of syb2. Actually, the analysis of individual amperometric events showed that the duration of foot signals was two times longer in syb2 mutant cells compared to control cells. A longer foot signal means that the lifetime of the fusion pore is longer in the absence of syb2, that is, the fusion pore expands more slowly into full fusion events. This assumption was further supported by the finding that the percentage of “plateau events” (resulting from exocytotic "failures" in which the fusion pore closes again before reaching full fusion) in the syb2 mutant cells is increased by 2 fold.

Several synaptic proteins (if they are part of the SNARE complex or not) are known to have differential effects on the duration of fusion pore expansion. The actual duration of this phase of exocytosis would depend on the presence and correct function of all of the proteins. SNAP25 would seem to have the opposite effect as syb2, since in the corresponding mutant mouse single vesicular fusion events in the chromaffin cell show shorter duration of the expansion phase (Sorensen *et al.*, 2003). Synaptotagmin, proposed to be the Ca^{2+} sensor of the synaptic vesicle (Wang *et al.*, 2001), is present in the cell under different isoforms originated by alternative splicing (Berton *et al.*, 1997; Geppert *et al.*, 1991; Hilbush and Morgan, 1994; Marqueze *et al.*, 1995). Synaptotagmin I has been shown to prolong the fusion pore expansion (or dilation) time, while synaptotagmin IV decreases its duration (Wang *et al.*, 2001). Munc18, the protein that binds to syntaxin, seems to increase the duration of the expansion phase also

(Fisher *et al.*, 2001).

Can the pore expansion phase be "accelerated" by overexpression of syb2? I have determined that chromaffin cells deficient in syb2 have longer pore expansion phases. From this I deduce that syb2 has the effect of accelerating this phase, making it shorter. If now I made mutant cells express more syb2 than wild type cells have, perhaps I can not only "rescue" the wild type phenotype (*i.e.*, an expansion phase of normal duration), but even "accelerate" this phase, making it faster than normal. The results of the overexpression experiments, however, are clear: overexpression of syb2 in syb2-deficient cells rescues indeed the wild type phenotype, giving the chromaffin cells back the normal duration of their expansion phase; however, in no case could I detect shortened expansion periods in the rescued cells, even after reaching overexpression levels of up to 17-fold (17 times more syb2 than in wild type cells). This indicates that the effect of syb2 is not dose-dependent. Similar results have been obtained with SNAP25 (Sorensen *et al.*, 2003).

3.4 The deficiency of syb2 does not change the spike phase of individual events

Our data show an important function of syb2 in presynaptic processes, particularly during the expansion phase of the fusion pore. Has syb2 a function also after complete expansion? No significant difference in the spike phase of events was observed between syb2 mutant and wild type cells, showing that once the fusion pore expands, exocytosis proceeds normally in the absence of syb2. Similar reasoning and methods have allowed Sorensen *et al.* to reach similar conclusions about SNAP25. Not all presynaptic proteins lack normal effects on the spike phase. Munc18 function, for instance, seems to have an effect on rise time and decaying time of the spikes (Fisher *et al.*, 2001).

3.5 The remaining release in syb2 mutant cells was carried on by synaptobrevin isoforms

Coming back to the initial observation that deficiency in syb2 is responsible only

for a 20% decrease in exocytosis: which other proteins are responsible for the 80% that remain? A powerful tool to investigate this matter is the toxin produced by the microorganism Clostridium tetani, tetanus toxin (TeNT). This is a protease able to specifically cleave the proteins of the synaptobrevin / VAMP family, *e.g.*, syb1, syb2, and VAMP3 (Schiavo *et al.*, 2000b). Micro-injection of TeNT in the presynaptic neurons produces a complete block of transmitter release (Bruns *et al.*, 1997), due to the cleavage of syb2. In our study, the remaining exocytotic capacity present in syb2 mutant cells was completely abolished by overexpression of TeNT LC, indicating that this residual capacity was carried out by the proteins belonging also to the synaptobrevin / VAMP family. This indicates that synaptobrevin proteins are functionally redundant. Which of the synaptobrevin isoforms substitutes for syb2 in the mutant cell? Syb1, syb2 and VAMP3 have been extensively characterized and are responsible for the exocytosis. Since syb1 in adrenal glands is undetectable by standard biochemistry method, VAMP3 would seem like the ideal candidate, because of several reasons: 1) VAMP3 can be easily detected in adrenal glands (McMahon *et al.*, 1993); 2) like synaptobrevin2 and 1, VAMP3 is a substrate for the proteolytic action of TeNT (Galli *et al.*, 1994; Yamasaki *et al.*, 1994b; Yamasaki *et al.*, 1994a); 3) VAMP3 shares a very similar SNARE motif with synaptobrevin2, and they share the same cleavage site for TeNT.

The hypothesis that VAMP3 substitutes for syb2 in the syb2-deficient chromaffin cell is supported by the fact that, in hippocampal cells, where syb2 deficiency abolishes completely exocytosis, VAMP3 is not expressed (Chilcote *et al.*, 1995). If I assume that VAMP3 can carry on the exocytosis in the absence of syb2, then how to explain the 20% decrease of release frequency in syb2 mutant chromaffin cells? One possibility is that syb2 and VAMP3 functionally cooperate in the wild type cell, in such a way that, in the syb2 mutant, the remnant partner can do the job only imperfectly, due to the large differences between them in terms of amino acid sequence of the transmembrane and cytosolic domains (despite their almost total resemblance in the SNARE motif). Alternatively, syb2 could function

independently in wild type conditions; in the mutant, VAMP3 would be able to take over some of the functions of syb2, but less efficiently.

3.6 VAMP3 overexpression does not rescue normal expansion duration in syb2 deficient chromaffin cells

In this context, our results with overexpression of VAMP3 in the syb2-deficient chromaffin cells seem contradictory. VAMP3 actually further prolongs the abnormally long expansion phase found in $syb2^{-/-}$ chromaffin cells. It has been suggested that, while the SNARE complex is known to increase the probability of vesicle fusion, it also may counteract the expansion of the pore once the fusion pore is formed (Sorensen *et al.*, 2003). Our results coincide fully with such insight. At present I cannot offer any more detailed explanation of this paradox.

3.7 No phenotype was found in VAMP3-deficient chromaffin cells

At this point, analyzing exocytosis in the VAMP3-deficient chromaffin cell would be an obvious experiment. The VAMP3 mutant line is available (Yang *et al.*, 2001). In addition, it has been reported that one special kind of neuro-endocrine cells, the pancreatic beta cells (which release insulin), has normal function in these mutants. Our results on the VAMP3 mutant chromaffin cells are in agreement: I have not found any abnormal phenotype in chromaffin exocytosis in the absence of VAMP3. One hypothesis comes immediately to mind when trying to explain these results: syb2, as well as other synaptobrevins, is functionally redundant with VAMP3.

4. Summary

SNAREs (soluble NSF-attachment protein receptors) are generally acknowledged as central components of membrane fusion reactions. During fusion, SNAREs (the vesicle SNARE synaptobrevin and the plasma membrane SNAREs syntaxin 1 and SNAP-25) form complexes through their SNARE motifs. Although SNAREs have been studied in great detail, their precise role in membrane fusion has remained unclear. In my study, I examined the exocytosis in the chromaffin cells from synaptobrevin2 (syb2) and cellubrevin (VAMP3, one member of the synaptobrevin / VAMP family of SNAREs) null mice.

In the absence of syb2, exocytosis persisted, but the release frequency was decreased by 20 %. Single vesicular fusion events showed normal characteristics of spike phase, but the duration of foot signal was prolonged by two-fold compared to wild type. Expression of TeNT light chain in syb2$^{-/-}$ chromaffin cells completely abolished the residual release. The prolonged foot duration and the decreased release frequency were fully rescued to wild type level by over-expressing syb2 protein. However, over-expression of cellubrevin (VAMP3) in syb2$^{-/-}$ cells had an opposite effect on the foot duration, that exogenous VAMP3 even prolonged the foot duration by 3-fold compared to wild type. I also examined the exocytosis in VAMP3$^{-/-}$ chromaffin cells, no significant differences were found between mutant and control cells, with respect to secretion and individual fusion events.

I conclude that synaptobrevin proteins support exocytosis, and they are functionally redundant. Both synaptobrevin isoforms (syb2 and VAMP3) are involved in the stage of fusion pore dilation, but they have opposite effects on this stage.

Reference List

Ahnert-Hilger,G., Bader,M.F., Bhakdi,S., and Gratzl,M. (1989). Introduction of macromolecules into bovine adrenal medullary chromaffin cells and rat pheochromocytoma cells (PC12) by permeabilization with streptolysin O: inhibitory effect of tetanus toxin on catecholamine secretion. J. Neurochem. 52, 1751-1758.

Albillos,A., Dernick,G., Horstmann,H., Almers,W., Alvarez,d.T., and Lindau,M. (1997). The exocytotic event in chromaffin cells revealed by patch amperometry. Nature 389, 509-512.

Almers,W., Breckenridge,L.J., and Spruce,A.E. (1989). The mechanism of exocytosis during secretion in mast cells. 2. Soc. Gen. Physiol Ser. 44, 269-282.

Alvarez,d.T., Fernandez-Chacon,R., and Fernandez,J.M. (1993). Release of secretory products during transient vesicle fusion. Nature 363, 554-558.

Amatore,C., Arbault,S., Bonifas,I., Bouret,Y., Erard,M., and Guille,M. (2003). Dynamics of full fusion during vesicular exocytotic events: release of adrenaline by chromaffin cells. Chemphyschem. 4, 147-154.

Apland,J.P., Adler,M., and Oyler,G.A. (2003). Inhibition of neurotransmitter release by peptides that mimic the N-terminal domain of SNAP-25. J. Protein Chem. 22, 147-153.

Ashery,U., Betz,A., Xu,T., Brose,N., and Rettig,J. (1999). An efficient method for infection of adrenal chromaffin cells using the Semliki Forest virus gene expression system. Eur. J. Cell Biol. 78, 525-532.

Aunis,D. and Langley,K. (1999). Physiological aspects of exocytosis in chromaffin cells of the adrenal medulla. Acta Physiol Scand. 167, 89-97.

Baltazar,G., Tome,A., Carvalho,A.P., and Duarte,E.P. (2000). Differential contribution of syntaxin 1 and SNAP-25 to secretion in noradrenergic and adrenergic chromaffin cells. Eur. J. Cell Biol. 79, 883-891.

Barnard,R.J., Morgan,A., and Burgoyne,R.D. (1997). Stimulation of NSF ATPase activity by alpha-SNAP is required for SNARE complex disassembly and exocytosis. J. Cell Biol. 139, 875-883.

Berton,F., Iborra,C., Boudier,J.A., Seagar,M.J., and Marqueze,B. (1997). Developmental regulation of synaptotagmin I, II, III, and IV mRNAs in the rat CNS 2. J. Neurosci. 17, 1206-1216.

Bittner,M.A., Habig,W.H., and Holz,R.W. (1989). Isolated light chain of tetanus toxin inhibits exocytosis: studies in digitonin-permeabilized cells. J. Neurochem. 53, 966-968.

Block,M.R., Glick,B.S., Wilcox,C.A., Wieland,F.T., and Rothman,J.E. (1988). Purification of an N-ethylmaleimide-sensitive protein catalyzing vesicular transport. Proc. Natl. Acad. Sci. U. S. A 85, 7852-7856.

Bruns,D., Engers,S., Yang,C., Ossig,R., Jeromin,A., and Jahn,R. (1997). Inhibition of transmitter release correlates with the proteolytic activity of tetanus toxin and botulinus toxin A in individual cultured synapses of Hirudo medicinalis. J. Neurosci. 17, 1898-1910.

Bruns,D. and Jahn,R. (1995). Real-time measurement of transmitter release from single synaptic vesicles. Nature 377, 62-65.

Bruns,D., Riedel,D., Klingauf,J., and Jahn,R. (2000). Quantal release of serotonin. Neuron 28, 205-220.

Burgoyne,R.D. (1995). Mechanisms of catecholamine secretion from adrenal chromaffin cells

50. J. Physiol Pharmacol. 46, 273-283.Baumert,M., Maycox,P.R., Navone,F., De Camilli,P., and Jahn,R. (1989). Synaptobrevin: an integral membrane protein of 18,000 daltons present in small synaptic vesicles of rat brain. EMBO J. 8, 379-384.

Calakos,N. and Scheller,R.H. (1996). Synaptic vesicle biogenesis, docking, and fusion: a molecular description 1. Physiol Rev. 76, 1-29.

Camacho,M., Montesinos,M.S., Machado,J.D., and Borges,R. (2003). [Exocytosis as the mechanism for neural communication. A view from chromaffin cells]. Rev. Neurol. 36, 355-360.

Chilcote,T.J., Galli,T., Mundigl,O., Edelmann,L., McPherson,P.S., Takei,K., and De Camilli,P. (1995). Cellubrevin and synaptobrevins: similar subcellular localization and biochemical properties in PC12 cells 1. J. Cell Biol. 129, 219-231.

Chow,R.H., von Ruden,L., and Neher,E. (1992). Delay in vesicle fusion revealed by electrochemical monitoring of single secretory events in adrenal chromaffin cells 1. Nature 356, 60-63.

Clements,J.D., Lester,R.A., Tong,G., Jahr,C.E., and Westbrook,G.L. (1992). The time course of glutamate in the synaptic cleft 1. Science 258, 1498-1501.

Elferink,R.P., Ottenhoff,R., Liefting,W., de Haan,J., and Jansen,P.L. (1989). Hepatobiliary transport of glutathione and glutathione conjugate in rats with hereditary hyperbilirubinemia 1. J. Clin. Invest 84, 476-483.

Fahey,P.F. and Webb,W.W. (1978). Lateral diffusion in phospholipid bilayer membranes and multilamellar liquid crystals 2. Biochemistry 17, 3046-3053.

Fasshauer,D., Sutton,R.B., Brunger,A.T., and Jahn,R. (1998). Conserved structural features of the synaptic fusion complex: SNARE proteins reclassified as Q- and R-SNAREs. Proc. Natl. Acad. Sci. U. S. A 95, 15781-15786.

Fernandez,J.M., Neher,E., and Gomperts,B.D. (1984a). Capacitance measurements reveal stepwise fusion events in degranulating mast cells. Nature 312, 453-455.

Fernandez,J.M., Neher,E., and Gomperts,B.D. (1984). Capacitance measurements reveal stepwise fusion events in degranulating mast cells. Nature 312, 453-455.

Fleig,A. and Penner,R. (1995). Excessive repolarization-dependent calcium currents induced by strong depolarizations in rat skeletal myoballs. J. Physiol 489 (Pt 1), 41-53.

Galli,T., Chilcote,T., Mundigl,O., Binz,T., Niemann,H., and De Camilli,P. (1994). Tetanus toxin-mediated cleavage of cellubrevin impairs exocytosis of transferrin receptor-containing vesicles in CHO cells . J. Cell Biol. 125, 1015-1024.

Geppert,M., Archer,B.T., III, and Sudhof,T.C. (1991). Synaptotagmin II. A novel differentially distributed form of synaptotagmin. J. Biol. Chem. 266, 13548-13552.

Graham,M.E., Fisher,R.J., and Burgoyne,R.D. (2000). Measurement of exocytosis by amperometry in adrenal chromaffin cells: effects of clostridial neurotoxins and activation of protein kinase C on fusion pore kinetics. Biochimie 82, 469-479.

Haller,M., Heinemann,C., Chow,R.H., Heidelberger,R., and Neher,E. (1998). Comparison of secretory responses as measured by membrane capacitance and by amperometry. Biophys. J. 74, 2100-2113.

Hamill,O.P., Marty,A., Neher,E., Sakmann,B., and Sigworth,F.J. (1981). Improved patch-clamp techniques for high-resolution current recording from cells and cell-free membrane patches. Pflugers Arch. 391, 85-100.

Hilbush,B.S. and Morgan,J.I. (1994). A third synaptotagmin gene, Syt3, in the mouse. Proc. Natl. Acad. Sci. U. S. A 91, 8195-8199.

Hohne-Zell,B. and Gratzl,M. (1996). Adrenal chromaffin cells contain functionally different SNAP-25 monomers and SNAP-25/syntaxin heterodimers. FEBS Lett. 394, 109-116.

Huang,L., Ozato,K., and Pagano,R.E. (1978). Interactions of phospholipid vesicles with murine lymphocytes. I. Vesicle-cell adsorption and fusion as alternate pathways of uptake. Membr. Biochem. 1, 1-25.

Jahn,R. and Sudhof,T.C. (1999). Membrane fusion and exocytosis. Annu. Rev. Biochem. 68, 863-911.

Jankowski,J.A., Schroeder,T.J., Ciolkowski,E.L., and Wightman,R.M. (1993). Temporal characteristics of quantal secretion of catecholamines from adrenal medullary cells. J. Biol. Chem. 268, 14694-14700.

Kawagoe,K.T., Jankowski,J.A., and Wightman,R.M. (1991). Etched carbon-fiber electrodes as amperometric detectors of catecholamine secretion from isolated biological cells. Anal. Chem. 63, 1589-1594.

Kelly,R.B. (1993). Storage and release of neurotransmitters. Cell 72 Suppl, 43-53.

Khanin,R., Parnas,H., and Segel,L. (1997). A mechanism for discharge of charged excitatory neurotransmitter. Biophys. J. 72, 507-521.

Land,B.R., Salpeter,E.E., and Salpeter,M.M. (1980). Acetylcholine receptor site density affects the rising phase of miniature endplate currents. Proc. Natl. Acad. Sci. U. S. A 77, 3736-3740.

Leszczyszyn,D.J., Jankowski,J.A., Viveros,O.H., Diliberto,E.J., Jr., Near,J.A., and Wightman,R.M. (1990). Nicotinic receptor-mediated catecholamine secretion from individual chromaffin cells. Chemical evidence for exocytosis. J. Biol. Chem. 265, 14736-14737.

Liljestrom,P. and Garoff,H. (1991). A new generation of animal cell expression vectors based on the Semliki Forest virus replicon. Biotechnology (N. Y.) 9, 1356-1361.

Liljestrom,P. and Garoff,H. (1991). A new generation of animal cell expression vectors based on the Semliki Forest virus replicon. Biotechnology (N. Y.) 9, 1356-1361.

Lindau,M., Rosenboom,H., and Nordmann,J. (1994). Exocytosis and endocytosis in single peptidergic nerve terminals. Adv. Second Messenger Phosphoprotein Res. 29, 173-187.

Lomneth,R., Martin,T.F., and DasGupta,B.R. (1991). Botulinum neurotoxin light chain inhibits norepinephrine secretion in PC12 cells at an intracellular membranous or cytoskeletal site. J. Neurochem. 57, 1413-1421.

Lundstrom,K. (1999). Alphaviruses as tools in neurobiology and gene therapy. J. Recept. Signal. Transduct. Res. 19, 673-686.

Marqueze,B., Boudier,J.A., Mizuta,M., Inagaki,N., Seino,S., and Seagar,M. (1995). Cellular localization of synaptotagmin I, II, and III mRNAs in the central nervous system and pituitary and adrenal glands of the rat. J. Neurosci. 15, 4906-4917.

Matthews-Bellinger,J. and Salpeter,M.M. (1978). Distribution of acetylcholine receptors at frog neuromuscular junctions with a discussion of some physiological implications. J. Physiol 279, 197-213.

McMahon,H.T., Ushkaryov,Y.A., Edelmann,L., Link,E., Binz,T., Niemann,H., Jahn,R., and Sudhof,T.C. (1993). Cellubrevin is a ubiquitous tetanus-toxin substrate homologous to a putative synaptic vesicle fusion protein. Nature 364, 346-349.

Moser,T. and Neher,E. (1997). Estimation of mean exocytic vesicle capacitance in mouse adrenal chromaffin cells. Proc. Natl. Acad. Sci. U. S. A 94, 6735-6740.

Murthy,V.N. and Stevens,C.F. (1999). Reversal of synaptic vesicle docking at central synapses. Nat. Neurosci. 2, 503-507.

Nagy,A., Baker,R.R., Morris,S.J., and Whittaker,V.P. (1976). The preparation and characterization of synaptic vesicles of high purity. Brain Res. 109, 285-309.

Neher,E. (1998). Vesicle pools and Ca2+ microdomains: new tools for understanding their roles in neurotransmitter release. Neuron 20, 389-399.

Neher,E. and Zucker,R.S. (1993). Multiple calcium-dependent processes related to secretion in bovine chromaffin cells. Neuron 10, 21-30.

Neher,E. and Marty,A. (1982a). Discrete changes of cell membrane capacitance observed under conditions of enhanced secretion in bovine adrenal chromaffin cells. Proc. Natl. Acad. Sci. U. S. A 79, 6712-6716.

Neher,E. and Marty,A. (1982b). Discrete changes of cell membrane capacitance observed under conditions of enhanced secretion in bovine adrenal chromaffin cells. Proc. Natl. Acad. Sci. U. S. A 79, 6712-6716.

Ohnuma,K., Whim,M.D., Fetter,R.D., Kaczmarek,L.K., and Zucker,R.S. (2001). Presynaptic target of Ca2+ action on neuropeptide and acetylcholine release in Aplysia californica. J. Physiol 535, 647-662.

Perlman,R.L. and Chalfie,M. (1977). Catecholamine release from the adrenal medulla. Clin. Endocrinol. Metab 6, 551-576.

Poirier,M.A., Xiao,W., Macosko,J.C., Chan,C., Shin,Y.K., and Bennett,M.K. (1998). The synaptic SNARE complex is a parallel four-stranded helical bundle. Nat. Struct. Biol. 5, 765-769.

Roth,D. and Burgoyne,R.D. (1994). SNAP-25 is present in a SNARE complex in adrenal chromaffin cells. FEBS Lett. 351, 207-210.

Rothman,J.E. (1994). Intracellular membrane fusion. Adv. Second Messenger Phosphoprotein Res. 29, 81-96.

Rusakov,D.A. and Kullmann,D.M. (1998). Geometric and viscous components of the tortuosity of the extracellular space in the brain. Proc. Natl. Acad. Sci. U. S. A 95, 8975-8980.

Ryan,T.A. (2003). Kiss-and-run, fuse-pinch-and-linger, fuse-and-collapse: the life and times of a neurosecretory granule. Proc. Natl. Acad. Sci. U. S. A 100, 2171-2173.

Schiavo,G., Benfenati,F., Poulain,B., Rossetto,O., Polverino,d.L., DasGupta,B.R., and Montecucco,C. (1992a). Tetanus and botulinum-B neurotoxins block neurotransmitter release by proteolytic cleavage of synaptobrevin. Nature 359, 832-835.

Schiavo,G., Malizio,C., Trimble,W.S., Polverino,d.L., Milan,G., Sugiyama,H., Johnson,E.A., and Montecucco,C. (1994a). Botulinum G neurotoxin cleaves

VAMP/synaptobrevin at a single Ala-Ala peptide bond. J. Biol. Chem. 269, 20213-20216.

Schiavo,G., Matteoli,M., and Montecucco,C. (2000). Neurotoxins affecting neuroexocytosis. Physiol Rev. 80, 717-766.

Schoch,S., Deak,F., Konigstorfer,A., Mozhayeva,M., Sara,Y., Sudhof,T.C., and Kavalali,E.T. (2001). SNARE function analyzed in synaptobrevin/VAMP knockout mice. Science 294, 1117-1122.

Schroeder,T.J., Jankowski,J.A., Kawagoe,K.T., Wightman,R.M., Lefrou,C., and Amatore,C. (1992). Analysis of diffusional broadening of vesicular packets of catecholamines released from biological cells during exocytosis. Anal. Chem. 64, 3077-3083.

Sollner,T., Bennett,M.K., Whiteheart,S.W., Scheller,R.H., and Rothman,J.E. (1993). A protein assembly-disassembly pathway in vitro that may correspond to sequential steps of synaptic vesicle docking, activation, and fusion. Cell 75, 409-418.

Sorensen,J.B., Nagy,G., Varoqueaux,F., Nehring,R.B., Brose,N., Wilson,M.C., and Neher,E. (2003). Differential control of the releasable vesicle pools by SNAP-25 splice variants and SNAP-23. Cell 114, 75-86.

Sorensen,J.B., Matti,U., Wei,S.H., Nehring,R.B., Voets,T., Ashery,U., Binz,T., Neher,E., and Rettig,J. (2002). The SNARE protein SNAP-25 is linked to fast calcium triggering of exocytosis. Proc. Natl. Acad. Sci. U. S. A 99, 1627-1632.

Spruce,A.E., Breckenridge,L.J., Lee,A.K., and Almers,W. (1990). Properties of the fusion pore that forms during exocytosis of a mast cell secretory vesicle. Neuron 4, 643-654.

Sutton,R.B., Fasshauer,D., Jahn,R., and Brunger,A.T. (1998). Crystal structure of a SNARE complex involved in synaptic exocytosis at 2.4 A resolution. Nature 395, 347-353.

Tagaya,M., Toyonaga,S., Takahashi,M., Yamamoto,A., Fujiwara,T., Akagawa,K., Moriyama,Y., and Mizushima,S. (1995). Syntaxin 1 (HPC-1) is associated with chromaffin granules. J. Biol. Chem. 270, 15930-15933.

Thomas,K.R. and Capecchi,M.R. (1987). Site-directed mutagenesis by gene targeting in mouse embryo-derived stem cells. Cell 51, 503-512.

Thomas,P., Wong,J.G., Lee,A.K., and Almers,W. (1993). A low affinity Ca2+ receptor controls the final steps in peptide secretion from pituitary melanotrophs. Neuron 11, 93-104.

Van der,K.W. (1995). The rise times of miniature endplate currents suggest that acetylcholine may be released over a period of time. Biophys. J. 69, 148-154.

Wang,C.T., Grishanin,R., Earles,C.A., Chang,P.Y., Martin,T.F., Chapman,E.R., and Jackson,M.B. (2001). Synaptotagmin modulation of fusion pore kinetics in regulated exocytosis of dense-core vesicles. Science 294, 1111-1115.

Wathey,J.C., Nass,M.M., and Lester,H.A. (1979). Numerical reconstruction of the quantal event at nicotinic synapses. Biophys. J. 27, 145-164.

Wightman,R.M., Jankowski,J.A., Kennedy,R.T., Kawagoe,K.T., Schroeder,T.J., Leszczyszyn,D.J., Near,J.A., Diliberto,E.J., Jr., and Viveros,O.H. (1991). Temporally resolved catecholamine spikes correspond to single vesicle release from individual chromaffin cells. Proc. Natl. Acad. Sci. U. S. A 88, 10754-10758.

Xu,T., Rammner,B., Margittai,M., Artalejo,A.R., Neher,E., and Jahn,R. (1999a). Inhibition of SNARE complex assembly differentially affects kinetic components of exocytosis. Cell 99, 713-722.

Xu,T., Rammner,B., Margittai,M., Artalejo,A.R., Neher,E., and Jahn,R. (1999b). Inhibition of SNARE complex assembly differentially affects kinetic components of exocytosis. Cell 99, 713-722.

Yamasaki,S., Baumeister,A., Binz,T., Blasi,J., Link,E., Cornille,F., Roques,B., Fykse,E.M., Sudhof,T.C., Jahn,R., and . (1994a). Cleavage of members of the synaptobrevin/VAMP family by types D and F botulinal neurotoxins and tetanus toxin. J. Biol. Chem. 269, 12764-12772.

Yamasaki,S., Hu,Y., Binz,T., Kalkuhl,A., Kurazono,H., Tamura,T., Jahn,R., Kandel,E., and Niemann,H. (1994b). Synaptobrevin/vesicle-associated membrane protein (VAMP) of Aplysia californica: structure and proteolysis by tetanus toxin and botulinal neurotoxins type D and F. Proc. Natl. Acad. Sci. U. S. A 91, 4688-4692.

Yang,C., Mora,S., Ryder,J.W., Coker,K.J., Hansen,P., Allen,L.A., and Pessin,J.E. (2001). VAMP3 null mice display normal constitutive, insulin- and exercise-regulated vesicle trafficking. Mol. Cell Biol. 21, 1573-1580.

Zucker,R.S. (1996). Exocytosis: a molecular and physiological perspective. Neuron 17, 1049-1055.

Acknowledgement

I would like to express my deep gratitude to Prof. Dr. Reinhard Jahn, who has granted me the opportunity to pursue the work of this PhD thesis under the excellent working conditions in his department and who has kindly supported me with advice and suggestions. I would especially like to thank Prof. Dr. Dieter Bruns for having given me two challenging and interesting PhD projects, the supervision and advice throughout the three years. I thank Prof. Dr. Hans-Dieter Söling for his kind and crucial help, advice and support particularly for handling the formal study matters for the University of Göttingen. I would like to thank Prof. Dr. F.W. Schürmann for being the referent of my thesis. I also thank Prof. Dr. Gottfried Mieskes for his support and help in this department.

I would like to thank Dr. Xunlei Zhou and Dr. Gonzalo Alvarez-Bolado warmly for the critical reading and correction of the thesis manuscript, Dr. Xunlei Zhou especially for her expertise concerning the techniques of molecule biology. I also would like to thank Dr. Dagmar Schütz for the correction of my thesis and the data discussion and Dr. Christian Derst for critical reading of the PhD manuscript. Thank you also to my good friends of the department "Neurobiology" Dr. Dagmar Schütz, Dr. Undine Lippert, Dr. Thorsten Lang, Dr. Shigeo Takamori for the helpful discussions. Thank you to Dr. Jakob Soerensen from Prof. Dr. Erwin Neher's department "Membrane biophysics" for kindly providing his overexpression viral constructs for my project.

Finally, I would like to thank all other members of the department "Neurobiology" Kathrin Barnewitz, Marcin Barszczewski, Dr. Christina Schütte, Dorothea Schieding, Olga Vites, Stephan Schenck, Dr. David Ferrari and Chaoshe Guo for the excellent working atmosphere.